Molecular Analysis of Type IV Pilus Assembly in *Clostridium perfringens*

William A. Hendrick

Dissertation submitted to the Faculty of the Virginia Polytechnic Institute and State University in partial fulfillment of the requirements for the degree of

Doctor of Philosophy
in
Biological Sciences

Stephen B. Melville, Chair
Ann M. Stevens
Florian D. Schubot
Daniel G. Capelluto

June 29, 2016
Blacksburg, Virginia

Keywords: Type IV Pili, *Clostridium perfringens*

Molecular Analysis of Type IV Pilus Assembly in *Clostridium perfringens*

William A. Hendrick

ABSTRACT

Clostridium perfringens is a Gram-positive anaerobe capable of causing disease in humans and many animals. *C. perfringens* is able to move across surfaces in a manner that is dependent on growth and type IV pili.

Type IV pili are filaments that can be extended away from the cell by rapid polymerization, and retracted by depolymerization. Furthering the understanding of the initial and final energetic states of the pilins will reveal insights into possible mechanisms of type IV pilus assembly. Toward that end, a pilin was purified from the Gram-negative pathogen *Pseudomonas aeruginosa* and incorporated into an artificial membrane. The pilin was probed by a solid state nuclear magnetic resonance (ssNMR) technique that can determine the angle and depth of insertion of a helical peptide, as well as fluorescent and electron microscopy.

All type IV pilus systems involve the action of an assembly ATPase to provide energy to polymerize the pilus. One proposed mechanism involves two primary proteins: an ATPase and an integral membrane core protein (IMCP). Other type IV pilus proteins are thought to play supportive roles in aiding the traversal of the cell envelope. In order to evaluate this model, the assembly ATPase PilB2 and IMCP PilC2 from *C. perfringens* were purified and examined for interactions. The evidence presented here suggest that PilB2 and PilC2 do not interact directly, and cannot function as a core assembly apparatus.

The carbonic anhydrase (Cpb) from *C. perfringens* strain 13 was characterized both biochemically and physiologically. Cpb belongs to the type I subclass of the β class and is the first β

class enzyme investigated from a strictly anaerobic bacteria. Kinetic analyses revealed a two-step, ping-pong, zinc-hydroxide mechanism of catalysis. Analyses of a *cpb* deletion mutant of *C. perfringens* strain HN13 showed that Cpb is strictly required for growth when cultured in semi-defined medium and an atmosphere without CO_2. The grew well in nutrient-rich media with or without CO_2 in the atmosphere, although elimination of glucose resulted in decreased production of acetate, propionate, and butyrate. The results suggest a role for Cpb in anaplerotic CO_2 fixation reactions by supplying bicarbonate to carboxylases.

This work received funding from the NSF and NIH

DEDICATION

This work is dedicated first and foremost to my wife Kelly, for being supportive of my goals, and for helping me through this long journey. Also to my family, especially my parents, for being encouraging of my curiosity and love of science at an early age. Also to Mrs. Stacy Costello, who taught the very first microbiology and biochemistry courses I took. Also to all of the other faculty and staff at Ocean Lakes High School Mathematics and Science Academy I interacted with, for fostering an interest in more advanced sciences. And finally to all those who struggle with mental illness and the staff at Cook Counseling Center.

ACKNOWLEDGEMENTS

I want to thank my advisor, Dr. Stephen Melville for his guidance in my projects. He was consistently supportive, even when my personal problems directly threatened my ability to continue, and encouraged me to always work harder. I do wish I had been better able to take his advice and urgings and turn them into actual positive change for the better.

I want to thank my committee members, Dr. Ann Stevens, Dr. Florian Schubot, and Dr. Daniel Capelluto, for all of the care and support throughout my studies.

My lab mates over the years, Andrea Hartman, Hualan Liu, Sarah Nikraftar, Gary Camper, and Samantha Murray, are an amazing group of people that I am very lucky to have known. I miss, and shall miss, each of you deeply.

The undergraduates I have mentored directly, Tara Gallagher and Haley Krem, have both gone on to careers of their own within science. Not scaring them off from science is the best praise I can receive as a mentor.

The Life Sciences I building/microbiology at VT community is something that I will miss, and don't expect to ever experience the likes of again.

Table of Contents

List of Figures

List of Tables

List of Equations

Chapter 1 Introduction and Review of Literature

Clostridium perfringens

Characteristics of *C. perfringens*

C. perfringens is an anaerobic, Gram-positive, spore-forming, rod-shaped bacterium within the Firmicutes (1). It is extremely widespread and is found in the intestinal tract of humans and many animals (2), as well as soil (3) and freshwater and marine sediments (1). *C. perfringens* is an aerotolerant anaerobe with a short generation time (4). A broad array of extracellular toxins are produced by *C. perfringens*, which are responsible for its pathogenicity (5). *C. perfringens* is capable of a form of gliding motility across solid surfaces which is thought to be dependent on type IV pili (6).

Diseases caused by *C. perfringens* and its toxins

C. perfringens causes gas gangrene, as well as food poisoning and other gastrointestinal diseases in humans and animals (7). Like many other Clostridia, *C. perfringens* produces a number of extracellular toxins (Table 1.1) that are important in pathogenesis. As many as 19 different toxins are produced, though not all are present in each strain.

Table 1.1 Toxins of *C. perfringens* and their activities
Compiled from (2, 8-10).

Toxin	Biological Activity	Biochemical Activity
α	Lethal, Necrotizing, Hemolytic	Phospholipase C, Sphingomyelinase
β	Lethal, Necrotizing	Pore-forming
ε	Lethal, Necrotizing	Pore-forming
ι	Lethal, Necrotizing	ADP-ribosyltransferase
δ	Lethal, Hemolytic	Pore-forming
θ	Lethal, Hemolytic	Pore-forming
κ	Lethal, Necrotizing	Collagenase
λ	Edema	Protease
μ		Hyaluronidase
ν	Leukocidal	Deoxyribonuclease
cpe	Diarrhea, Cytotoxic	Pore-forming
NanI		Sialidase

C. perfringens strains are divided into five toxin types (A – E, Table 1.2) based on which of four

major toxins (α, β, ε, and ι) they produce (11). Type A is associated with gas gangrene, a severe, life threatening infection with sudden onset. Several species of *Clostridium*, such as *C. novyi*, *C. septicum*, and *C. histolyticum* can also cause gas gangrene, but *C. perfringens* is the most common cause (12, 13). The symptoms of gas gangrene include fever, pain, edema, myonecrosis, and gas accumulation. Later stages include necrotizing fasciitis and cutaneous necrosis. Left untreated, this infection leads inevitably to death due to systemic toxemia. The primary toxin involved in gas gangrene is α-toxin, which is produced by all *C. perfringens* types, although Type A produces the highest amounts (7, 12). This toxin has phospholipase C and sphingomyelinase activities, and functions to disrupt the membranes of host cells by degradation of phospholipids and sphingolipids (14). Type B isolates produce toxins α, β, and ε, and cause lamb dysentery (2). Type C isolates of *C. perfringens* produce α- and β-toxin, and can cause a rare form of enteritis known as enteritis necroticans or pigbel. This disease occurs most frequently in undernourished people, on consumption of a high protein meal. Symptoms include severe abdominal pain, vomiting, and bloody diarrhea (15). Low trypsin production caused by a low protein diet reduces inactivation of β-toxin, which is responsible for the symptoms of the disease. Additionally, in areas of New Guinea where this disease is prevalent, large feasts of pork are usually consumed with sweet potatoes. Sweet potatoes contain a trypsin inhibitor which further reduces inactivation of β-toxin (7). Type D isolates produce α- and ε-toxins, and cause enterotoxemia of sheep and goats, and pulpy-kidney disease (8). Although ε-toxin is also produced by type B, it is primarily responsible for the virulence of type D strains. Following cleavage by trypsin, chymotrypsin, or λ-toxin, mature ε-toxin binds to host cell membranes in the intestine and many other organs. Once bound to membranes, ε-toxin oligomerizes and forms pores (16).

C. perfringens is also a major cause of food poisoning. Ingestion of improperly handled food contaminated with *C. perfringens* spores, especially those foods containing meat, can lead to vegetative cells growing in the intestinal tract. If these cells carry the gene for *C. perfringens* enterotoxin (*cpe*), production of the enterotoxin (CPE) occurs when the cells sporulate (7, 17). CPE accumulates in the

cytoplasm of the mother cell, and is released when the cell lyses to release the mature spore. Binding of the enterotoxin to the intestinal epithelium is followed by loss of fluid and electrolytes into the intestinal lumen, causing cramping and diarrhea (17).

Table 1.2 Diseases Caused by *C. perfringens*
Compiled from (2, 8).

Type	Major Toxins	Disease
A	α	Human and animal gas gangrene, Food poisoning, Human and canine gastroenteritis, Necrotic enteritis of poultry
B	α, β, ε	Lamb dysentery, Foal/sheep/goat enterotoxemia
C	α, β	Enteritis necroticans (pigbel, Darmbrand), Sheep/calf/lamb/piglet/foal necrotic enteritis
D	α, ε	Enterotoxemia of sheep, goats, and cattle
E	α, ι	Possible association with cattle/sheep/rabbit gastroenteritis

Gliding motility of *C. perfringens*

C. perfringens is capable of a form of gliding motility across solid surfaces, where a large group of cells, held tightly in bundles side-to-side and end-to-end, are propelled away from the central area of growth. The mechanism underlying this motility is not well understood, although it has been determined that type IV pili play some role (6). Strains with plasmid insertions in *pilT* (retraction ATPase) and *pilC* were found to have a significantly reduced ability to glide on an agar surface. Interestingly, genes for type IV pili were found in all species of *Clostridium* examined, and gliding motility was demonstrated in *Clostridium beijerinckii* on high percentage agar (6). It was later found, by random transposon mutagenesis, that in addition to type IV pili, a variety of genes impact the ability to glide on a surface (18). Many of the genes identified are involved in metabolic processes, indicating that this motility is partially dependent on proper growth conditions.

Type IV pili

Type IV pili (TFP) are flexible appendages produced by many Gram-negative bacteria (19), as well as many Gram-positive bacteria, including *C. perfringens* (6). TFP have a large diversity of function,

from attachment and motility, to DNA uptake and even electron transport (19, 20). The assembled filaments are composed of many copies of a small (15-20 kDa) pilin protein (PilA2 in *C. perfringens*), and are 6-9 nm wide and up to several micrometers long. TFP are extraordinarily strong, with retraction forces as high as 110 pN (21), and rupture forces as high as 150 pN (22). These filaments are assembled and disassembled by molecular motors using the hydrolysis of ATP as an energy source, called PilB2 and PilT in *C. perfringens*, respectively. There are a number of additional proteins involved in TFP assembly, including a prepilin peptidase (PilD), an integral membrane protein (PilC2) that binds the assembly and retraction ATPases, and proteins that form a channel through the cell wall for the growing pilus (PilM, PilN, PilO) (6, 19). TFP have been studied extensively in *Pseudomonas aeruginosa*; so much so that it is considered a model system (23). Unless noted otherwise, all further discussions of prior studies will be limited to *P. aeruginosa*.

Functions of type IV pili

TFP are used by bacteria to accomplish a wide variety of functions. In *P. aeruginosa*, pili have been implicated in surface attachment, surface motility, DNA binding, conjugation, and biofilm formation (24-26).

TFP are known to act as adhesins, allowing *P. aeruginosa* to attach to a wide variety of surfaces, both organic (epithelial tissues, erythrocytes) and inorganic (minerals, glasses, metals) (27). By functionalizing the tip of an AFM probe with bacteria, Touhami *et al.* (27) were able to determine that TFP of *P. aeruginosa* PAO1, when attached to a mica surface, could withstand an average tension of 95 pN before rupturing. This was done by gently placing the coated probe onto a phosphate-buffered saline coated mica surface, and allowing the pili of the cells to attach to the surface. The probe was then slowly (3 μm/s) retracted, measuring the force required to move the probe. Interestingly, the probe/bacteria/pilus/mica system was found to have an elastic constant that does not vary with respect to pilus length, suggesting that pili are very ‘rigid’ to tension: that is, they do not lengthen under load the way an elastic band would. This would mean that any load applied to the base of the filament by the

retraction ATPase would be transmitted in full to the surface to which the pilus is adhered.

DNA binding by TFP was demonstrated in 2004 by van Schaik *et al.* (28). This was done by binding pUCP19 plasmid and salmon sperm DNA to microtiter plates, and observing the binding of biotinylated pili from strains PAK, K122-4, and KB-7 using streptavidin conjugated to horseradish peroxidase. This binding was thought to be a property of the intact pilus, and mediated by non-specific electrostatic interaction with a positively charged band on the surface of the pilus. The authors tested this by testing the ability of pilin monomers to bind DNA under similar conditions, and found that they did not bind. Additionally, the binding of DNA by intact pili was shown to be inhibited by polyphosphate and both mono- and polyclonal antibodies to PAK pili. Specific oligonucleotide sequences did not have an effect on DNA binding, although random sequences composed of pyrimidine bases did inhibit binding of other oligonucleotides. *P. aeruginosa* is not known to be naturally competent; however, *P. aeruginosa pilA* has been shown to restore natural competence in a *Pseudomonas stutzeri pilA* mutant, showing that *P. aeruginosa* pili can function to take up DNA from the extracellular environment.

Although *P. aeruginosa* does not use TFP for natural transformation, a TFP system has been identified that allows for lateral gene transfer. Carter *et al.* (29) demonstrated that the pathogenicity island (PI) PAPI-1 of strain PA14 is transferred using TFP machinery encoded in the PI via a conjugation mechanism.

TFP have also been shown (30) to allow UV-irradiated cells of the archaeal order *Sulfolobales* to transfer DNA between cells. This DNA transfer is dependent on aggregation of the cells (31), and mutants deficient in the UV-inducible pili (*ups*) are still able to form aggregates with wild-type cells, and perform the transfer. UV-induced transfer between two bacterial strains with mutations in different sites of *pyrE*, a gene involved in uracil biosynthesis, was able to restore function of *pyrE*, demonstrating that this transfer allows cells to exchange chromosomal DNA fragments, which are then used by the cells' DNA repair machinery to recombine these fragments into the chromosome to repair damage.

Structure of type IV pili

TFP are long, proteinaceous filaments that can be extended away from (and in many cases retracted toward) the surface of bacterial cells. These filaments can be up to 7 μm in length, and have a helical structure (19, 27, 32, 33). The TFP of *P. aeruginosa* strains K and O (PAK, PAO) have very similar dimensions: 5.2 nm in diameter with a ring of hydrophobic residues at 3.1 nm from the center (33). This helical architecture gives the individual pilus filament great strength as well as a degree of flexibility. Indeed, when viewed under transmission electron microscopy (TEM), *P. aeruginosa* PAO1 pili can form sharp bends with loop diameters as small as 50 nm. Additionally, the average rupture force of the same pilus has been measured using atomic force microscopy (AFM) to be 95 pN when attached to mica (27). This is thought to be the release of the pilus tip from the mica surface, rather than the breaking of the pilus filament or release of the pilus from the bacterium, but this has not been conclusively demonstrated. In Gram-negative bacteria, the pilus assembly machinery can be broken down into subcomplexes; the pilus itself, the outer membrane secretin, the alignment subcomplex, and the motor subcomplex (34).

Pilins

Type IV pilins are produced as prepilins, with an N-terminal class III signal peptide (35) consisting of hydrophilic residues that are cleaved by a prepilin peptidase (36). Following cleavage, the N-terminus of the mature pilin is generally a N-methylated phenylalanine residue, followed by 20-25 hydrophobic amino acids in an α-helical stalk (α1-N), with the fifth residue almost always being a glutamate (35, 37). Aside from this, pilins vary greatly in size and structure, although they share a general architecture. The α1-N motif is continued into another α-helix (α1-C), which composes the ’backbone’ of the pilin’s globular head domain. This is followed by an αβ-loop region between α1 and a central 4-5 strand β-sheet. A pair of conserved cysteine residues forms a disulfide bond linking the C-terminal region to this β-sheet; the region between the two residues is referred to as the D-region. The αβ-loop and the

D-region vary substantially (19).

There are three subtypes of pilins, Type IVa, Type IVb, and Tad, based on sizes of their signal peptide and mature pilin. Type IVa pilins are widely distributed, tend to have shorter signal peptides, are smaller in the mature form, and feature a simple N to N+1 β-sheet architecture. Type IVb pilins are generally found in enteric organisms, have longer signal peptides and mature forms, and have a more complex β-sheet architecture, with the C-terminal strand in the center of the sheet (19, 35, 38, 39). Tad pilins can be considered a subset of Type IVb, but are much smaller (38).

Pilus

The pilus fiber is composed of many copies of pilin proteins, which are held together by a mixture of hydrophobic and ionic interactions. Each incorporated pilin monomer increases the length of the pilus by 10.5 Å (25), and participates in interactions with multiple pilins. These interactions are in the form of a bundle of three N terminal alpha helices, composed of the N terminal alpha helices of subunit n (residues 24-39), subunit n+3 (residues 4-19), and subunit n+4 (residues 1-13). Along the length of one pilin, the bundles change interaction partners twice (25). The packing arrangement of pilins within the pilus leads to a surface with ridges and deep helical grooves; in *Neisseria gonorrhoeae*, some of these grooves are positively charged which would allow for non-specific DNA binding, which may play a role in pilus-dependent competence (19).

Outer membrane secretin

The pilus fiber exits the outer membrane via the secretin pore, which is composed of ~12-15 PilQ subunits, each of which adopts a beta barrel structure with 14-16 transmembrane strands with an extracellular C-terminus (26, 40). In *Myxococcus xanthus*, it has been demonstrated that the secretin is the first part of the Type IV pilus system to be assembled, and requires an outer membrane bound pilotin

(41). The secretin has been demonstrated to be a 'gated' system that can open and close, through the use of electron cryo-tomography (42). This pore recruits and interacts with the alignment subcomplex via the C-terminal domain of the lipoprotein PilP (41, 43). The secretin provides a stable, controlled route for the pilus to exit the cell envelope.

Alignment subcomplex

The purpose of the alignment complex is to physically align the motor subcomplex with the secretin. This complex is composed of the proteins PilM, PilN, PilO, and PilP. PilN and PilO are inner membrane proteins that form a heterotrimer with the lipoprotein PilP (26, 43). Both PilN and PilO have similar organization: small, cytoplasmic N-termini, a single transmembrane helix, and periplasmic C-termini composed of a long coiled-coil and ferredoxin fold (38). PilP has a long, unstructured N-terminus that interacts with PilN and PilO, followed by a β-sandwich fold that interacts with the N-terminus of PilQ (26, 38). PilM is an actin-like cytoplasmic protein that binds to PilN (38), as well as ATP and the motor protein PilB (24). As a whole, this subcomplex provides a scaffold-like link between the secretin, the inner membrane, and the cytoplasmic motor subcomplex, while allowing the growing pilus to traverse the periplasmic space into the secretin.

Motor subcomplex

The motor subcomplex provides the energy for pilus extension and retraction. The enzymes involved are PilB, PilT, and in some cases PilU. Pilus extension and retraction can be regulated through the motor subcomplex by altering the activities of the enzymes. PilB, through hydrolyzing ATP to ADP, provides energy to extend the pilus, while PilT and PilU both function to retract the pilus (19, 34, 39).

Model of type IV pilus extension

The mechanism of TFP assembly is not well understood. It is known that an enzyme provides energy for the assembly of the filament through hydrolysis of ATP, but it is not known exactly how this energy is transferred across the cytoplasmic membrane. These assembly ATPases are hexameric, and fully soluble in the cytoplasm. The subunits of the ATPases have a distinct two-part structure, with N-terminal and C-terminal domains (NTD, CTD respectively) linked by a hinge-like region. It has been shown in crystal structures of related proteins (Type 2 secretion ATPase EpsE, *Vibrio cholerae*, VirB11 Type 4 secretion ATPase HP0525, *Helicobacter pylori*, retraction ATPase PilT, *Aquifex aeolicus*, and secretion ATPase GspE, *Archaeoglobus fulgidus* (19)) that these domains come together to bind ATP, and swing away from each other in the absence of ATP. This provides a means of energy generation, but still does not explain how this energy is transmitted across the membrane to the growing pilus. The integral membrane protein (IMP) associated with TFP may provide the means of energy transmission. A model of TFP assembly has been proposed by Lisa Craig (19). This model states that hydrolysis of ATP by the assembly ATPase causes the NTD of the ATPase to move away from the CTD. This movement forces the IMP upwards out of the membrane, which in turn lifts the base of the pilus out of the membrane. This, combined with docking of free pilin monomers to the base of the pilus by electrostatic interactions, allows for a cyclic mechanism whereby newly docked pilins are locked into the fiber, and new sites for binding of free pilin are opened (19).

Type IV Pili and Cyclic di-GMP

Cyclic di-GMP is a universal bacterial second messenger molecule. It is involved in regulating many processes within the cell, including type IV pili. It is produced from two molecules of GTP by a diguanylate cyclase enzyme and hydrolyzed by a phosphodiesterase, and there are several types of protein and ribonucleic acid receptors that bind cyclic di-GMP. It is thought that two type IV pilus accessory proteins, PilZ and FimX, serve as an adaptor protein and cyclic di-GMP receptor,

respectively. Cyclic di-GMP levels influence the extension and retraction of the pilus through these two proteins. In *Xanthomonas*, it appears that PilZ recruits FimX to the assembly ATPase PilB, possibly promoting pilus extension. Meanwhile, a homolog of PilZ recruits a complex containing a diguanylate cyclase and a phosphodiesterase as well as a periplasmic receptor protein, possibly promoting pilus retraction.

It was found (44) that the type IV pilus assembly ATPase MshE from *Vibrio cholerae* binds cyclic di-GMP. This binding required an extended N-terminal domain known as the Type 2 Secretion System N-Terminal Domain (T2SSE_N), which is found on the PilB2 assembly ATPase from *C. perfringens*. As *C. perfringens* does not have any homologs of PilZ or FimX, it is possible that this domain allows the function of the pilus to be tied to cyclic di-GMP concentrations.

Carbonic Anhydrase

As a side project, a strain of *C. perfringens* with an in-frame deletion mutation in the gene encoding carbonic anhydrase was constructed. Carbonic anhydrase enzymes catalyze the interconversion of carbonic acid to water and carbon dioxide:

Equation 1.1 Hydration of carbon dioxide by carbonic anhydrase.

$$H_2O + CO_2 \leftrightarrow HCO_3^- + H^+$$

They are found throughout the domains of life, and occur in three classes, α, β, and γ. All three classes catalyze the reaction through a coordinated zinc ion, but differ greatly in structure and binding of zinc. The carbonic anhydrase produced by *C. perfringens* is a β-class CA; the members of this class typically bind zinc ions through coordination with two conserved cysteine residues and a conserved histidine residue. This carbonic anhydrase is of interest, because the active site may contain an iron cofactor instead of zinc, and this would be the first described instance of a β-class CA containing a cofactor other than zinc (45). However, the γ-class carbonic anhydrase of *Methanosarcina thermophila* has been

shown to have a higher activity with an iron cofactor when purified anaerobically from *E. coli*. This iron cofactor is in the form of Fe^{2+}, and on exposure to oxygen is oxidized to Fe^{3+} with concurrent loss of activity in the enzyme (46).

In this work, I sought to examine the assembly of type IV pili using a two-fold approach. First, in Chapter 2, I attempted to provide data that would be useful in determining how much energy was required to incorporate a pilin from *Pseudomonas aeruginosa* into a pilus, using solid-state nuclear magnetic resonance. Secondly, in Chapter 3, I examined a proposed model of type IV pilus extension by attempting to reconstitute the core assembly apparatus of the *C. perfringens* type IV pilus *in vitro*. Additionally, I participated in a collaborative project (Chapter 4) examining the carbonic anhydrase Cpb of *C. perfringens*.

Chapter 2 Solid-State Nuclear Magnetic Resonance of *Pseudomonas aeruginosa* Strain K Pilin in an Artificial Membrane

Abstract

Type IV pili are filaments that can be extended away from the cell by rapid polymerization. This polymerization involves the transition of pilin monomers from one energetically favorable state to another. As this requires an input of energy, understanding of the initial and final energetic states of the pilins will reveal insights into possible mechanisms of type IV pilus assembly. Toward that end, a type IV pilin was purified from the Gram-negative opportunistic pathogen *Pseudomonas aeruginosa* and incorporated into an artificial membrane. The pilin was probed by a solid-state nuclear magnetic resonance (ssNMR) technique that can determine the angle and depth of insertion of a helical peptide. The pilin was also examined in a giant unilamellar vesicle (GUV) system in an effort to determine if the pilins self-assemble into a structured array. The ssNMR yielded only preliminary data that this technique can be used to address these questions. The GUV system did not yield any information regarding pilin-pilin interactions in the membrane, but the process of producing the GUVs may have opened an alternate method to probing the energetics of the pilin to pilus transition.

Introduction

Type IV pili are extracellular filaments that mediate a wide array of functions. All type IV pilus systems operate on the same basic principle of cyclic extension and retraction. The extension of a type IV pilus is accomplished by the incorporation of pilin (PilA) monomers into the base of the growing pilus from a pool on the exterior surface of the cell membrane. Retraction of the pilus is accomplished by removing pilins from the base of the pilus back into the cytoplasmic membrane. Both of these states, pilin-in-pilus and pilin-in-membrane, are stable. Transitioning from one state to the other, however, requires an input of energy, which is provided by the hydrolysis of ATP by an assembly or retraction ATPase. For assembly of a pilus, there is thought to be an upper limit of 3 ATP molecules hydrolyzed per pilin incorporated (47), as determined by molecular dynamics simulations involving the removal of *P. aeruginosa* strain K (PAK) pilin from a simulated membrane. This approach involves exposure of the long, hydrophobic alpha-helical tail directly to aqueous solvent. This is not thought to actually occur in the assembly of type IV pili, but gives a theoretical upper bound on the energy required to remove a pilin from the membrane into the pilus. The primary output of the molecular dynamics modeling gives information on the geometry of the pilin in the membrane, including angle of insertion and depth of insertion. The goal of this study was to determine these parameters experimentally, by measuring the NMR spectra of PAK pilin in an artificial, defined lipid membrane. By using these parameters in the molecular dynamics studies, the upper limit of the amount of energy required can be further refined. Solid-state nuclear magnetic resonance (ssNMR), more specifically PISEMA (polarization inversion, spin exchange at the magic angle) ssNMR, offers the opportunity to measure these parameters directly. This method exploits the ability to control the orientation of a membrane, and therefore any proteins embedded in it, by mechanical means. With each peptide bond plane aligned in a specific, unique orientation relative to the detector, the angle of the entire helix can be determined by fitting the signal to a theoretical helical wheel. From this starting point, a more refined energetic picture of type IV pilus assembly may be proposed by examining interactions with other type IV pilus proteins.

Methods

Purification of *P. aeruginosa* strain K pilin

PAK PilA is prepared by shearing whole, intact pili from the surface of *P. aeruginosa* cells. These cells have deletions in *pil*A and *pil*T (retraction ATPase), with a plasmid containing the wild-type PAK *pil*A gene under an IPTG inducible promoter, and a carbenicillin resistance gene. To produce the pili, the cells were first grown overnight as a lawn on one LB agar plate containing 150 μg/mL carbenicillin. The next day the cells were suspended in 4 mL phosphate buffered saline (1 x PBS), and this suspension was used to swab a lawn of cells onto 40-45 1 x M9 Salts/100 mM Glucose/30 μg/mL carbenicillin/1 mM IPTG agar plates, and grown overnight. When required for ssNMR studies, the M9 salt solution was prepared using $^{15}NH_4Cl$, with all other procedures and materials remaining the same. The following morning, the cells were suspended in 40 - 45 mL 150 mM NaCl. The pili were sheared from the surface of the cells by vigorous mixing with a vortex mixer for 75 seconds. The cells were then removed from the suspension by centrifugation at 25,000 x g for 15 minutes at 4°C. After centrifugation, the supernatant was transferred to a 50 mL conical tube, and 1/10 volume of 1 M $MgCl_2$ was added to precipitate the pili. This was incubated overnight at 4°C. The following morning, the pili were pelleted by centrifugation at 100,000 x g for 1 hour at 4°C. Following centrifugation, the supernatant was discarded, and the tube was rinsed with 250 μL 1 x PBS to collect the pili. Purity was evaluated by SDS-PAGE and concentration was evaluated using the bicinchoninic acid (BCA) assay (Pierce) with bovine serum albumin (BSA) as the standard. Purified pili were dissociated by incubation in 1.5% beta-octyl glucoside overnight at 4°C. This solution was then subjected to stirred-cell ultrafiltration through a regenerated cellulose membrane with a nominal molecular weight cut-off of 100 kDa. This membrane only allows monomeric PilA to pass through, retaining any intact pili. After filtration, the PilA/detergent solution was stored at -20°C until needed.

Incorporation of *P. aeruginosa* strain K pilin into an artificial membrane

A solution of 3 moles palmitoyloleoyl phosphatidylethanolamine (POPE) to 2 moles

palmitoyloleoyl phosphatidylglycerol (POPG) was prepared by mixing chloroform stock solutions of each phospholipid (Avanti Polar Lipids). An appropriate amount of this phospholipid solution (100 mol lipid to 1 mol protein) was dried on to the interior surface of a glass tube using a gentle stream of nitrogen to remove the bulk solvent, and vacuum to remove the remaining chloroform. The prepared PilA/detergent solution was added to the dried film, and shaken gently until the lipid film solubilized. This phospholipid/PilA/detergent solution was then diluted 1:10 in 100 mM Tris, pH 7. The vesicles were collected and washed by ultrafiltration into 100 mM Tris, pH 7, using a stirred-cell concentrator fitted with a 100 kDa nominal molecular weight cut-off membrane. This removes any free pilin from the vesicle suspension. The vesicle suspension was analyzed by SDS-PAGE and BCA protein assay, and submitted for ssNMR analysis.

Fluorescent and transmission electron microscopy of PilA in electroformed giant unilamellar vesicles

A sample of PAK PilA was labeled with Alexa Fluor 488 and incorporated into vesicles as described above. A small quantity of these proteoliposomes was dried onto the surface of two platinum wires, approximately 1 cm long, and separated by 5 mm. The coated wires were immersed in 5 mM HEPES pH 7.2, 200 mM sucrose, and an AC voltage (3 V, 10 Hz, square wave) was applied across the wires for 2 hours. A sample of the ‘unpurified’ giant unilamellar vesicles (GUVs) was reserved for microscopy, while the remainder was dropped through a solution of 5 mM HEPES pH 7.2, 200 mM glucose to remove any other material. Both the purified and unpurified GUV’s were imaged by fluorescent microscopy. A similar protocol was performed with unlabeled PilA for transmission electron microscopy (TEM), with phosphotungstic acid used as a negative stain.

Results

Purification and incorporation of PAK PilA into an artificial membrane

The entirety of the PISEMA experimental procedure requires purification and incorporation of the protein in question (PilA) into a membrane whose orientation can be controlled mechanically. As shown in Figure 2.1, the shearing and precipitating method was able to yield semi-purified PilA. The primary contaminant at approximately 40 kDa is possibly flagellin, but this was not confirmed. Incorporation of PilA into liposomes by the detergent dilution method further purified PilA to homogeneity.

^{31}P ssNMR of artificial membranes containing ^{15}N-PilA

In order for subsequent analyses with PISEMA to be relevant, the orientation of the artificial membranes, and thereby the orientation of PilA, had to be verified to be parallel with the detector. In order to ensure that this was the case, the sample was scanned using ^{31}P ssNMR, which can determine directly the angle of the phosphate group of phospholipids. As shown in Figure 2.2, the samples prepared for the PISEMA experiment were flat and oriented. With a change in angle relative to the detector, the anisotropic ^{31}P signal changes from a chemical shift of approximately 25 ppm, to approximately -10 ppm. This indicates that the membrane normal, n, is parallel to B_0 when the glass plates supporting the lipid layers is perpendicular to B_0. The large, invariable, double peak on the spectrum represents some unknown isotropic phosphorus present in the sample, possibly carried-over phosphate buffer from purification.

PISEMA of ^{15}N-PilA in artificial membranes

As shown in Figure 2.3, PISEMA is clearly possible on this sample system. Given the flat, aligned membranes as demonstrated by the ^{31}P ssNMR, it can be said that the PilA contained in the membrane is constrained. The red diamonds on Figure 2.3A indicates the spectrum one would obtain from an idealized alpha helix embedded in a membrane at an angle of 25 degrees. There is some agreement between the data obtained and the theoretical wheel, giving a hint that PilA is embedded at an angle other

than the ~9 degrees obtained by molecular dynamics (47). Unfortunately, the spectrum is not complete and shows a lot of anisotropic background near the abscissa. A second experiment was conducted with more protein to hopefully alleviate the problems with the first experiment. As shown in Figure 2.3B, the helical wheel does have more signal, but there is also a greater degree of anisotropic noise.

Electroformation of GUVs containing fluorescent PilA

In an effort to resolve the conflict between the PISEMA data and the molecular dynamics modelling, fluorescent microscopy of PilA in GUVs was performed. It was hoped that higher-order pilin associations would become apparent as 'patchy' localization of fluorescence on the surface of the GUVs. This was not observed. However, electroformation of PilA containing GUVs yielded an interesting result. Prior to purification by a density differential, the sample material exhibited long, thin fluorescent fibers (Figure 2.4A). Given that the only fluorescent molecule in the system was labeled PilA, these fibers are undoubtedly composed of PilA. Purification by dropping the vesicles through a less dense buffer system removed the fibers from the sample (Figure 2.4B).

Discussion

The rapid purification of uniformly ^{15}N-labeled *P. aeruginosa* strain K PilA for use in PISEMA experiments is described. By shearing whole pili from *P. aeruginosa* cells grown on a medium containing $^{15}NH_4Cl$ as the sole nitrogen source, large amounts of purified, labeled PilA were obtained. Incorporation of this labeled protein into a lipid membrane of defined composition was easily accomplished by the detergent dilution method, to yield a source of proteoliposomes that served as a feedstock for PISEMA experiments. Unfortunately, with such a large globular head that was not constrained in the system, there was a high level of anisotropic signal, which complicates analysis. On the whole, this approach of measuring the angle and depth of insertion of a type IV pilin monomer shows promise, but needs refinement. The advantage of using the PAK PilA protein is that molecular dynamic modelling has already been done of the crystal structure of the protein in an idealized membrane. This gives the advantage of having a starting point for the analyses of the NMR spectra. Additionally, the outcome of the PISEMA experiments can then be fed back in to the molecular dynamics model, allowing for validation and refinement.

Interestingly, the preliminary data presented here show a large discrepancy between the simulated data and the measured data. A more complete PISEMA spectrum would be necessary to resolve this conflict. If the preliminary data is correct, one possible source of this discrepancy is higher-order pilin-pilin associations in the membrane. In order to polymerize at ~1000 subunits per second, a pool of thousands of subunits of PilA must be available at the base of the growing pilus. If the pilin proteins interact with each other in the membrane, they would be readily available at the pilus base.

In order to resolve this, fluorescent microscopy was used to attempt to detect pilin-pilin interactions in a GUV system. Patchy fluorescence, which would have indicated clumping of pilin monomers in the membrane, was not seen but it appears as though the electroformation process may induce polymerization of pilins into a fibrous structure. It is not known whether these fibers have the same architecture as biologically produces pili, but they are extremely thin. Indeed, when viewed under

transmission electron microscopy (Figure 2.5), fibers can be observed that appear to match the width of a biologically polymerized type IV pilus (~8.6 nm). If these fibers are indeed architecturally identical to type IV pili, then it may be possible to directly probe the energetics of pilus assembly using a controlled electroformation set-up, where one can slowly increase the voltage applied across a pilin containing membrane and observe polymerization.

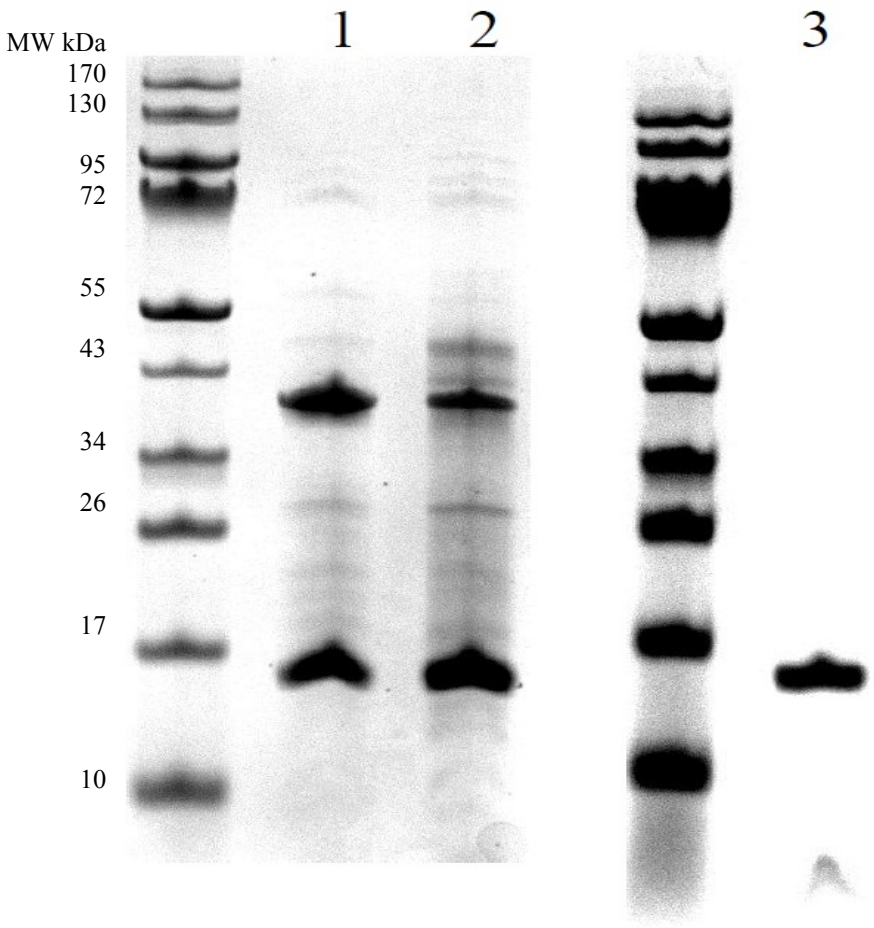

Figure 2.1 SDS-PAGE of purified PAK PilA and PilA incorporated into an artificial membrane

Lane 1: Unlabeled pili sheared from the surface of PAK cells scraped from 45 M9 plates
Lane 2: ^{15}N-labeled pili sheared from the surface of PAK cells scraped from 45 M9 plates
Lane 3: Unlabeled PAK PilA incorporated into POPE/POPG artificial membrane

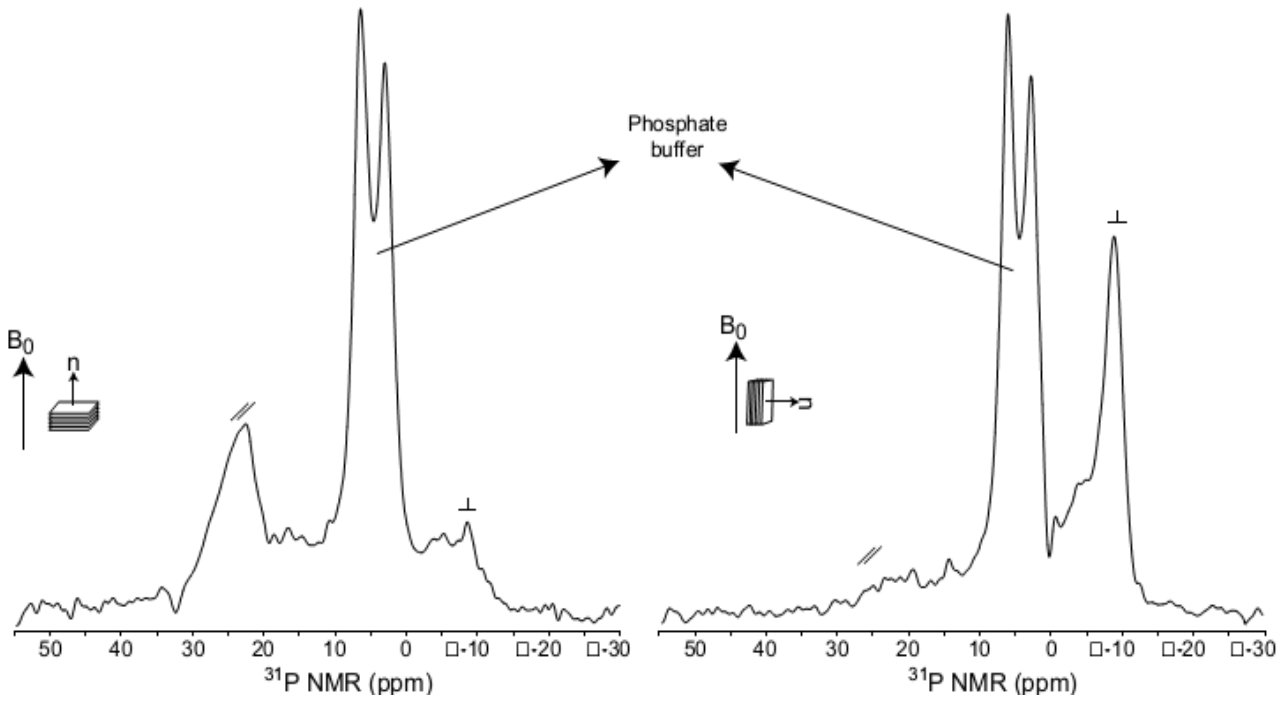

Figure 2.2 ^{31}P ssNMR of POPE/POPG membranes with PAK ^{15}N-PilA

The chemical shift of the ^{31}P signal is dependent on the angle of the phospholipid group to the NMR detector. The change of the chemical shift from ~25 ppm to ~-10ppm with tilting of the sample indicates that the vast majority of the lipids are flat and aligned properly on the glass plates.

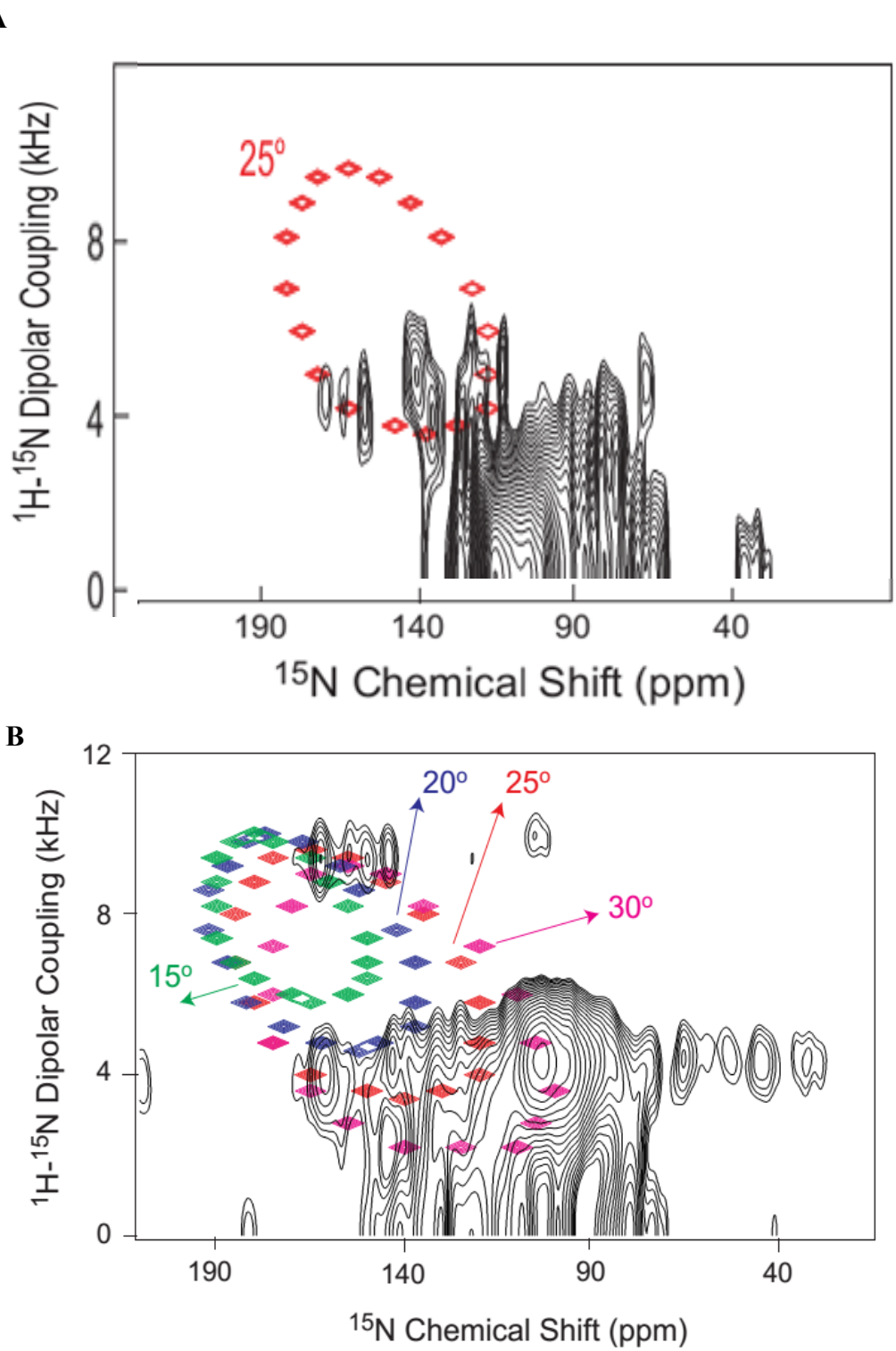

Figure 2.3 PISEMA of ^{15}N-PilA in POPE/POPG membranes

A) Experiment 1. PilA content of 5 mg. B) Experiment 2. PilA content of 20 mg. Colored diamonds indicate positions of spectral peaks from an idealized α-helix embedded in a membrane at the specified angle.

A

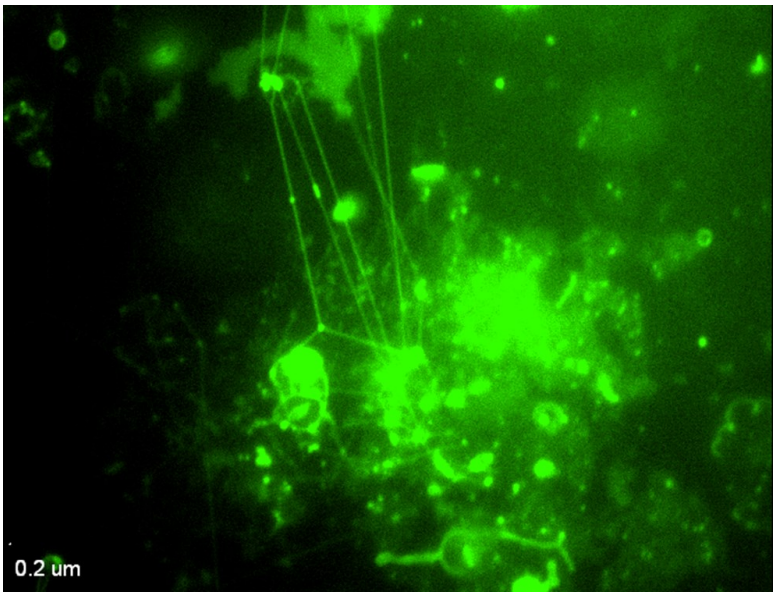

B

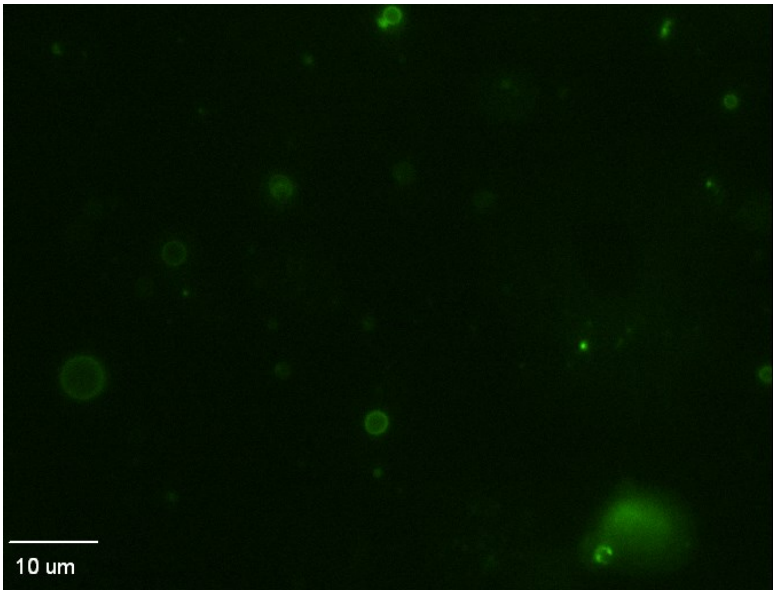

Figure 2.4 Fluorescent microscopy of PilA in electroformed GUVs

A) Pre density differential purification. **B)** Post density differential purification. GUVs were formed by drying a mixture of fluorescently labeled PilA and POPE/POPG lipids on a pair of wire electrodes, immersing the electrodes in sucrose containing buffer, and applying an alternating electric field. Density differential purification consisted of adding a small volume of GUVs to a tube containing glucose buffer, and collecting material that pooled at the bottom of the tube. This removed the fluorescent fibers from the GUV sample.

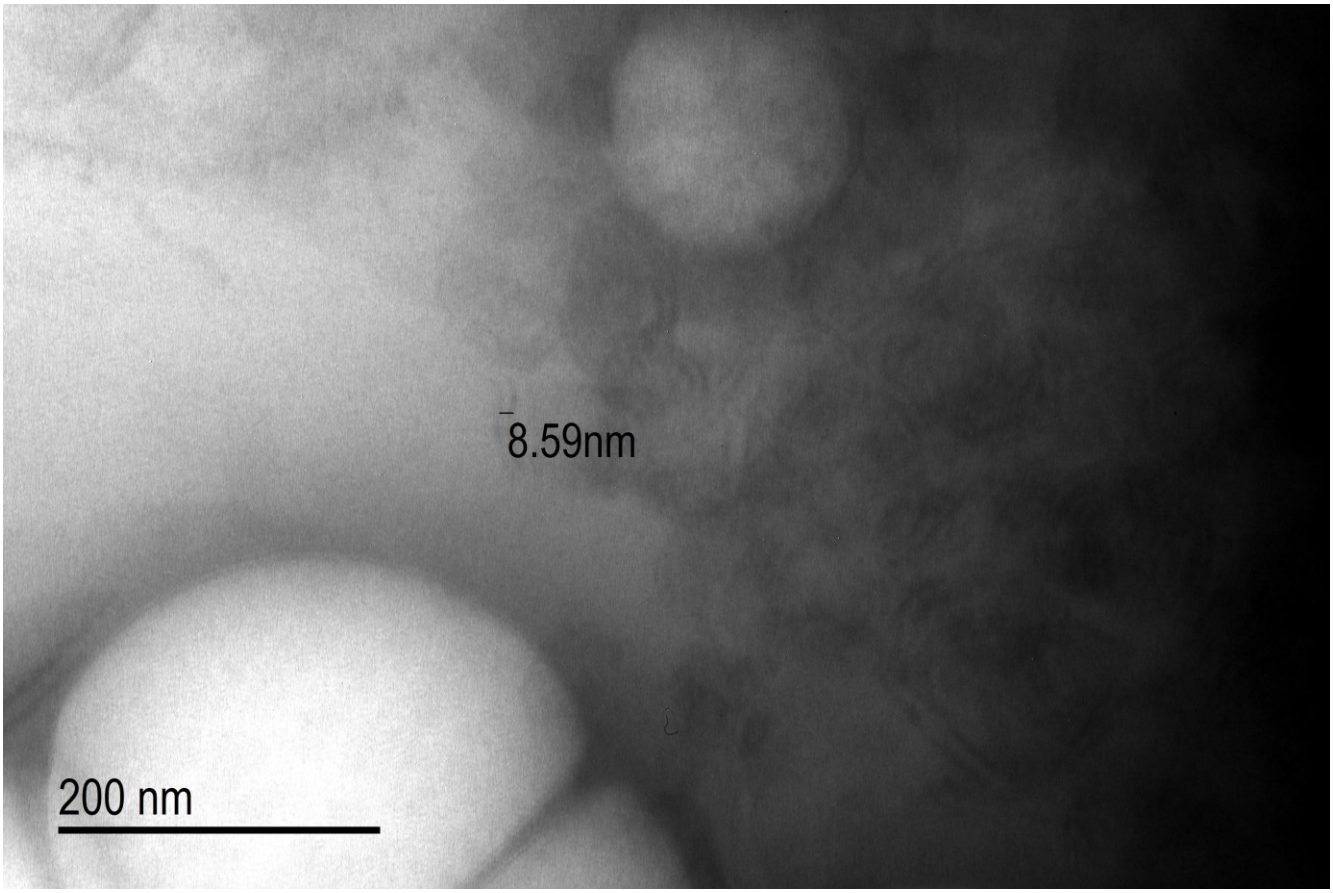

Figure 2.5 Transmission Electron Microscopy of unpurified electroformed PilA containing GUVs

TEM image of unpurified electroformed GUVs containing PilA, negatively stained using phosphotungstic acid. The structure labeled "8.59nm" is thought to be a fiber comprised of electroformed PilA.

Chapter 3 Characterization of the Type IV Pilus Proteins PilB2 and PilC2 of *C. perfringens*

Abstract

Type IV pili are extracellular filaments used by a broad range of bacteria. All type IV pilus systems involve the action of an assembly ATPase to provide energy to polymerize pilins in the membrane into a growing pilus. One proposed mechanism involves a large conformational shift in the assembly ATPase cyclically causing an integral membrane core protein (IMCP) to lift the base of the pilus away from the membrane a short distance. This simultaneously locks newly added pilins into the pilus, extends the pilus, and opens new sites for pilins to join the base of the pilus. This model would minimally require the assembly ATPase and the IMCP; the other type IV pilus proteins would play supportive roles in aiding the traversal of the cell envelope. In order to evaluate this model, the assembly ATPase PilB2 and IMCP PilC2 from the Gram-positive anaerobic pathogen *Clostridium perfringens* were purified and examined for interactions. The evidence presented here suggests that PilB2 and PilC2 do not interact directly, and thus cannot function as a core assembly apparatus. This does not invalidate the model, however, as other assembly ATPase/IMCP pairs have been demonstrated to interact.

Introduction

Type IV pili are extracellular filaments produced by bacteria that can mediate a large array of functions, including but not limited to, motility, cell-cell aggregation, DNA uptake, and adherence to surfaces (19). All of these functions rely on the type IV pilus' cyclic extension (polymerization) and retraction (depolymerization). Numerous proteins have been determined, in Gram-negative bacteria, to be involved in the biogenesis of a pilus: pilins (PilA), a prepilin peptidase (PilD), an inner membrane core protein (PilC), an assembly ATPase (PilB), a retraction ATPase (PilT), an actin-like cytoplasmic accessory protein (PilM), two similar inner membrane accessory proteins (PilN and PilO), a secretin (PilQ), and a pilotin that binds PilQ to the PilMNO complex (PilP). Many of these components mediate the pilus' traversal of the periplasm, cell wall, and outer membrane (PilMNOPQ). Many Gram-positive organisms, including the Clostridia, also possess type IV pili. The major difference between the Gram-positive and Gram-negative systems is that the Gram-positive organisms lack an outer membrane secretin, as there is no outer membrane to cross (39).

The Gram-positive anaerobic pathogen *Clostridium perfringens* possesses two type IV pilus-like systems (Figure 3.1), with two separate PilB/PilC protein pairs (PilB1/PilC1, PilB2/PilC2) and four different pilins (PilA1-A4). It does not possess flagella, but is capable of a growth dependent gliding motility (6, 18). Type IV pili do play some role in this motility, but it is not well understood. The pilin PilA2 has been shown to be present on the surface of *C. perfringens* (6), and when expressed in *Neisseria gonorrhoeae*, allows cells to adhere to mouse muscle cells instead of the genitourinary epithelium (37). As *pilA2* is immediately downstream of *pilB2* and *pilC2* on the *C. perfringens* chromosome, PilB2 and PilC2 are likely responsible for polymerizing PilA2 into a pilus.

Which proteins constitute the minimum necessary to polymerize pilins into a pilus? Without the need to cross the cell envelope, is it possible to reconstitute a functional 'core assembly apparatus' *in vitro*? It has been proposed as a model (Figure 3.2, (19)) that a PilB protein and a PilC protein would

constitute the minimum necessary for polymerizing pilin into a pilus, and thus comprise the core assembly apparatus. The assembly ATPase binds to the cytoplasmic face of the inner membrane core protein. The extracellular face of the inner membrane core protein is bound to the base of a growing pilus. In the base of the pilus, there is a 'docking site' that a pilin monomer may freely diffuse into. The pilin is held in place by an electrostatic interaction between the N-methyl-phenylalanine residue at position one of a pilin in the pilus and the side chain of the glutamate residue at position five of the incoming pilin (19). The assembly ATPase hydrolyzes ATP to ADP, undergoing a conformational shift. This, in turn, causes the inner membrane core protein to act as a piston, elevating the base of the pilus and locking the newly incorporated pilus in place. A new docking site opens in the base of the pilus, and the cycle repeats. In *Clostridium perfringens*, the assembly ATPase PilB2 and inner core membrane protein PilC2 are thought to be the type IV pilus core assembly apparatus. In other systems, including PilB and PilC from *C. perfringens* (which are thought to comprise part of a type II secretion system), this interaction has been demonstrated (48).

Type IV pili are often regulated by the universal second messenger molecule cyclic-di-GMP. This molecule is produced from two molecules of GTP by a diguanylate cyclase enzyme and hydrolyzed by a phosphodiesterase. It is thought that two type IV pilus accessory proteins, PilZ and FimX, serve as an adaptor protein and cyclic di-GMP receptor, respectively (34). *C. perfringens* lacks proteins with any significant homology to PilZ or FimX. Recently, MshE from *Vibrio cholerae* was demonstrated to directly bind cyclic-di-GMP (44). PilB2 shares an extended N-terminal domain with MshE, known as the Type 2 Secretion System N-Terminal Domain (T2SSE_N). This domain was demonstrated to be required for binding of cyclic-di-GMP to MshE (44).

This work was done with the initial purpose of characterizing the interaction between these two proteins, to serve as a starting point for investigating the concept of the core assembly apparatus as a functional unit. The results presented here indicate that PilB2 and PilC2, in contrast to other systems, do

not interact directly, and potentially represent a broader class of type IV pili that do not have interacting PilB/PilC pairs. The binding of c-di-GMP was not found to alter the binding of PilB2 to PilC2, or increase the ATPase activity of PilB2. Further study on other c-di-GMP binding PilBs and their cognate PilCs is required to determine if c-di-GMP binding and lack of PilB/PilC interaction are correlated. Given the ubiquity of type IV pilus systems, the similarity of the *C. perfringens* PilB2 and *V. cholerae* MshE T2SSE_N domain function, the lack of PilZ/FimX adaptor proteins, and the evolutionary distance between Clostridia and other bacteria (especially Gram-negative organisms), the Clostridial system can be considered a simple model system for studying type IV pilus function.

Methods

Bacterial Strains and Culture Conditions

All bacterial strains and plasmids used in this study are listed in Table 3.1. *Escherichia coli* was grown in Luria-Bertani (LB) medium with antibiotics added as necessary (100 μg/mL kanamycin, 20 μg/mL chloramphenicol, or 100 μg/mL ampicillin), 100 μg/mL X-gal for blue/white screening, and 1.5% agar for plates. *C. perfringens* was grown in a Coy anaerobic chamber in brain heart infusion (BHI) medium with 20 μg/mL chloramphenicol and/or 1.5% agar when necessary. TY medium (30 g/L tryptone, 20 g/L yeast extract, 1 g/L sodium thioglycollate), supplemented with 3% galactose and/or 1.5% agar as needed, was used for mutagenesis work in *C. perfringens*. *Pseudomonas aeruginosa* was grown in LB with 150 or 30 μg/mL carbenicillin, and 1.5% agar for plates as appropriate.

Purification of PilB2-HA-His_6

The gene encoding PilB2 was amplified from *C. perfringens* strain 13 chromosomal DNA using primers oWH32 and oWH34 (Table 3.1) and Phusion polymerase (New England Biolabs). Taq polymerase was used to generate 3'-A overhangs, and this product was ligated into pGEM-T Easy (Promega). The insert encoding PilB2-HA was excised by digestion with SalI and NheI and ligated into pET-24 (also digested with SalI and NheI) to yield pWH3, encoding PilB2-HA-His_6. BL21-CodonPlus(DE3)-RIL cells were transformed with pWH3 by electroporation, and grown at 37 °C in LB supplemented with 20 μg/mL chloramphenicol and 100 μg/mL kanamycin with shaking to an OD600 of 0.7. IPTG was then added to a final concentration of 1 mM, and the cells were grown overnight. Cells were harvested by centrifugation at 10,000 x g, and resuspended in 0.5 x Tris buffered saline (12.5 mM Tris pH 7.4 + 75 mM NaCl) containing one tablet of complete Mini protease inhibitor cocktail (Roche) and 40 mM imidazole, and lysed with a Model 500 Sonic Dismembrator (Fisher). The lysate was cleared by centrifugation at 20,000 x g, followed by filtration through a 0.22 μm syringe filter. The clarified lysate was applied to a 5 mL HisTrap FF column (GE Healthcare Life Sciences), and eluted with a linear

gradient of 0.5 x TBS + 1 M imidazole. Fractions containing PilB2-HA-His_6 (as evaluated by SDS-PAGE) were pooled and applied to a 5 mL Q-Sepharose anion exchange column (GE Healthcare Life Sciences), and eluted with a stepwise gradient of 0.5 x TBS + 1 M NaCl. The fractions containing PilB2-HA-His_6 were pooled, concentrated, and applied to a Superose 6 10/300 gel filtration column (GE Healthcare Life Sciences) equilibrated with 0.5 x TBS. Unless otherwise indicated, these and all subsequent chromatography procedures were performed using an ÄKTApurifier 10 FPLC system (GE Healthcare Life Sciences) at 4 °C. Fractions were evaluated for purity by SDS-PAGE, and those that contained >90 % PilB2-HA-His_6 were pooled, concentrated, and diafiltered using Amicon Ultra 2 mL centrifugal filters (Millipore, UFC210024, 100 kDa NMWCO) into 0.5 x TBS + 25 % glycerol, and stored at 4 °C. Protein concentration was determined with the Micro BCA Protein Assay kit (Thermo).

Purification of His_6-FLAG-PilC2

P. aeruginosa strain K cells, containing a pMMB-HisFlg-PilC2, encoding His_6-FLAG-PilC2, were grown overnight in 50 mL LB + 150 µg/mL carbenicillin at 37 °C with shaking in a baffled flask. The following morning, this culture was subcultured into 2 L fresh, prewarmed LB containing 30 µg/mL carbenicillin, and incubated at 37 °C (also with shaking in a baffled flask) until they reached an OD600 of ~1.0. IPTG was added to a final concentration of 200 µM, and the cells were grown overnight. The following morning, the cells were harvested by centrifugation at 25,000 x g. The cells were then suspended in 1 X TBS (25 mM Tris pH 7.4 + 150 mM NaCl) and lysed with a Model 500 Sonic Dismembrator. Urea and sarkosyl were added to a final concentration of 8 M and 2%, respectively, and the lysate was incubated overnight at 4 °C with gentle agitation (4). The following morning, the solubilized lysate was diluted with an equal volume of ultrapure water. Insoluble debris was removed by centrifugation at 40,000 x g and filtration through a 0.45 µm filter. The clarified, solubilized lysate was applied at a rate of 0.1 mL/min to a 5 mL HisTrap FF column equilibrated with 0.5 x TBS + 0.1% sarkosyl. The column was washed extensively with 0.5 x TBS + 0.1% sarkosyl, and this buffer was replaced to refold the protein with 0.5 x TBS + 0.1% beta-octyl glucoside (BOG) over the course of 10

hours. The refolded His_6-FLAG-PilC2 was then eluted with a linear gradient of 0.5 x TBS + 0.1 % BOG + 500 mM imidazole. Fractions were evaluated for purity by SDS-PAGE, and those that contained >90% His_6-FLAG-PilC2 were pooled, concentrated, and diafiltered using Amicon Ultra 2 mL centrifugal filters (Millipore, UFC201024, 10 kDa NMWCO) into 0.5 x TBS + 0.1% BOG + 25% glycerol, and stored at 4 °C. Protein concentration was determined with the Micro BCA Protein Assay kit (Thermo).

Inductively Coupled Plasma-Atomic Emission Spectroscopy (ICP-AES) of PilB2-HA-His_6

PilB2-HA-His_6 was suspended in 0.5 X TBS and analyzed by ICP-AES (analytes: S, Ni, Ca, Cd, Mn, Mg, Co, Cu, Zn, and Fe) with a Spectro ARCOS SOP (Spectro Analytical Instruments, Inc.).

Binding of TNP-ATP to PilB2-HA-His_6

Solutions of 0.5 μM of the fluorescent ATP analog TNP-ATP, with increasing amounts of PilB2-HA-His_6, were prepared in 0.5 x TBS, and placed in a black, flat bottomed 96 well plate. Fluorescence was measured using a TECAN infinite M200, using an excitation wavelength of 409 nm, and emission wavelength of 541 nm.

Kinetics and Specific Activity of PilB2-HA-His_6

Rate of ATP hydrolysis of PilB2-HA-His_6 was determined using a linked continuous assay. PilB2-HA-His_6 was added to a solution containing 25 mM HEPES pH 7.5, 10 mM DTT, 20 μg/mL BSA, 200 μM phosphoenol pyruvate, 300 μM NADH, 25 mM $MgCl_2$, and 2.5 μL of a pyruvate kinase/lactate dehydrogenase solution (Sigma, P0294-5ML). The reaction was initiated by the addition of ATP.

Equation 3.1 Continuous, linked assay for ATP hydrolysis.

A) $ATP \xleftrightarrow{PilB2-HA-His_6} ADP + PO_4^{3-}$

B) $ADP + PEP \xleftrightarrow{Pyruvate\ Kinase} ATP + Pyruvate$

C) $Pyruvate + NADH \xleftrightarrow{Lactate\ Dehydrogenase} Lactate + NAD^+$

Conversion of ATP to ADP by PilB2-HA-His_6 (Equation 3.1A) results in pyruvate kinase transferring the phosphoryl group from phosphoenol pyruvate to ADP, yielding ATP and pyruvate (Equation 3.1B). Lactate dehydrogenase converts pyruvate and NADH to lactate and NAD^+ (Equation 3.1C). Oxidation of NADH, as the signal of ATP hydrolysis, was monitored by reduction in absorbance at 340 nm. The data were plotted in Excel, and the rate of the reaction from t = 15 min to t = 30 min was determined by a line of best fit.

Analytical Gel Filtration Chromatography of PilB2-HA-His_6

A Superose 6 10/300 column was calibrated using thyroglobulin, pyruvate kinase, lactate dehydrogenase, and lysozyme as the molecular size standards. The approximate size of PilB2-HA-His_6 was determined by comparing the retention volume of purified protein (with and without 50 μM ATP) to the retention volumes of the standards.

Circular Dichroism Spectroscopy of His_6-FLAG-PilC2

A sample containing 1 μM His_6-FLAG-PilC2 in 0.5x TBS + 0.1% BOG was analyzed using a JASCO J815 spectrometer. Far UV spectra (190-260 nm) were recorded at 25°C in a 2 mm path length cuvette using 1 nm bandwidth, 1 nm data pitch, data integration time of 2 s, and a scanning speed of 100 nm/min. The spectra were recorded three times and averaged. The data were analyzed using the K2D3 server (5) accessible at http://k2d3.ogic.ca//index.html.

Antibody Production and Western Blotting

Rabbit antibodies were produced (GenScript) against synthetic peptides from PilB2 and PilC2. The peptide used for anti-PilB2 production was composed of 15 amino acid residues starting from position 155 of PilB2, and had a sequence of N-LTDKASDEESNELC-C. The peptide used for anti-PilC2 production was composed of 15 amino acid residues starting from position 9 of PilC2, and had a sequence of N-INSEGQRIEGSQSAC-C. Both antibodies were affinity purified against the antigen peptide. Western blotting was performed using an iBlot 2.0 transfer system (Life Technologies) and a

SNAP i.d. 2.0 blot development system (Millipore). Antibodies were diluted in 1 x Tris buffered saline with Tween 20 (TBS-T, Santa Cruz Biotechnology), and 0.5% gelatin (Sigma, G-8150) in 1 x TBS-T was used as a blocking agent. The secondary antibody used, unless otherwise noted, was goat anti-rabbit IgG:HRP (Thermo). Reactive bands were visualized by incubating with SuperSignal West Dura Extended Duration Substrate (Thermo) and imaging with a Typhoon TRIO Variable Mode Imager (GE).

Co-immuno Affinity Chromatography of PilB2-HA-His_6 and His_6-FLAG-PilC2

Rabbit anti-PilB2 antibodies were crosslinked to Protein A HP SpinTrap (GE Healthcare) columns according to the manufacturer's instructions. Samples of PilB2-HA-His_6, His_6-FLAG-PilC2, and a mixture of PilB2-HA- His_6 and His_6-FLAG-PilC2 were pre-incubated in 0.5x TBS + 0.1% BOG for 60 minutes at 37 °C, and separated with the prepared anti-PilB2 columns according to the manufacturer's instructions. The flow through, wash, and elution fractions from the columns were collected and analyzed by SDS-PAGE and western blotting with anti-PilB2 and anti-PilC2 antibodies.

Construction of WH2

A mutant strain of *C. perfringens* with an in-frame deletion in *pilC*2 was constructed according to the method of Nariya et al (1). To create the plasmid pWH5, the region upstream of the *pilC*2 gene, including the first three codons, was amplified from *C. perfringens* strain 13 chromosomal DNA with primers oWH17 and oWH18. The region downstream of the *pilC*2 gene, including the codons coding for amino acids 400, 401, and a stop codon, was amplified from *C. perfringens* strain 13 chromosomal DNA with primers oWH19 and oWH20. These two partially overlapping products were then used as the template, allowing for amplification of *pilC*2$\Delta_{4\text{-}399}$ with primers oWH17 and oWH20. Taq polymerase was used to give this product 3'-A overhangs to allow for ligation into pGEM-T Easy. The insert was then digested out of this plasmid with the enzymes BamHI and SalI, and ligated into pCM-GALK digested with the same enzymes to form pWH5. This plasmid was introduced into strain HN13 by electroporation. The first crossover event was selected for by the addition of chloramphenicol to the

growth medium. An overnight culture of HN13 + pWH5 was grown at 37 °C in BHI with 20 μg/mL chloramphenicol, and subcultured into TY + 3% galactose, and grown for 24 hours at room temperature. This culture was then serially diluted and plated onto TY + 3% galactose plates. Resultant colonies were patched on to TY + 3% galactose and BHI with 20 μg/mL chloramphenicol. Clones that underwent a second recombination event, and thus were sensitive to chloramphenicol, were screened by PCR to confirm deletion of *pilC*2.

in vivo imaging of YFP-PilB2 in *C. perfringens*

To create the plasmid pKRAH-YB2 (previously performed by Andrea Hartman, (48)), the *yfp* gene was amplified from the pSW4-YFP plasmid with the primers oAH14 and oAH40. The *pilB*2 gene was amplified from *C. perfringens* strain 13 chromosomal DNA with the primers oAH39 and oAH41. These two partially overlapping products were then used as the template, allowing for amplification of *yfp-pilB*2 with primers oAH14 and oAH40. Taq polymerase was used to give this product 3'-A overhangs to allow for ligation into pGEM-T Easy. The insert was then digested out of this plasmid with the enzymes SacII and SacI, and ligated into pKRAH1 digested with the same enzymes to form pKRAH-YB2. This plasmid was electroporated into *C. perfringens* strain HN13 and WH2. These strains were incubated at 37 °C overnight in liquid BHI with 20 μg/mL chloramphenicol. The following morning, the cultures were inoculated onto BHI agar with 20 μg/mL chloramphenicol + 0.5 mM lactose. The plates were incubated at 37 °C for 2 hours, and the cells were scraped from the surface of the plate into 1 x phosphate buffered saline (PBS, 25 mM sodium phosphate, 150 mM NaCl). The cell suspensions were placed onto polylysine coated slides (Thermo) and allowed to stand for 10 minutes before a coverslip was added. The cells were then imaged on an Olympus IX71 using DIC and YFP filters. The position of YFP-PilB2 was analyzed using the MicrobeTracker suite for MATLAB and the spotFinderZ function.

in vitro imaging of Fluorescently Labeled PilB2-HA-His_6 and His_6-FLAG-PilC2 in POPE/POPG liposomes

PilB2-HA-His_6 and His_6-FLAG-PilC2 were labeled with Alexa Fluor 488 and 594, respectively,

using the Molecular Probes labeling kits (Invitrogen). The His_6-FLAG-PilC2 was diluted in 0.5x TBS + 2% BOG. This protein/detergent solution was used to solubilize a lipid film of 3:2 molar ratio POPE:POPG. A sufficient amount of lipid was used to give a 1:10,000 molar ratio of His_6-FLAG-PilC2 to lipid. Liposomes were formed by dilution to less than 0.25% BOG, and collected by ultracentrifugation. His_6-FLAG-PilC2 liposomes, with and without PilB2-HA-His_6, were imaged on an Olympus IX71 using DIC, mCherry, and GFP filters.

Results

PilB2 localization is not changed in a *pilC2* deletion strain

Previous work by Andrea Hartman (48) showed that an insertion mutant of *pilC* resulted in a loss of localization of YFP-PilB, suggesting an interaction between PilC and PilB. In order to determine if this applied to PilB2 and PilC2, a strain with an in-frame, markerless deletion in *pilC2* (strain WH2) was constructed. Plasmid pAH10, containing a lactose-inducible *yfp-pilB2* gene fusion was introduced into strains HN13 and WH2, and the localization patterns of YFP-PilB2 fusion protein were determined. As shown in Figure 3.3, YFP-PilB2 continues to localize in a similar manner in strain WH2, as compared to the wild-type HN13. This suggests that PilB2 and PilC2 do not interact directly.

PilB2 binds zinc and forms a hexameric complex in the absence of ATP

PilB2-HA-His_6 was purified from *E. coli* to homogeneity through Ni-IMAC, anion exchange, and gel filtration chromatography (Figure 3.4A). An approximate molecular weight of 440 kDa was determined for PilB2-HA-His_6 by analytical gel filtration (Figure 3.4). This is indicates that PilB2-HA-His_6 is in a hexameric state, since this is 6.6 times the molecular weight of the monomer (67 kDa), and other assembly and retraction ATPases have been reported to be hexameric. When 50 μM ATP was added, the retention volume of PilB2-HA-His_6 was not affected.

Purified, concentrated PilB2 exhibited a faint pink color. In order to determine if the color was caused by bound metals, ICP-AES was conducted to measure the following elements: S, Ni, Ca, Cd, Mn, Mg, Co, Cu, Zn, and Fe (Table 3.2). As one PilB2 monomer contains 18 sulfur containing amino acid residues, ion counts were normalized to moles sulfur per moles analyte. Considering there is one mole of zinc per 22 moles sulfur, each hexamer contains 4.98 moles of zinc, suggesting 1 zinc ion bound per monomer. PilB2 contains a tetracysteine motif that has been shown in other similar proteins to coordinate zinc. This has been shown to contribute to protein stability and promote hexamer formation, but is not required for ATPase activity (49).

Binding and hydrolysis of ATP by PilB2-HA-His$_6$

The fluorescent ATP analog, trinitrophenyl-ATP (TNP-ATP) was used to investigate ATP binding by PilB2-HA-His$_6$. It was found to bind in a non-cooperative fashion with a K_d of 18.7 ± 0.45 μM (Figure 3.5C). Because this compound is an analog of ATP, this should only be taken as an indication that PilB2-HA-His$_6$ binds ATP, and not as a reliable indicator of the kinetics of ATP binding. The use of a continuous, linked assay that coupled the hydrolysis of ATP to the oxidation of NADH to NAD^+ allowed for the determination of a specific activity of PilB2-HA-His$_6$ of 9.9 nmol/min/mg (Figure 3.5B), which is comparable to other assembly ATPases characterized thus far (24, 44). PilB2-HA-His$_6$ showed Michaelis-Menten kinetics with a K_m of 53.2 ± 14.5 μM and a V_{max} of 0.27 ± 0.03 μM/min (Figure 3.5A).

Binding of cyclic-di-GMP by PilB2-HA-His$_6$

The T2SSE_N domain has recently been shown in assembly ATPases from Gram-negative organisms to bind the second messenger cyclic-di-GMP and regulate polymerization of the pilus (44, 50). As PilB2 has this T2SSE_N domain, as well as several of the conserved motifs that are required for cyclic-di-GMP binding, the binding of cyclic-di-GMP to PilB2-HA-His$_6$ was investigated (Figure 3.6) using the Differential Radial Capillary Action of Ligand Assay (DRaCALA) technique (51). Binding of cyclic-di-GMP to PilB2-HA-His$_6$ was observed to be cooperative, and analysis using a one-binding-site model gave a K_d of 1.34 ± 0.10 μM (Figure 3.6A). This binding was shown to be specific by adding unlabeled nucleotide competitors to the reaction, with only unlabeled cyclic-di-GMP inhibiting binding (Figure 3.6B). As this method can also be used to investigate kinetics of ATP binding directly without the use of an analogous molecule or competition assays, the binding of ATP to PilB2-HA-His$_6$ was also investigated. This binding was also determined to be specific (Figure 3.6D), and a dramatically different K_d (2.74 ± 0.26 μM) was found (Figure 3.6C) as compared to the TNP-ATP assay (18.67 ± 0.45 μM). This further reinforces the need to keep the limitations of TNP-ATP data in mind. As TNP-ATP is an *analog* of ATP, it can be reasonably assumed that the K_d should be different between the two molecules, and as there is a large additional group on the ATP molecule, it is not unreasonable to assume that the

K_d for TNP-ATP would be higher than that of ATP. Interestingly, the addition of cyclic-di-GMP to ATPase assay mixtures did not have any discernable effect on the activity of PilB2-HA-His_6 (Figure 3.6E).

Purification of His-FLAG-PilC2 from *P. aeruginosa*

Initially, attempts were made to purify PilC2 from the membrane fraction of *E. coli* but induction of the *pilC2* gene on a pET-24 or pET-28 vector caused the culture to stop growing almost immediately. A variety of different growth conditions were tried, but ultimately it was decided to express the protein in *P. aeruginosa*. On induction of the *pilC2* gene, *P. aeruginosa* continued to grow, and the presence of PilC2 was demonstrated by western blotting. The protein that was produced was in an insoluble form, not in the cytoplasm or the membrane fraction. As a result, whole *P. aeruginosa* lysates were denatured using urea and Sarkosyl, and refolded on a Ni-IMAC column by exchange with urea free, Sarkosyl buffer, and finally a slow, linear exchange of Sarkosyl buffer with buffer containing β-octyl glucoside. Protein eluted by an imidazole gradient showed a single band that was reactive to anti-PilC2 by western blotting (Figure 3.7A and B). Circular dichroism spectroscopy was performed on the resulting His_6-FLAG-PilC2 to evaluate refolding (Figure 3.7C). The secondary structure content (70% alpha helix, 3.9% beta sheet) that was calculated from the CD spectrum closely match the predicted values (74% alpha helix, 4.7% beta sheet) for PilC2 made by the JPred4 server (http://www.compbio.dundee.ac.uk/jpred) (52), indicating that His_6-FLAG-PilC2 likely adopted its native secondary structure through the refolding process.

Purified PilB2 and PilC2 do not bind and the ATPase activity of PilB2 is unaffected by the presence of PilC2

Direct binding of PilB2 and PilC2 was evaluated using a Protein A sepharose column loaded with anti-PilB2 antibodies. Mixtures of PilB2-HA-His_6 and/or His_6-FLAG-PilC2 were pre-incubated prior to loading onto the anti-PilB2 column. Flow through and elution fractions were evaluated by non-reducing SDS-PAGE (Figure 3.8A). Whole IgG (150 kDa) was present in each elution fraction. When loaded

alone (Figure 3.8A Column A), PilB2-HA-His_6 was visible in the elution fraction (Figure 3.8A lane 2) but not the flow through (Figure 3.8A lane 1). When His_6-FLAG-PilC2 was loaded alone, (Figure 3.8A Column B), the protein was visible in the flow through fraction (Figure 3.8A lane 3) and not in the elution fraction (Figure 3.8A lane 4). When PilB2-HA-His_6 was pre-incubated with His_6-FLAG-PilC2 and loaded onto the column (Figure 3.8A Column C), the elution profiles of each protein were unaffected. His_6-FLAG-PilC2 remained in the flow through fraction (Figure 3.8A lane 5) while only PilB2-HA-His_6 was present in the elution fraction (Figure 3.8A lane 6). The addition of cyclic-di-GMP (100 μM, not shown) did not alter the elution profile of either protein. Adding His_6-FLAG-PilC2 to ATPase reaction mixtures with PilB2-HA-His_6 showed no discernable effect on the rate of ATP hydrolysis by PilB2-HA-His_6 (Figure 3.8B).

Reconstitution of His_6-FLAG-PilC2 into unilamellar vesicles does not cause co-localization with PilB2-HA-His_6

In order to investigate whether PilB2/PilC2 binding requires a membrane environment, PilB2-HA-His_6 was labeled with Alexa Fluor 488 and His-FLAG-PilC2 was labeled with Alex Fluor 594. The fluorescently labeled His_6-FLAG-PilC2 was reconstituted into unilamellar proteoliposomes with a mixture of POPE/POPG that resembles the lipid mixture of bacterial cytoplasmic membranes. An excess of PilB2-HA-His_6 was added to these proteoliposomes, and the vesicles were imaged on a fluorescent microscope. Figure 3.9 shows a typical vesicle. Figure 3.9A shows the phase contrast image of the vesicle, Figure 3.9B demonstrates the localization of His_6-FLAG-PilC2 and Figure 3.9C shows PilB2-HA-His_6. Figure 3.9D shows the merged image of the PilB2 and PilC2 signals, and shows that most of the PilB2 signal does not co-localize with the PilC2 signal.

Discussion

The assembly ATPase and IMCP, PilB2 and PilC2, from *C. perfringens* were purified and analyzed, and represent the first Gram-positive members of these protein classes that have been biochemically characterized to date. Originally, the goal was to purify these two proteins and use them

to assess the viability of the core assembly apparatus as a valid theory. This would have involved the purification of a pilin protein and incorporating the IMCP and the pilin into unilamellar vesicles, plus the assembly ATPase and probe for pilus polymerization. This system was chosen for its relative genetic simplicity, as the only known accessory proteins in the genome of *C. perfringens* are PilM, PilN, and PilO. However, from the data presented here it appears that the PilB2/PilC2 system from *C. perfringens* do not interact directly, in contrast to most other type IV pilus/type II secretion systems described thus far (34). This provides a glimpse into possible biological and mechanistic differences in type IV pilus/type II secretion systems. It appears that there are two distinct classes of type IV pilus/type II secretion systems that can be differentiated based on direct vs. indirect PilB/C interactions. The presence of this split casts doubt on the viability of the 'core assembly apparatus' as a universal model for assembly of pili; however, it may still be of use in describing the assembly mechanism of the PilB/C pairs that do directly interact.

The question then becomes: what are the determinants of this grouping? PilB2/PilC2 do not directly interact, while PilB/PilC from *C. perfringens* do interact directly (48). There are Gram-negative representatives of both classes as well: PilB/PilC from *P. aeruginosa* interact directly (53), while PilF and PilG (PilB/PilC homolog pair) from *Neisseria meningitidis* do not interact directly (54). The fact that this division has been maintained across such evolutionary distance, and that both types can be present in one organism, suggests different functions and/or modes of regulation. Currently, prediction of whether a given PilB/PilC pair falls into the direct or indirect group cannot be made until more PilB/PilC pairs are studied. There are currently 4 distinct characteristics of PilB-like proteins that may influence the interaction between the PilB/PilC pairs: Length of N-terminal domain, oligomeric state in the absence of ATP, binding of zinc, and binding of cyclic-di-GMP. These characteristics are not totally independent however. The binding of cyclic-di-GMP, for example, would appear to require an extended N-terminal domain, although the presence of the T2SSE_N domain is not a guarantee that the protein will bind

cyclic-di-GMP (44). Likewise, oligomerization of the PilB-like proteins in the absence of ATP may be correlated to zinc binding (49).

Table 3.1 Strains, plasmids and primers used in this study

Strains		
Name	**Relevant characteristics or sequence**	**Source**
E. coli		
DH10B	F- *mcrA*Δ *mrr-hsdRMS mcrBC* ϕ80d*lacZ*ΔM15 *lacX74 deoR recA1 araD139*Δ *ara, leu7697 galU galK*Δ*rpsL endA1 nupG*	
BL21-CodonPlus(DE3)-RIL	*E. coli* B F– ompT hsdS(rB – mB –) dcm+ Tetr gal λ(DE3) endA Hte [argU ileY leuW Cam^R]	
C. perfringens		
HN13	*galKT* deletion strain of parent, strain 13, used for constructing in-frame deletions	(55)
WH2	In-frame deletion of the *pilC2* gene in strain HN13	This study
Plasmids		
pGEM-T Easy	PCR cloning vector	Promega
pET-24a	Protein expression vector	Novagen
pKRAH1	Lactose-inducible expression vector	(56)
pCM-GALK	Contains a *C. beijerinckii galK* gene under control of a ferredoxin promoter from *C. perfringens*	(55)
pAH9	pGEM-T Easy with *yfp-pilB2*	This study
pAH10	*yfp-pilB2* in pKRAH1	This study
pWH3	PilB2-HA-His_6 construct in pET24a	This study
pWH5	Vector, based on pCM-GALK, for making a *pilC2* in-frame deletion	This study
pMMB-HisFlg-PilC2	Vector for expressing a gene encoding His_6-FLAG-PilC2 in *P. aeruginosa*	This study

Primers	
Name	Sequence (5' to 3')
OAH14	CCGCGGTAAATAACAAAAAGGAGAACGCATAATGTCAAAAGGAG
OAH39	CACACGGAATGGATGAATTATATAAGTTGATTAGTTATCA GAAAAAGCGTTTAGGAG
OAH40	CTAAACGCTTTTTCTGATAACTAATCAACTTATATAATTC ATCCATTCCGTGTGTAATTCC
OAH41	CTTTCGAGCTCTTACATATCATAAGTTATATTTAAC
OWH17	GGATCCCCTATGATAACAGGAGAAAAGATAG
OWH18	CTTTTAATTCTTATTAATTATGCTTTTAACCTATATTTGCCATAATTCCTCTCC
OWH19	GGAGAGGAATTATGGCAAATATAGGTTAAAAGCATAATTAATAAGAATTAAAAG
OWH20	GTCGACTCTCACTTCCAATATCAATAGAAATAG
OWH32	GCTAGCATGATTAGTTATCAGAAAAAGCGTTTAGGAGATATACTAATTG
OWH34	GTCGACAGCGTAATCTGGAACATCGTATGGGTACATATCATAAGTTATATTTAACATTTCTTCA ACTGTGGTATTCCCC
5'-1 HisFlgPilC2	CGATTACAAAGACGATGACGATAAACTGCTGGTTGCAAATTTTAAATATAAAGCTAT
5'-2 HisFlgPilC2	GAGGAGGATATTCATGATGGTTCATCACCATCACCATCACGATTACAAAGACGATG
3'PilC2	AGAAAGCTGGGTTTCAACCTATACTGTTATACATTTTA

Table 3.2 ICP-AES of PilB2-HA-His_6 in 0.5 x TBS

Analyte	Wavelength (nm)	Detection Limit	Blank, ug/mL	Sample, ug/mL	Ions, g/L	Ions, mol/L	Mole S/ Mole Ion	Ions/Hexamer
S	182.034	0.002	0.044	0.178	1.34E-04	4.18E-06	1	108
Ca	317.933	0.003	0.019	0.023	4.30E-06	1.07E-07	38.985	2.77
Fe	259.941	0.0003	0.001	0.004	2.80E-06	5.01E-08	83.424	1.295
Ni	231.604	0.001	<0.0008	0.002	7.00E-07	1.19E-08	350.717	0.308
Zn	213.856	0	0.002	0.015	1.26E-05	1.93E-07	21.704	4.976
Cd	214.438	0.0004	<0.0004	<0.0004	---	---	---	---
Co	228.616	0.0009	<0.0009	<0.0009	---	---	---	---
Cu	324.754	0.003	<0.003	<0.003	---	---	---	---
Mg	279.079	0.013	<0.013	<0.013	---	---	---	---
Mn	257.611	0.0002	<0.0002	<0.0002	---	---	---	---

Figure 3.1 Genetic structure of type IV pili genes in *C. perfringens*

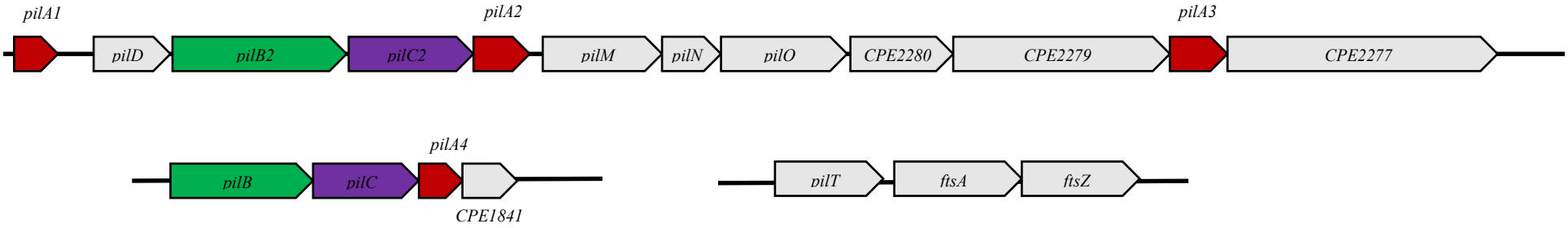

Type IV pilus associated genes in *C. perfringens*. Assembly ATPases are green, integral membrane core proteins are purple, pilins are red. Two PilB/PilC pairs can be seen (*pilB/pilC* and *pilB2/pilC2*). The genetic arrangement of the B/C pairs suggests that PilB and PilC work together, while PilB2 and PilC2 work together.

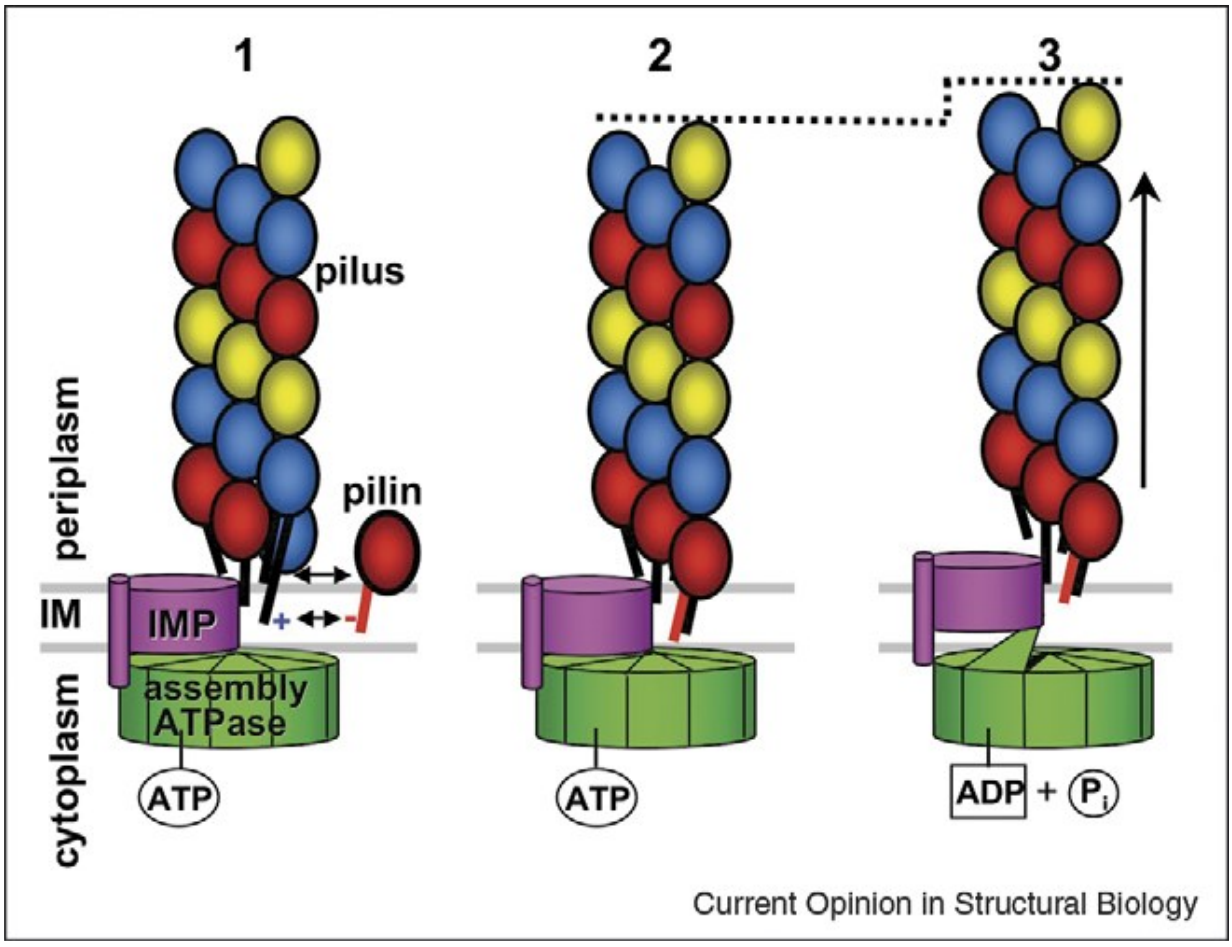

Figure 3.2 Proposed core assembly apparatus and mechanism for Type IV Pili

1) Pilin subunits diffuse along inner membrane, and approach TFP assembly apparatus. A negative charge (Glu5) on the free pilin is attracted to the positively charge N-terminus of a pilin in the base of the filament.
2) Attractive forces between the free pilin and the base of the filament cause the free pilin to bind to the filament base.
3) ATP is hydrolyzed by the assembly ATPase, inducing a large conformational shift. This shift is transmitted by the integral membrane protein to the base of the filament. This transmitted motion causes the pilus filament to rise slightly out of the membrane, both locking the newly incorporated pilin into the filament, and opening a new potential binding site for free pilins (19).
Reproduced with permission.

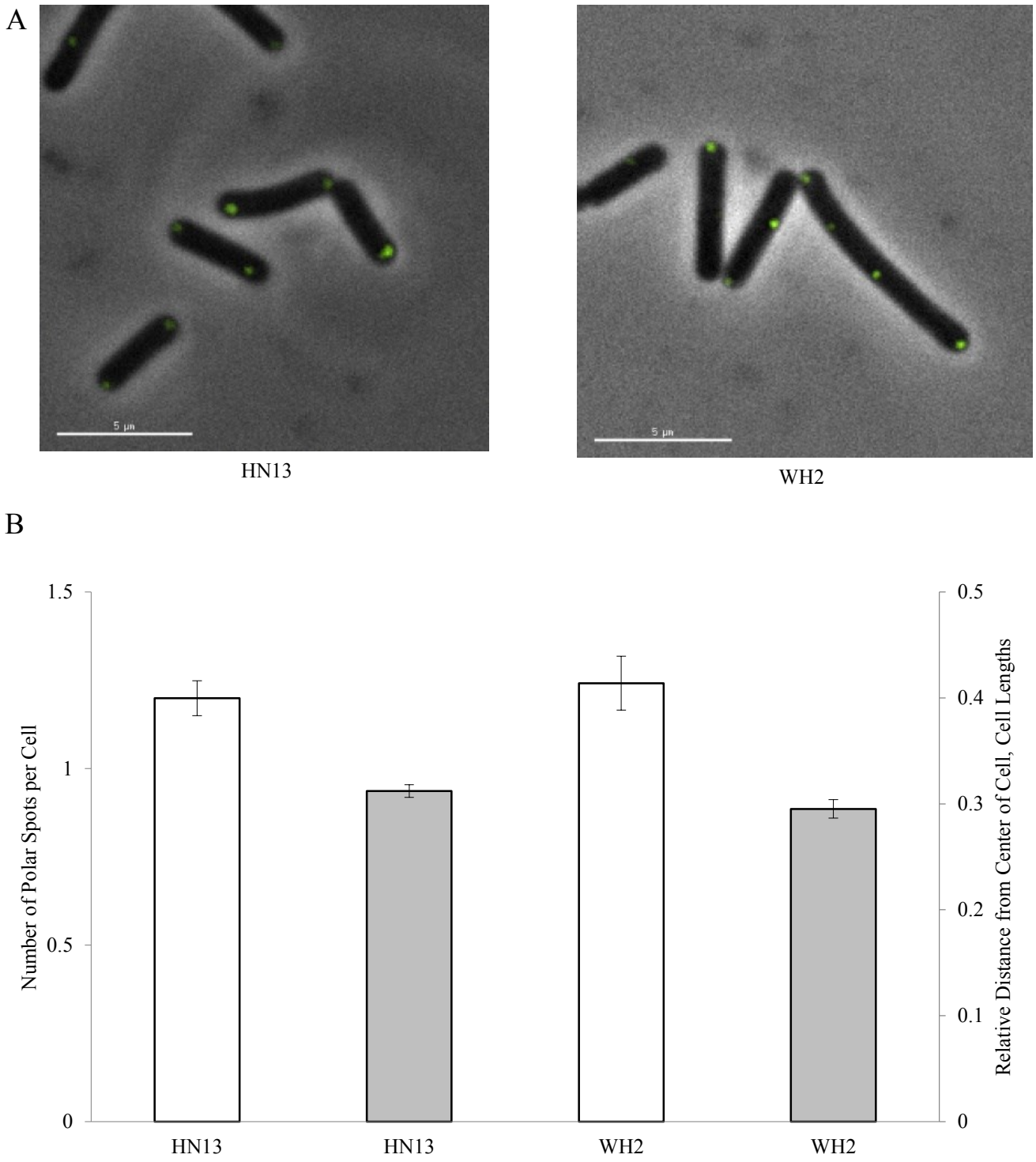

Figure 3.3 YFP-PilB2 localization does not change in the absence of PilC2

A) *in vivo* imaging of PilB2-YFP. Phase-contrast and fluorescent imaging of PilB2-YFP in strain HN13 (wild type), and WH2 (pilC2 mutant). PilB2-YFP appears as green spots in the cells. **B)** The number of polar spots per cell (white bars, n = 286 cells and n = 120 cells for HN13 and WH2, respectively) and relative distance from the center of cells (gray bars, n = 612 spots and n = 307 spots for HN13 and WH2, respectively).

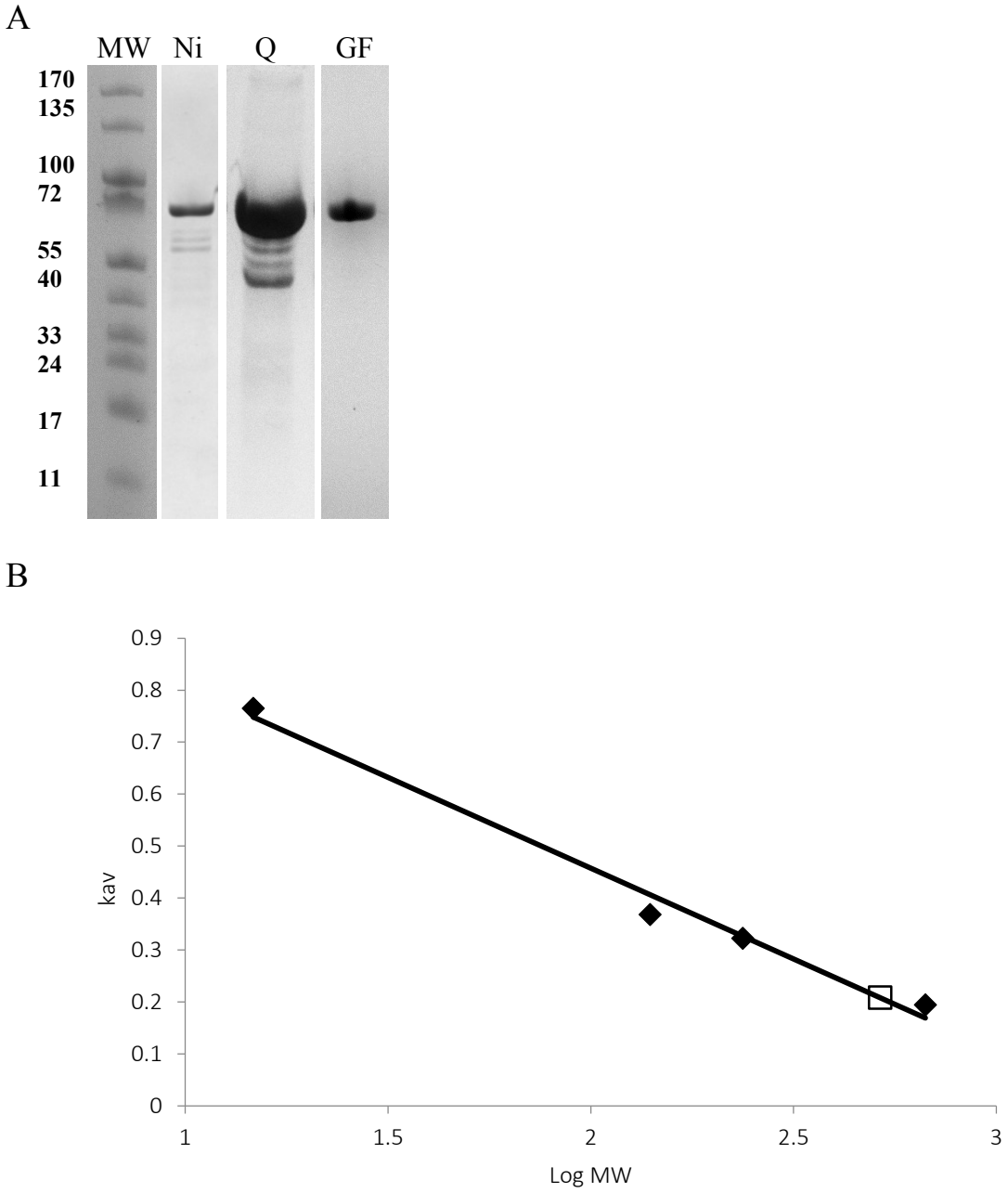

Figure 3.4 Purified PilB2-HA-His_6 is hexameric

A) Purification of PilB2-HA-His_6. MW, Molecular weight markers. Ni, elution fraction from nickel-charged immobilized metal affinity chromatography column. Q, elution fraction from Q-sepharose anion-exchange column. GF, elution fraction from Superose 6 column. **B)** Gel filtration was performed using a Superose 6 10/300 column, equilibrated with 0.5x Tris Buffered Saline. The calibration sample contained thyroglobulin (669 kDa), pyruvate kinase (237 kDa), lactate dehydrogenase (140 kDa), and lysozyme (14.7 kDa) (shown as black diamonds in the graph). PilB2-HA-His_6 size estimation was 440 kDa (white square). Representative analytical chromatography result, repeated in duplicate.

A

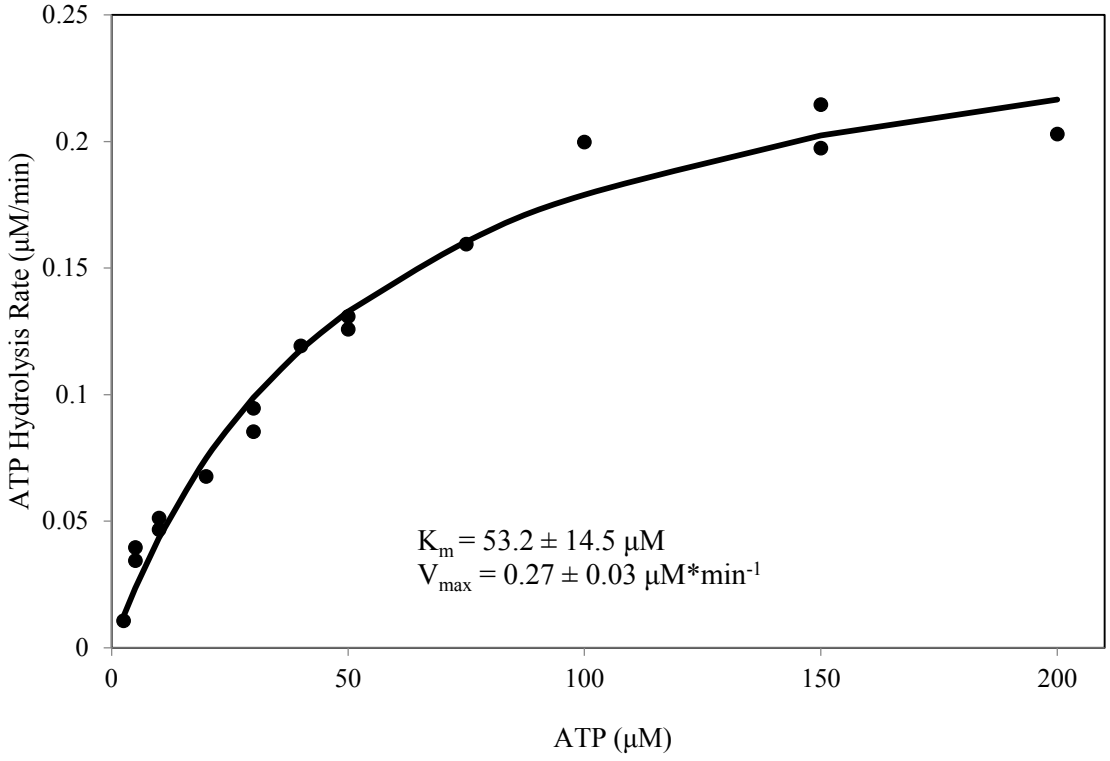
0.25
0.2
0.15
0.1
0.05
0
ATP Hydrolysis Rate (µM/min)
K_m = 53.2 ± 14.5 µM
V_{max} = 0.27 ± 0.03 µM*min^{-1}
0
50
100
150
200
ATP (µM)

B

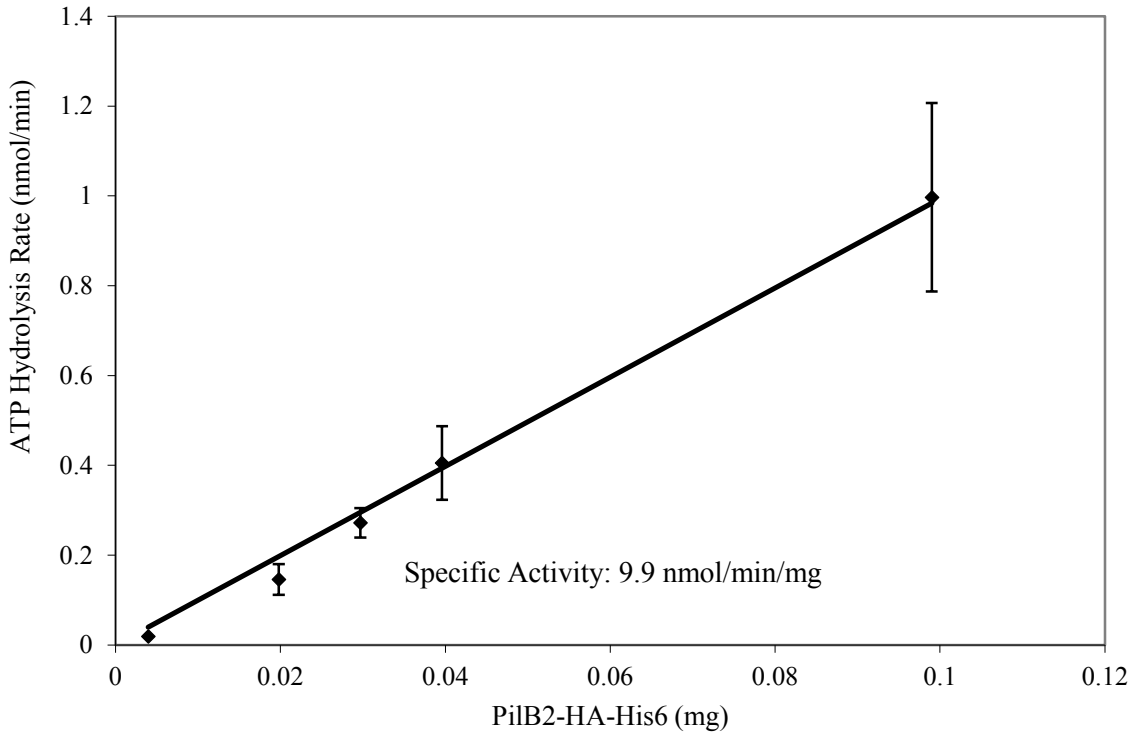
1.4
1.2
1
0.8
0.6
0.4
0.2
0
ATP Hydrolysis Rate (nmol/min)
Specific Activity: 9.9 nmol/min/mg
0
0.02
0.04
0.06
0.08
0.1
0.12
PilB2-HA-His6 (mg)

C

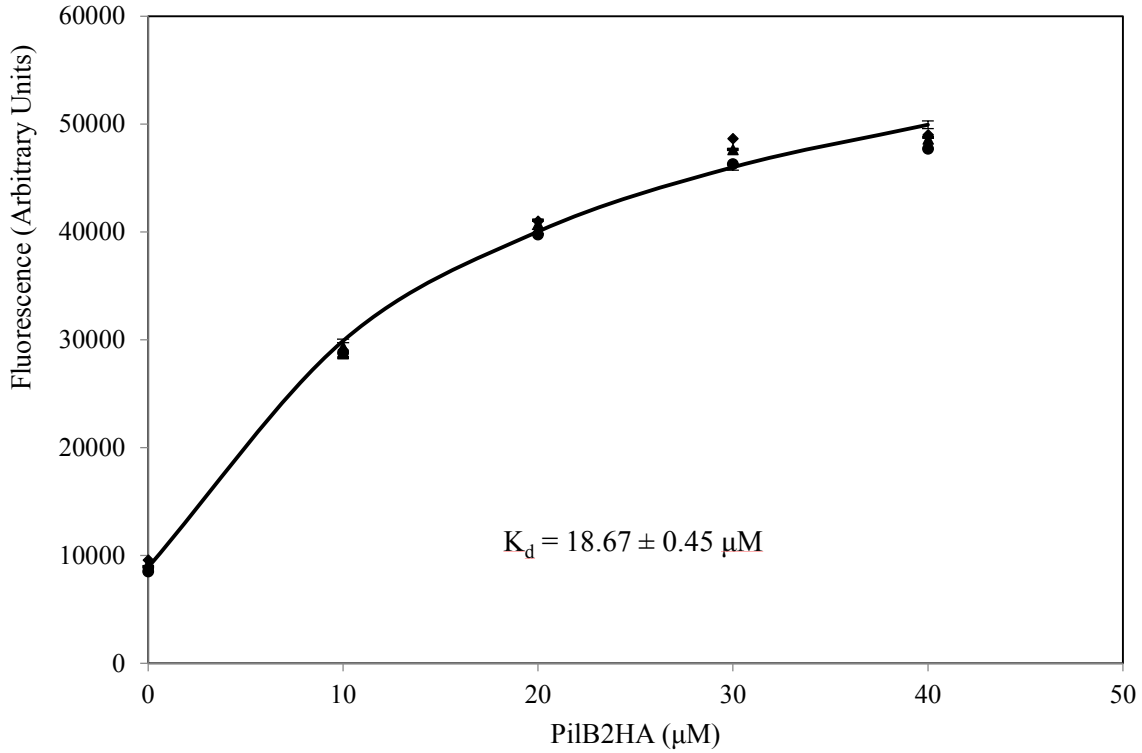

Figure 3.5 PilB2-HA-His_6 hydrolyzes ATP and binds the ATP analog TNP-ATP

(A) Using the disappearance of NADH as a marker for ATP hydrolysis, rates of ATP hydrolysis were determined for a 1 μM sample of PilB2-HA-His_6 in the presence of increasing amounts of ATP. Each point represents one replicate, line indicates line of best fit determined using Least Squares regression to fit the data to the Michaelis-Menten equation. **(B)** Specific activity of PilB2-HA-His_6 was determined by adding increasing amounts of PilB2-HA-His_6 to assay mixtures containing 100 μM ATP. The mean and SEM of triplicate samples is plotted for each point. **(C)** Increasing amounts of PilB2-HA-His_6 were incubated with 0.5 μM TNP-ATP. For each replicate (performed in triplicate), the theoretical fluorescence curve ($F=F_0+$[PilB2-HA-His_6]$*F_{max}(K_d+$[PilB2-HA-His_6]$)$) was fit to the data using Least Squares regression. The average of these curves is plotted. Error bars indicate SEM.

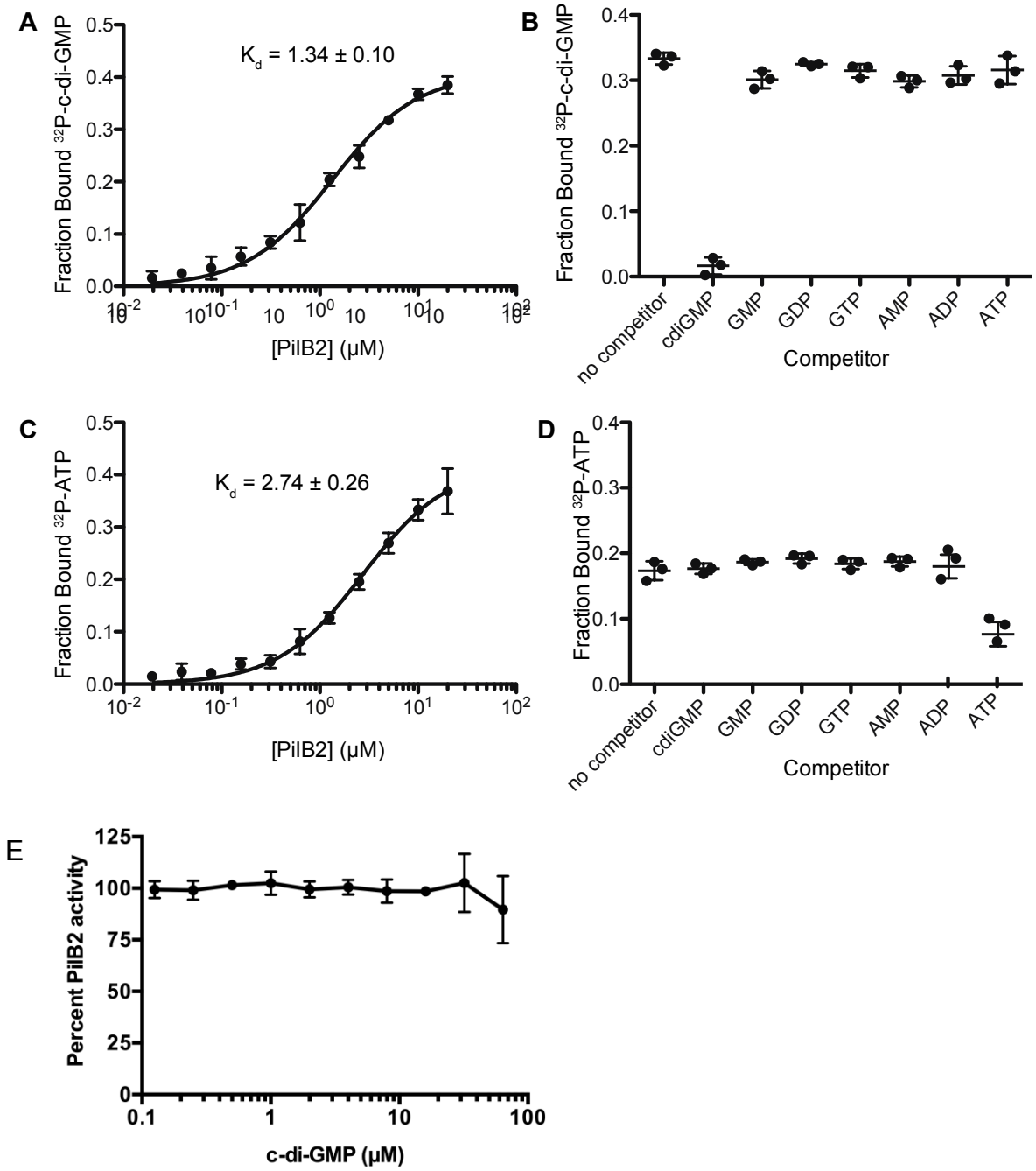

Figure 3.6 PilB2 binds the nucleotide cyclic-di-GMP.

The dissociation constants (K_d) and specificity of PilB2 binding to ^{32}P-c-di-GMP and ^{32}P-ATP was measured using the DRaCALA assay described under "Experimental Procedures". (**A** and **B**) ^{32}P-c-di-GMP and (**C** and **D**) ^{32}P-ATP (**A** and **C**). K_d was calculated using $Y = B_{max}*X/(K + X)$. (**B** and **D**) 100 μM of the indicated unlabeled nucleotide competitor was used. (**E**) Increasing concentrations of cyclic-di-GMP were added to ATPase assay mixtures as in Figure 3.5. Activity was recorded as percent activity relative to a reaction mixture with no added cyclic-di-GMP.

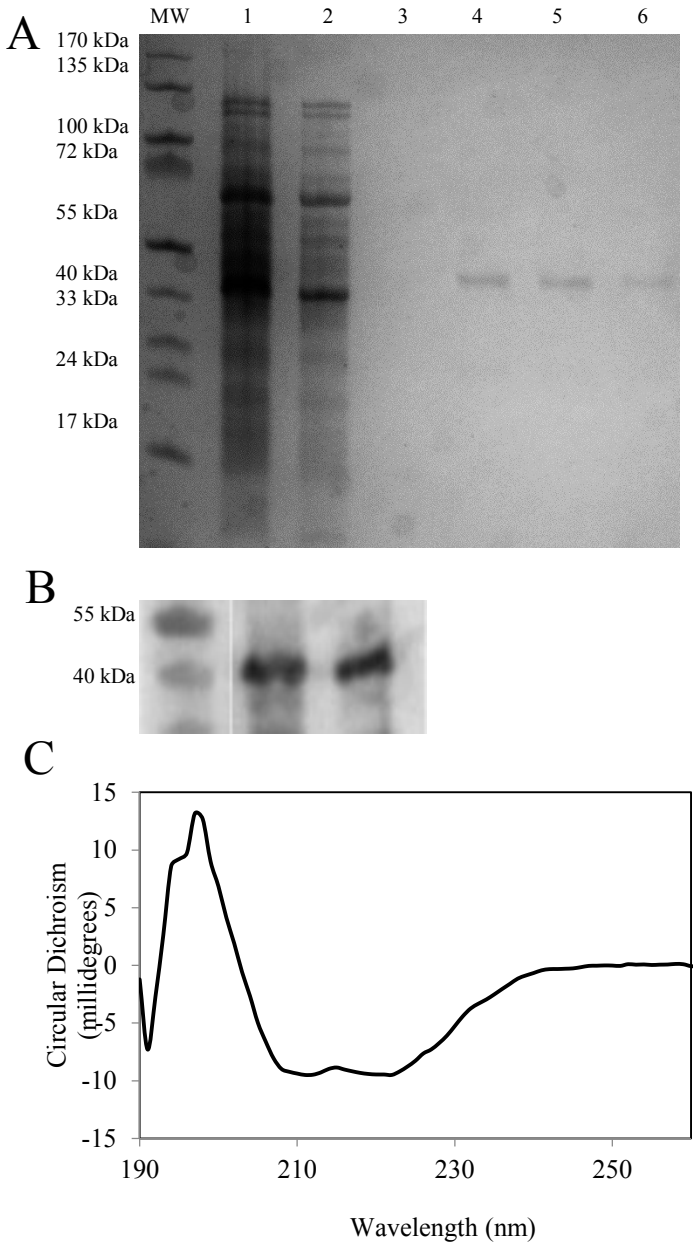

Figure 3.7 Purification and Circular Dichroism of His_6-FLAG-PilC2

A) SDS-PAGE of elution fractions following on-column refolding His_6-FLAG-PilC2. MW, molecular weight marker. Lane 1, denatured sample applied to column. Lane 2, flow through. Lanes 3 through 6, elution fractions of refolded PilC2. **B)** Western blot of elution fractions (lanes 4 and 5, Fig. 5A) following on-column refolding of PilB2-HA-His_6. Blot was probed with rabbit anti-PilC2 sera. **C)** Circular dichroism of purified His_6-FLAG-PilC2. The circular dichroism spectrum of His_6-FLAG-PilC2 was measured with a JASCO J815 spectrometer. Secondary structure estimates (74% alpha helix, 4.7% beta sheet) obtained from the K2D3 server at http://k2d3.ogic.ca//index.html.

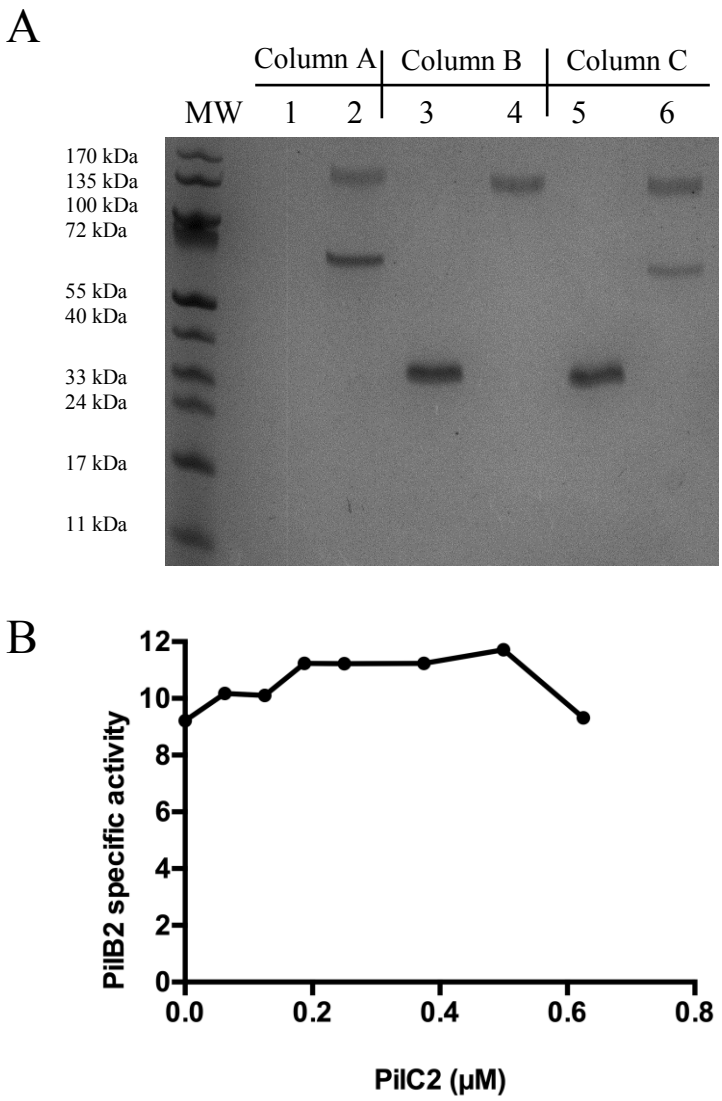

Figure 3.8 PilC2 does not co-immunoprecipitate with, or activate ATPase activity of, PilB2

A) Antibody pull down assay with Protein A columns loaded with anti-PilB2 antibodies. Ten micrograms of each protein were applied to the columns. Each fraction was analyzed by non-reducing SDS-PAGE. Intact IgG is visible in all elution fractions at 150 kDa. Column A: Loaded with PilB2-HA-His_6. PilB2-HA-His_6 (67 kDa) visible in elution (lane 2), but not in flow through (lane 1). Column B: loaded with His_6-FLAG-PilC2. His_6-FLAG-PilC2 (43 kDa) visible in flow through (lane 3), not visible in elution (lane 4). Column C: Loaded with PilB2-HA-His_6 and His_6-FLAG-PilC2. His_6-FLAG-PilC2 in flow through only (lane 5), PilB2-HA-His_6 in elution only (lane 6).
B) Specific activity of PilB2-HA-His_6 in the presence of His_6-FLAG-PilC2. Performed once.

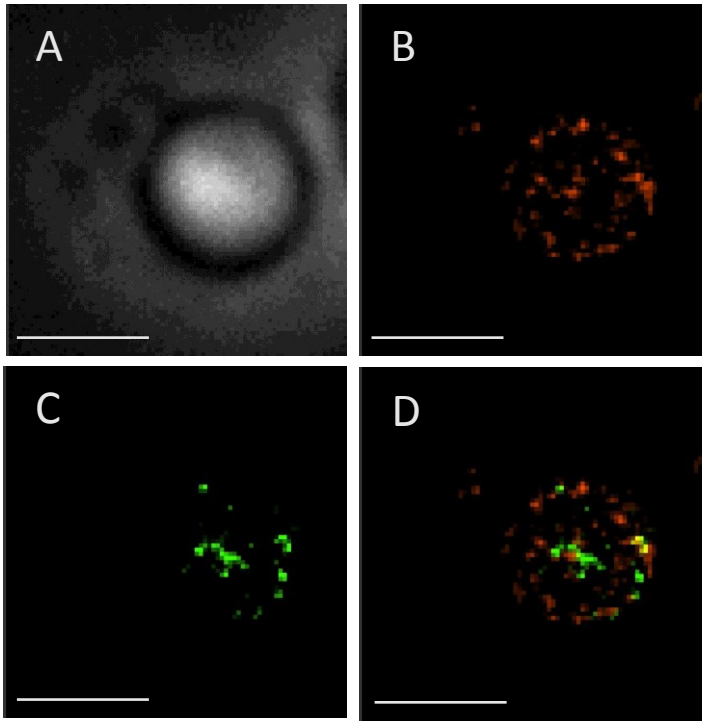

Figure 3.9 PilB2-HA-His_6 does not co-localize with His_6-FLAG-PilC2 in artificial membranes.

Representative images of fluorescently labeled PilB2-HA-His_6 (green) and His_6-FLAG-PilC2 (red) in liposomes. **(A)** Phase contrast image of a liposome. **(B)** Fluorescent imaging in the TRITC channel showing the location of His_6-FLAG-PilC2. **(C)** Fluorescent imaging in the FITC channel showing the location of PilB2-HA-His_6. **(D)** Merged image showing both His_6-FLAG-PilC2 and PilB2-HA-His_6. Bar equals 2 μm. Absence of yellow coloration indicates no colocalization of the two proteins. Not quantified, performed once.

Chapter 4 Biochemistry and Physiology of the Beta Class Carbonic Anhydrase from *Clostridium perfringens* Strain 13

R. Siva Sai Kumar[a], William Hendrick[b], Jared B. Correll[c], Andrew D. Patterson[c], Stephen B. Melville[b], James G. Ferry[a]

Department of Biochemistry and Molecular Biology, Pennsylvania State University, University Park, Pennsylvania, USA[a]; Department of Biological Sciences, Virginia Tech, Blacksburg, Virginia, USA[b]; Department of Veterinary and Biomedical Science, Pennsylvania State University, University Park, Pennsylvania, USA[c]

Journal of Bacteriology. 195(10):2262-9

Co-Author's Contribution:

My work on this project involved creation of the Cpb deletion strain, complementing the mutant, and analyzing the growth of the mutant. I examined the mutant for growth rate and ability to grow in nutrient limiting conditions, CO_2 depletion, and both nutrient/CO_2 limiting conditions. Additionally, I noted that the mutant had greatly reduced odor, which lead to the mass spectrometry analysis of spent medium. I also prepared a cell pellet of His-tagged Cpb produced in *C. perfringens* with iron supplementation, for determination of the native cofactor of Cpb.

Abstract

The carbonic anhydrase (Cpb) from *Clostridium perfringens* strain 13, the only carbonic anhydrase encoded in the genome, was characterized both biochemically and physiologically. Heterologously produced and purified Cpb was shown to belong to the type I subclass of the β class, the first β class enzyme investigated from a strictly anaerobic species of the domain Bacteria. Kinetic analyses revealed a two-step, ping-pong, zinc-hydroxide mechanism of catalysis with K_m and k_{cat}/K_m values of 3.1 mM CO_2 and 4.8×10^6 s^{-1} M^{-1}, respectively. Analyses of a *cpb* deletion mutant of *C. perfringens* strain HN13 showed that Cpb is strictly required for growth when cultured in semi-defined medium and an atmosphere without CO_2. The growth of the mutant was the same as that of the parent wild-type strain when cultured in nutrient-rich media with or without CO_2 in the atmosphere, although elimination of glucose resulted in decreased production of acetate, propionate, and butyrate. The results suggest a role for Cpb in anaplerotic CO_2 fixation reactions by supplying bicarbonate to carboxylases. Potential roles in competitive fitness are discussed.

Introduction

Carbonic anhydrase (CA) is a metalloenzyme catalyzing the reversible interconversion of CO_2 and bicarbonate ($CO_2 + H_2O = HCO_3^+ + H^+$). To date, five independently evolved classes (αβγζδ) are known (45). The β class is abundant in higher plants and photosynthetic algae of the domain Eukarya (57). Several β class CAs from the domain Bacteria have been described, including those from photosynthetic (58-60) and nonphotosynthetic species of which several are pathogenic (61-65). The β class CAs of photosynthetic species function to concentrate atmospheric CO_2, whereas it is proposed that nonphotosynthetic species utilize β class CAs to retain intracellular CO_2 by conversion to bicarbonate for anaplerotic carboxylation reactions (66-69). The only characterized β class CA from the domain Archaea (Cab) is that from *Methanothermobacter thermoautotrophicus* (formerly *Methanobacterium thermoautotrophicum* strain ΔH) (70-73), a microbe that obtains energy for growth by reducing CO_2 to methane. It is proposed that Cab functions to concentrate CO_2 for both methanogenesis and anaplerotic carboxylation reactions.

CAs are important for survival and growth of several pathogens and, therefore, a potential target for development of novel antimicrobial agents (74-77). *Clostridium perfringens* strains are ubiquitous, strictly anaerobic pathogens that inhabit many environmental niches, including soil, sediments, and the intestinal tracts of mammals (11). In humans, different strains of C. perfringens cause gas gangrene (myonecrosis), acute food poisoning, and necrotic enteritis. The *CPE0413* gene of strain 13 is annotated as encoding a probable CA (Comprehensive Microbial Resource [http://cmr.tigr.org/tigr-scripts/CMR/CmrHomePage.cgi]) that has yet to be investigated for enzymatic activity or physiological function. Here, we report the results of a phylogenetic, biochemical, and physiological characterization of the protein encoded by *CPE0413*. The results show that the protein is a type I β class CA, the first biochemical and physiological investigation of a CA from the genus *Clostridium*. The results further reveal that Cpb is essential for growth in semidefined media with no added CO_2, suggesting that Cpb functions in nature to retain intracellular levels of CO_2 and supply bicarbonate for anaplerotic reactions.

Methods

Bacterial strains, growth conditions

Bacterial strains, plasmids, and primers used in this study are listed in Table 4.1. *Escherichia coli* was grown in Luria-Bertani (LB) medium supplemented with antibiotics as needed: 400 μg/ml erythromycin, 100 μg/ml ampicillin, or 20 μg/ml chloramphenicol. C*lostridium perfringens* was grown in a Coy anaerobic chamber at 37°C. Four different media were used for growth of *C. perfringens*: brain heart infusion (BHI) medium (Difco), TY medium (3% tryptone, 2% yeast extract, 0.1% sodium thioglycolate), PGY medium (3% proteose peptone 3, 2% glucose, 1% yeast extract, 0.1% sodium thioglycolate) and semidefined media (0.1% yeast extract, 50 mM glucose, 50 mM $NaKPO_4$ [pH 7.0], 19.79 mg/liter $MnCl_2 \cdot 4H_2O$, 122 mg/liter $MgCl_2 \cdot 6H_2O$, 29.4 mg/liter $CaCl_2 \cdot 2H_2O$, 11.5 mg/liter $ZnSO_4 \cdot 7H_2O$, 0.025 mg/liter $CuSO_4 \cdot 5H_2O$). Strains were first inoculated onto plates containing BHI medium (with chloramphenicol for growth of the complemented strain) incubated in a 100% nitrogen atmosphere and then inoculated onto two identical agar plates containing semidefined media, one incubated in the anaerobic chamber (10% CO_2) and the other in an anaerobic jar containing 100% nitrogen.

In-frame deletion of *CPE0413* (*cpb*)

Mutagenesis of *C. perfringens* HN13, a derivative of *C. perfringens* strain 13, was performed as previously described (55). Briefly, overlap extension PCR using primers OWH9, OWH10, OWH11, and OWH12 was used to amplify ~900-bp regions flanking *CPE0413* (*cpb*). The resulting DNA fragment was cloned into pGEM-T Easy (pWH5) and then pCM-GALK (55), yielding pWH6. In-frame deletion mutagenesis was then performed using this construct (55), resulting in a deletion of the region from 18 to 555 bp out of the 570-bp *cpb* gene reading frame; this strain was named WH1. The mutation was confirmed using PCR with flanking primers OWH13 and OWH14.

Complementation

To complement the *cpb* mutation in strain WH1, a plasmid was constructed by amplifying the cpb gene plus 134 bp upstream with primers OWH15 and OWH24, cloning the *cpb* gene into plasmid pGEM-T Easy (pWH7) and then into pKRAH1 (pWH8), which placed the gene under the control of the lactose-inducible promoter, P_{bgaL} (48). Plasmids were introduced into strain WH1 by electroporation (78).

Cloning and heterologous production of Cpb

The *CPE0413* gene encoding Cpb was amplified by PCR using *Clostridium perfringens* strain 13 genomic DNA as a template. The forward primer (CA forward) partially corresponds to nucleotides encoding amino acids 1 to 9, and the reverse primer (CA reverse) corresponds to nucleotides 536 to 572 downstream of the beginning of the gene (Table 4.1). NdeI and HindIII restriction sites were introduced in the forward and reverse primers, respectively. The PCR product was digested with NdeI and HindIII and cloned into the digested pET22b(+) vector (Novagen) to yield pCPE0413. This constructed plasmid was transformed into E. coli strain Rosetta (DE3) pLacI (Novagen) which was used to inoculate Luria-Bertani broth containing 100 μg/ml ampicillin and 34 μg/ml chloramphenicol. The cells were grown at 37°C to an A_{600} of 0.6 to 0.8 and then induced with 1 mM isopropyl thiogalactopyranoside (IPTG) and 500 μM $ZnSO_4$ to overproduce Cpb. Induced cultures were allowed to continue growth for 4 to 5 h. The cells were harvested by centrifugation and stored frozen at −80°C until lysis.

Enzyme purification

Cell paste (5 g [wet weight]) was thawed in 30 ml of buffer A (50 mM potassium phosphate [pH 7.0]) containing 0.1 mM zinc and passed twice through a chilled French pressure cell at 138 MPa. The cell debris was removed by centrifuging the cell lysate at 29,000 × g for 30 min. After centrifugation, the supernatant was passed through a 0.45-μm filter before loading onto a Q-Sepharose (GE Healthcare) column equilibrated with buffer A. The column was developed with the same buffer to elute unbound protein. Bound proteins were then eluted with a linear gradient (0 to 1 M) of NaCl in buffer A. The

fractions with CA activity were concentrated and chromatographed on a Sephadex G-150 superfine gel filtration column (GE Healthcare) using buffer B (50 mM potassium phosphate [pH 7.0]) containing 0.1 M NaCl. Fractions with CA activity were pooled and stored at −20°C. CA activity was measured at room temperature by using the electrometric method described previously (79).

Enzyme activity

Steady-state CO_2 hydration activity was measured by stopped-flow spectroscopy using the changing pH indicator method described previously (80). Saturated solutions of CO_2 (32.9 mM) were prepared by bubbling CO_2 into distilled, deionized water at 25°C. The CO_2 concentration was varied from 5 to 27 mM by mixing with an appropriate volume of N_2-saturated water. The buffer/indicator pairs (the wavelengths used shown in parentheses) were morpholineethanesulfonic acid (MES)/chlorophenol red (574 nm) at pH 5.5 to 6.8, morpholinepropanesulfonic acid (MOPS)/p-nitrophenol (400 nm) at pH 6.8 to 7.5, HEPES/phenol red (557 nm) at pH 7.5 to 8.0, and *N*-Tris(hydroxymethyl)methyl-3-aminopropanesulfonic acid (TAPS)/*m*-cresol purple (578 nm) at pH 8.0 to 9.0. Buffer concentrations were 50 mM. The total ionic strength was adjusted to 150 mM with Na_2SO_4. The final pH indicator concentration was 50 μM. The initial 5 to 10% of the total absorbance change was used to calculate the initial steady-state rate with the mean of 5 to 10 reaction traces per experiment. The steady-state parameters k_{cat} and k_{cat}/K_m and their standard errors were determined by fitting the observed initial rates (corrected for the uncatalyzed reaction) to the Michaelis-Menten equation using the KaleidaGraph data analysis and graphing software. The pH-independent values of k_{cat} and pK_a for the CO_2 hydration reaction were determined by fitting the experimental pH-dependent Michaelis-Menten parameters to equations **Equation 4.1**A and **Equation 4.1**B where k_{cat}^{obs} is the observed k_{cat} and K_m^{obs} is the observed K_m.

Equation 4.1 Determination of k_{cat} and K_m of Cpb.

A) $k_{cat}^{obs} = {k_{cat}}/{(1 + 10^{pK_a - pH})}$

B) $$k_{cat}/K_m^{obs} = \frac{k_{cat}}{K_m}/(1 + 10^{pK_a - pH})$$

Esterase activity, using *p*-nitrophenylacetate as a substrate, was determined as previously described (81).

Protein, metal, and volatile fatty acid (VFA) analyses

Protein concentrations were estimated by measuring the absorbance of solutions (A_{280}), using a theoretical monomer extinction coefficient of 11, 710 cm^{-1} M^{-1} and a calculated monomer molecular mass of 21,351 Da. For analysis of metals, protein concentrations were determined by the biuret method (82) using bovine serum albumin as the standard.

The homogeneity of the enzyme was determined by 12% SDS-PAGE (83). The gels were stained for protein with Coomassie brilliant blue. Markers in the molecular mass range from 20 to 250 kDa were used to estimate the molecular mass. The native molecular mass was determined by gel filtration chromatography using a Sephadex G-150 gel filtration column (GE Healthcare) equilibrated with buffer B and calibrated with lysozyme (14.7 kDa), bovine erythrocyte CA (29 kDa), bovine serum albumin (monomer, 66 kDa; dimer, 132 kDa), the β class CA (Cab) from M. thermautotrophicus (90 kDa), and urease (trimer, 272 kDa; hexamer, 545 kDa). The column was developed with a flow rate of 0.2 ml/min using buffer B.

A comprehensive metal analysis (20 elements) was conducted using inductively coupled plasma (ICP) atomic emission spectroscopy at the Chemical Analysis Laboratory, University of Georgia, Athens. All solutions were made metal free by treating with Chelex 100 (Sigma). Prior to metal ion analysis, samples were dialyzed for about 24 h at 4°C with 4 to 6 changes against 20 mM potassium phosphate (pH 7.0).

Lactate and formate were determined using commercial kits (Megazymes, Ireland). Cells were grown for ~15 h to stationary phase and then removed by centrifugation, and the supernatant was filtered through a 0.22-μm filter and stored at −80°C until analyzed.

Acetate, butyrate, and propionate were determined by liquid chromatography-mass spectrometry

(LC-MS). Samples were analyzed using an Agilent 6890 N gas chromatograph (GC) with a Waters GCT classic mass spectrometer operated in electron ionization (EI) mode. Aliquots (2 µl) were injected using a split/splitless injector at 250°C with a 5:1 split onto a VF5 (5% diphenyl–95% dimethyl polysiloxane) capillary column (Varian) (20-m column with 150-µm internal diameter and 0.15-µm film thickness) using helium as the carrier gas at a flow rate of 1.4 ml/min. The column was held at an initial temperature of 50°C for 1 min and then heated at 10°C/min to 100°C where it was held for 2 min before heating at 30°C/min to a final temperature of 230°C. Following a 6-min solvent delay, EI mass spectra were acquired over the mass range of 45 to 400 kDa at 1 scan/second. Under these conditions, the pentafluorobenzyl (PFB) derivatives of acetic acid, propionic acid-2,2-d2, propionic acid (internal standard), and butyric acid had retention times of 7.05, 8.74, 8.78, and 9.69 min, respectively. The reconstructed ion chromatograms (RIC) for *m/z* 240, 256, 254, and 268 were generated, and the integrated areas were used for quantitation. A standard curve was prepared from a mixture of the three VFAs at a concentration of 240, 120, 60, 30, 15, 7.5, and 3.75 µg/ml containing 8 µg/ml of the internal standard. The amounts of each of the VFAs in the samples were calculated from the integrated area of the RIC, using the response factor for each VFA and normalized for the internal standard (IS) response.

Results and Discussion

Purification and characterization of Cpb encoded by *CPE0413*

The protein encoded by the *CPE0413* locus of the *C. perfringens* genome is annotated as a probable CA (84). The gene was amplified by PCR from C. perfringens genomic DNA using primers shown in Table 4.1. The PCR product was cloned into pET22b(+) to yield the expression vector pCPE0413 that was transformed into *E. coli* strain Rosetta (DE3) p*Lac*I for overproduction of the encoded protein. The protein was purified to homogeneity (Figure 4.1) from cell extract of IPTG-induced cells by ion-exchange and gel filtration chromatography. CA activity was monitored using the electrometric method (85). The purified protein showed CO_2 hydration activity comparable to the activities of kinetically characterized β class CAs (Table 4.2) validating the annotation; therefore, the gene is designated *cpb* (*Clostridium perfringens* beta class carbonic anhydrase). SDS-PAGE (Figure 4.1) revealed a molecular mass of 23 kDa consistent with 21.3 kDa calculated from the deduced amino acid composition. The molecular mass of ~88 kDa, determined by gel filtration chromatography (data not shown), indicated that the native enzyme is a tetramer. A comprehensive metal analysis (20 elements) performed by plasma emission spectroscopy, using two independent enzyme preparations with similar specific activities, revealed 0.89 and 0.93 zinc per subunit, indicating that the enzyme contains one active site zinc per subunit. The kinetic constants and subunit composition of Cpb (Table 4.2) most resemble those of the β class CA (Cab) from *M. thermautotrophicus* of the domain Archaea (70-72). Both Cpb and Cab have lower K_m values for CO_2 compared to all other β class CAs (Table 4.2), a result consistent with a role for Cpb and Cab in capturing environmental CO_2 and retaining intracellular levels for anaplerotic CO_2 fixation reactions. Cpb and Cab belong to one of two clades identified in the phylogenetic analysis of prokaryotic β class CAs (Figure 4.2) from species other than *Clostridium* species. A search of the nonredundant databases revealed 23 closely related homologs of *C. perfringens* strain 13 *cpb* belonging to the genus *Clostridium* represented by pathogenic species and nonpathogenic species of environmental and biotechnological importance (see Figure 4.7 in the supplemental material).

CAs characterized thus far employ a two-step, ping-pong, metal-hydroxide mechanism of catalysis (Equation 4.2 and Equation 4.3) where *E* represents enzyme residues, *M* is metal, and *B* is buffer.

Equation 4.2 Generation and release of bicarbonate.

A) $(E - M^{2+} - OH^{-}) + CO_2 = (E - M^{2+} - HCO_3^{-})$

B) $(E - M^{2+} - HCO_3^{-}) + H_2O = (E - M^{2+} - H_2O) + HCO_3^{-}$

Equation 4.3 Regeneration of metal-hydroxide.

A) $(E - M^{2+} - H_2O) = (H^{+} - E - M^{2+} - OH^{-})$

B) $(H^{+} - E - M^{2+} - OH^{-}) + B = (E - M^{2+} - OH^{-}) + BH^{+}$

In the first step, a pair of electrons residing on the metal-bound hydroxide attack the carbon of CO_2 (Equation 4.2A), producing metal-bound HCO_3^- that is next displaced by water (Equation 4.2B). In the next step, a proton is extracted from the metal-bound water (Equation 4.3A) and transferred to bulk solvent or buffer (Equation 4.3B), regenerating the metal-bound hydroxide (79). The steady-state parameters of k_{cat} and k_{cat}/K_m for Cpb increased with increasing pH (Figure 4.3A and B), suggesting that an unprotonated form is required for activity consistent with a metal-hydroxide mechanism of catalysis. Single ionizations with pK_a values of 6.9 ± 0.15 and 7.1 ± 0.2 were observed for k_{cat} and k_{cat}/K_m (Figure 4.3A and B). The dependence of CO_2 hydration on the concentration of HEPES buffer was determined at pH 7.5. The k_{cat} was dependent on the concentration of buffer in a saturable manner with an apparent K_m of 4 mM for HEPES (Figure 4.3C). This result indicates that buffer acts as the second substrate in a ping-pong mechanism accepting a proton from the enzyme during CO_2 hydration. The K_m parameter also increased with increasing buffer concentration, resulting in a k_{cat}/K_m that was independent of the buffer concentration (Figure 4.3D). These results are consistent with the metal-hydroxide mechanism in which the interconversion of CO_2 and HCO_3^- (Equation 4.2) reflected by k_{cat}/K_m is separate from the intermolecular proton transfer reflected by k_{cat} (Equation 4.3).

There are two distinct subclasses of the β class (2). The type 1 subclass is characterized by

ionizable water serving as a fourth ligand to zinc and pH rate profiles for CO_2 hydration featuring only one ionization (pK_a). In contrast, the type II subclass is characterized by Asp serving as the fourth ligand to zinc and a cooperative pH rate profile with multiple ionizations and only slight activity below pH 8 compared to type I. The type II subclass is further distinguished by a trio of residues (Trp, Tyr, and Arg) in a putative bicarbonate-binding allosteric site represented by the enzyme from *Haemophilus influenzae* (86). The Cpb CA does not contain the cognate Trp39 or Arg64 of the *H. influenzae* bicarbonate-binding allosteric site, and phylogenetic analyses place Cpb farthest from the *H. influenzae* enzyme (Figure 4.3). In contrast, Cpb from *C. perfringens* is in the same clade (Figure 4.2) and has substantial sequence identity with Cab from *M. thermautotrophicus* (Figure 4.4), which is representative of the type I subclass. Furthermore, the pH profiles of Cpb revealed only one pK_a each with activity extending well below pH 8 (Figure 4.3A and B). A distinctive feature of all β class CAs is ligation of the active site zinc with sulfur atoms of two Cys residues and a nitrogen atom of His (39). Comparison of sequences in Figure 4.4 indicates that zinc ligands in type I Cab are conserved in Cpb, in addition to the Asp/Arg pair essential for ensuring that water is the fourth ligand to zinc and playing a role in the proton transfer step in the mechanism of Cab (70, 73). Thus, the kinetic parameters, phylogeny, and sequence comparisons establish that Cpb of *C. perfringens* belongs to the type I subclass of β class CAs.

Physiological role of Cpb

Annotation of the genome of *C. perfringens* strain 13 indicated that a single CA-encoding gene, *CPE0413* (*cpb*), was present (87). To confirm that no other CAs are present, the deduced *cpb* gene product was entered into the BLASTP program and compared to the strain 13 genome sequence. No significant homology was seen to any other proteins, suggesting there is only a single CA in this strain. The same analysis was done with the other 8 *C. perfringens* strains with sequenced genomes, and only a single CA gene was detected in each, with 100 to 94% identity to the CA from strain 13 (blast.ncbi.nlm.nih.gov). The *cpb* gene of strain 13 is predicted to be monocistronic by the operon prediction software available in MicrobesOnline (http://www.microbesonline.org/cgi-bin/fetchLocus.cgi?locus=184876&disp=1). A

rho-independent transcription terminator is predicted to lie in the 141-bp intergenic region between *cpb* and *CPE0414* using the ARNold software (http://rna.igmors.u-psud.fr/toolbox/arnold/index.php).

CAs have been shown to mediate a wide variety of physiological effects on species from the domains *Bacteria* and *Eukarya* (66, 68, 76, 77, 88-94). Therefore, an in-frame deletion of the *cpb* gene was constructed in wild-type strain HN13, a derivative of *C. perfringens* strain 13 that has a deletion of the *gal*T-*gal*K genes (55). Introducing a heterologous *gal*K gene into the chromosome by insertion of a nonreplicating plasmid (pWH6) at the *cpb* locus established a counterselectable marker strategy where the addition of galactose is toxic to the cell due to the accumulation of galactose-1-phosphate (Gal-1-P) (55). Cells that have undergone a second recombination event that leads to deletion of the *cpb* gene are resistant to galactose treatment. This strategy was used to produce mutant strain WH1 for evaluating the physiological role of Cpb. There were no differences in the growth rate or final A_{600} of the mutant strain and wild-type strain when cultured in nutrient-rich PY, BHI, or PGY liquid medium (not shown). However, *E. coli* and other prokaryotes lacking a functional CA have shown deficiencies in the ability to grow in an atmosphere largely devoid of CO_2 required for anaplerotic carboxylation reactions (66, 68, 76, 93). Therefore, we tested the ability of the cpb deletion mutant WH1 to grow on solid media in the absence of CO_2 by replacing the headspace gas in anaerobic jars with 100% N_2. As shown in Figure 4.5, the *cpb* mutant strain WH1 was unable to grow in the absence of CO_2 on a semidefined medium comprised of 0.1% yeast extract, 50 mM glucose, and mineral salts. However, growth in semidefined medium was restored when a wild-type copy of the *cpb* gene was provided to strain WH1, yielding complemented strain WH1-pWH8 (Figure 4.5). In contrast, growth was comparable for wild-type strain HN13 and mutant strain WH1 when cultured on solid nutrient-rich medium (BHI, TY, or PGY) in an atmosphere of either 100% N_2 or 80% N_2, 10% H_2, and 10% CO_2 (not shown). These results demonstrate a strict requirement for Cpb during growth of *C. perfringens* in semidefined medium.

The absence of growth for the *cpb* deletion mutant strain WH1 when cultured in a semidefined medium and an atmosphere devoid of CO_2 is likely due to low activity of anaplerotic CO_2-fixing reactions

dependent on Cpb to supply HCO_3^- to carboxylases. One candidate anaplerotic enzyme is the phosphoenol pyruvate (PEP) carboxylase from *C. perfringens* (95) that produces oxaloacetate (Figure 4.6). Oxaloacetate is the first intermediate in the reverse tricarboxylic acid (TCA) cycle that *C. perfringens* strains use to synthesize the carbon backbones of amino acids (KEGG database [http://www.genome.jp/kegg/kegg2.html]) that are most likely present in nutrient-rich media although in low concentrations or absent in semidefined media. The PEP carboxylase from *C. perfringens* utilizes HCO_3^- and is homologous in sequence (96) (Figure 4.2) and similar in structure (95) to the PEP carboxylase of *M. thermautotrophicus* that also utilizes HCO_3^- (49). The *C. perfringens* archaeal-type PEP carboxylase is only one of three known in the domain *Bacteria* (96). The finding that Cpb has a relatively low K_m for CO_2 (Table 4.2) is, at least, consistent with a role for Cpb to supply HCO_3^- for anaplerotic reactions similar to that catalyzed by PEP carboxylase (Figure 4.6).

There was no statistically significant difference in the wild-type strain (HN13) and the *cpb* deletion mutant strain (WH1) in l-lactate, d-lactate, or formate production grown in either low-carbohydrate (PY) medium or high-carbohydrate (PGY) medium containing 111 mM glucose (data not shown). There was also no statistically significant difference in either the total or ratio of the acetate, butyrate, and propionate VFAs produced when the strains were cultured in PGY medium (data not shown). In contrast, mutant strain WH1 was deficient in the amount of total VFAs produced in PY medium compared to wild-type strain HN13, although the ratios of VFAs and final A_{600} were unchanged (Table 4.3). Addition of the wild-type *cpb* gene under the control of the lactose-inducible promoter P_{bgaL} to mutant strain WH1 restored VFA production in the complemented strain (WH1-pWH8) to wild-type levels (Table 4.3). While *C. perfringens* can ferment lactose, the amount of lactose added for induction had no significant effects on VFA production by the wild-type strain HN13 cultured in PGY or PY medium (data not shown). Finally, there was no significant difference in the growth rate or final A_{600} between wild-type strain HN13 and the *cpb* deletion mutant strain WH1 (data not shown). These results establish that

maximum production of VFAs in a low-carbohydrate medium is dependent on Cpb.

The finding that the *cpb* deletion mutant (WH1) showed no discernible defect in growth phenotype when cultured in nutrient-rich media diminishes the possibility that Cpb plays an important role in gas gangrene infections where *C. perfringens* is exposed to a surplus of nutrients by breaking down tissue and releasing soluble components. However, it remains to be determined whether Cpb has a more direct role in pathogenicity. Furthermore, although the results indicate that Cpb is necessary for maximum VFA production when carbohydrates are limiting, the effects of reduced VFA levels on pathogenicity have yet to be determined. Nonetheless, it appears likely that Cpb is valuable in soil environments where there is greater competition for nutrients and CO_2 levels are limiting. The results reported here encourage further research to determine whether Cpb homologs identified from other *Clostridium* species, isolated from diverse anaerobic environments, play important roles in the physiology and ecology of these organisms.

Table 4.1 Bacterial strains, plasmids, and primers used in this study

Strain, plasmid, or primer	Relevant characteristic(s) or sequence (5′ to 3′)	Source or reference
Strains		
E. coli		
DH10B	*F⁻ mcrAΔ mrr-hsdRMS mcrBC* Φ80d*lacZΔ*M15 *lacX74 deoR recA1 araD139Δ ara leu7697 galU galK ΔrpsL endA1 nupG*	Gibco/BRL
C. perfringens		
HN13	Strain 13; *ΔgalKT*	(55)
WH1	Strain HN13 with deletion of the region from bp 18 to 555 in *cpb*	This Study
Plasmids		
pGEM-T Easy	PCR cloning vector; ampicillin resistance	Promega
pKRAH1	Contains *bgaR* − P_{bgaL}; chloramphenicol resistance	(48)
pCM-GALK	Contains a *Clostridium beijerinckii galK* gene under the control of a ferredoxin promoter from *C. perfringens*	(55)
pET22b	Protein production vector	Novagen
pCPE0413	*cpb* gene in pET22b	This Study
pWH5	pGEM-T Easy with overlapping PCR product of DNA flanking the *cpb* gene	This Study
pWH6	pCM-GALK with *cpb* deletion fragment	This Study
pWH7	pGEM-T Easy with *cpb* gene from HN13	This Study
pWH8	pKRAH1 with *cpb* gene from HN13	This Study
Primers		
CA Forward	TTTTTTCATATGGAAAAGAATGTGAGAAGACTAGAAG	
CA Reverse	TTTTTTAAGGTTATTCGTATCCATTTACTATAACCTTAAGTTCTCC	
OWH9	GTCGACTTCACAAATCAATAGAAGAAATTGAAG	
OWH10	GTTTTTTAATTTTTATTTTATTCGTATCCATTCACATTCTTTTCCATACTAAATACC	
OWH11	GGTATTTAGTATGGAAAAGAATGTGAATGGATACGAATAAAATAAAAATTAAAAAAC	
OWH12	GGATCCCTTTTTGTTTATTTTCAATTCCAAATATAC	
OWH13	AATGAAAAAGGAGATAAAACTCCAG	
OWH14	CCATATACAGGACTAATTGGTCC	
OWH15	GTCGACGTGGGTTTAAAGTAAAGACTTTAAATC	
OWH24		

Table 4.2 Subunit composition and kinetic parameters of characterized prokaryotic β class carbonic anhydrases

Enzyme Source	Composition[a]		Kinetic parameters[a]			Reference(s)
	Subunit mass (kDa)	Holoenzyme	k_{cat} (s^{-1})	K_m (mM)	k_{cat}/K_m (s^{-1})(M^{-1})	
Clostridium perfringens strain 13	21.3	Tetramer	1.5×10^4	3.1	4.8×10^6	This study
Methanothermobacter thermautotrophicus	18.9	Tetramer	1.7×10^4	2.9	5.9×10^6	(71)
Mycobacterium tuberculosis (Rv1284)	18.2	Tetramer	3.9×10^5	10.5	3.7×10^7	(64, 97)
Mycobacterium tuberculosis (Rv3588c)	21.8	Dimer	NA	NA	NA	(64)
Brucella suis (bsCAI)	25	Dimer	6.4×10^5	16.4	3.9×10^7	(61)
Brucella suis (bsCAII)	25	NA	1.1×10^6	12.3	8.9×10^7	(75)
Helicobacter pylori	25.8	NA	7.1×10^5	14.7	4.8×10^7	(62)
Streptococcus pneumoniae	21.1	NA	7.4×10^5	11.3	6.5×10^7	(98)
Salmonella enterica (stCAI)	24.8	NA	1.0×10^6	12	8.3×10^7	(99)
Salmonella enterica (stCAII)	26.6	NA	7.9×10^5	15.2	5.2×10^7	(99)
Halothiobacillus neapolitanus	57.3	NA	8.9×10^5	3.2	2.8×10^7	(100)

[a]NA, not available.

Table 4.3 Volatile fatty acid production in three strains of *C. perfringens* cultured in PY medium

Trial	Total Ac/Pr/Bu[a] produced (μg/ml) [ratio] in strain:		
	HN13[b]	WH1[c]	WH1-pWH8[d]
1	1,310/460/280 [2.8/1/0.6]	300/110/63 [2.7/1/0.6]	970/415/240 [2.3/1/0.6]
2	1,230/430/280 [2.9/1/0.7]	311/110/62 [2.8/1/0.6]	1,030/420/580 [2.5/1/1.4]

[a]Ac/Pr/Bu, acetate/propionate/butyrate.

[b]HN13 is the wild-type strain.

[c]WH1 is the cpb deletion mutant strain.

[d]WH1-pWH8 is the cpb-complemented mutant cultured with lactose present in PY medium.

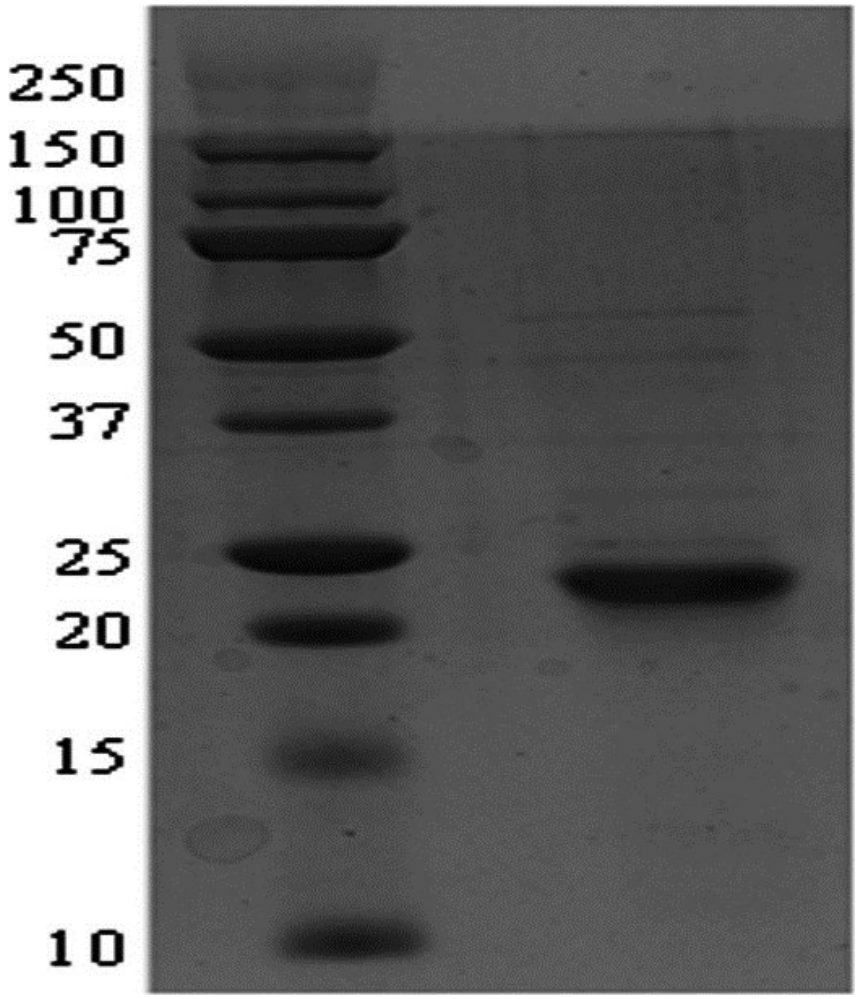

Figure 4.1 Denaturing polyacrylamide gel electrophoresis of Cpb.

The right lane contains 10 μg of purified protein. The left lane contains molecular mass standards. The positions of molecular mass standards (in kilodaltons) are shown to the left of the gel. The gel was stained for protein with Coomassie blue R-250.

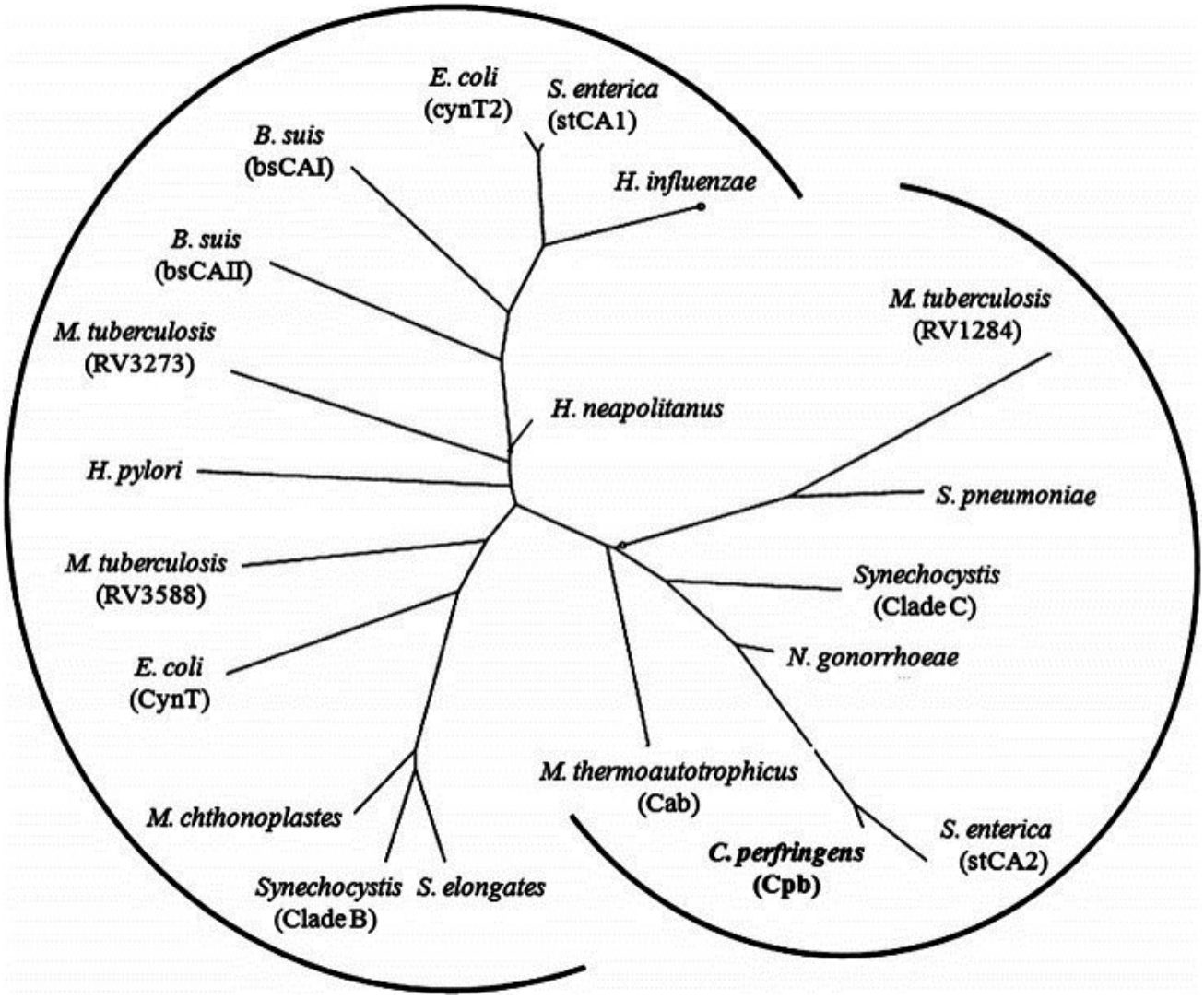

Figure 4.2 Phylogenetic analysis of prokaryotic β class carbonic anhydrases.

The sequences were from the following species (gene identification numbers shown in parentheses or brackets): *Clostridium perfringens* strain 13 (gi|18309395), *Methanothermobacter thermautotrophicus* strain ΔH (gi|15679577), *Escherichia coli* (cynT [gi|386607709] and cynT2 [gi|14277938]), *Brucella suis* (bsCAI [gi|260567947] and bsCAII [gi|260568899]), *Helicobacter pylori* (gi|188526816), *Mycobacterium tuberculosis* (strain RV1284 [gi|298524787], RV3588C [gi|15610724], and RV3273 [gi|15610409]), *Salmonella enterica* serovar Typhimurium (stCA2 [gi|378987335] and stCA1 [gi|16763561]), *Neisseria gonorrhoeae* (gi|59802380), *Streptococcus pneumoniae* (gi|307066706), *Haemophilus influenzae* (gi|99031788), *Synechocystis* (clade C [gi|1001130] and clade B [gi|1653251]), *Synechococcus elongates* (gi|56685078), *Microcoleus chthonoplastes* (gi|78057950), and *Halothiobacillus neapolitanus* (gi|88193005). The tree was constructed using the phylogeny/evolution analysis tools obtained at ExPASy (http://expasy.org/phylogeny_evolution). A distance-based method was used for the construction.

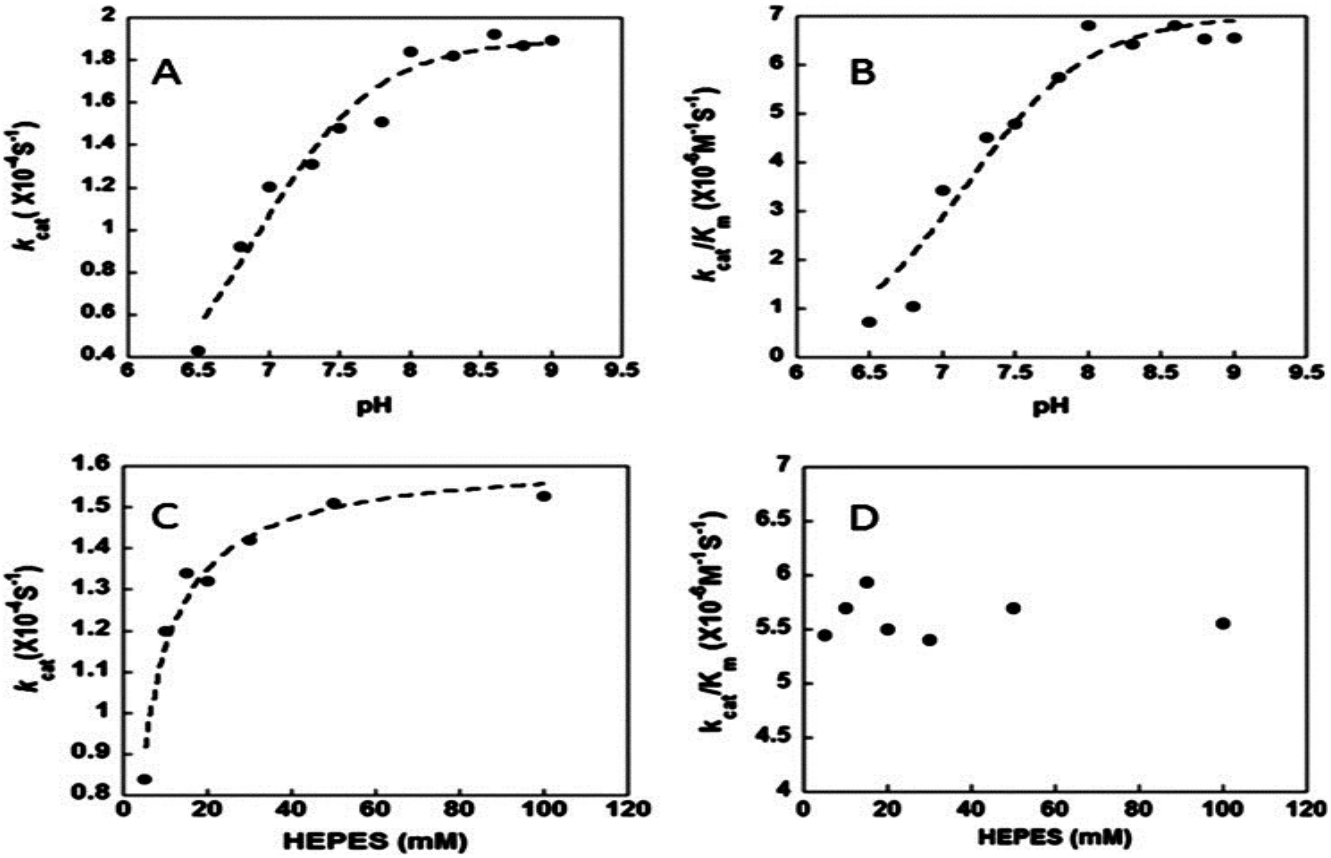

Figure 4.3 pH and buffer dependence of CO_2 hydration catalyzed by Cpb.
(A) pH versus k_{cat}; (B) pH versus k_{cat}/K_m; (C) HEPES concentration versus k_{cat}; (D) HEPES concentration versus k_{cat}/K_m.

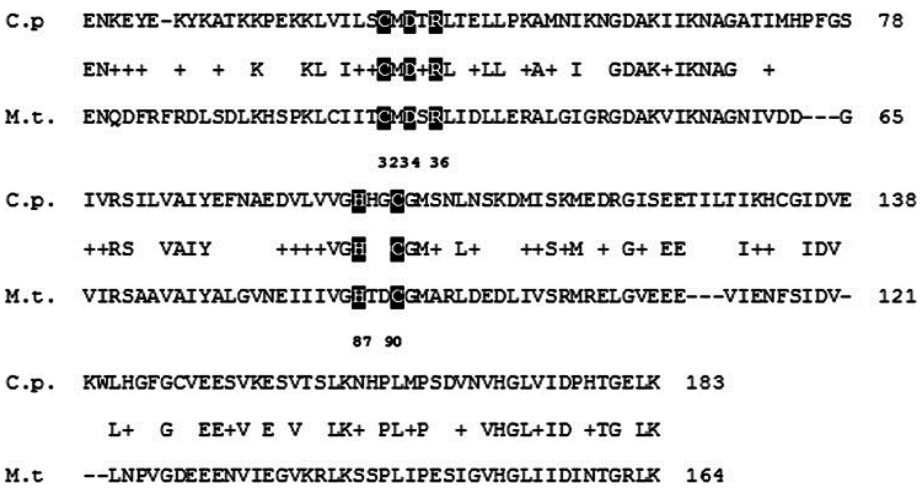

Figure 4.4 Alignment of the sequences for Cpb from *Clostridium perfringens* and Cab from *Methanothermobacter thermautotrophicus*.

The deduced sequences were aligned by using ClustalX (50). Abbreviations and gene identification numbers: C.p., *C. perfringe*ns, gi|110799007; M.t., *M. thermautotrophicus*, gi|1272331. The numbering corresponds to the *M. thermautotrophicus* sequence. Residues 32, 87, and 90 are ligands to zinc. Residues 34 and 36 are the Asp/Arg pair important for the proton transfer step of catalysis.

Although commercially available bovine α class CA showed an esterase activity of ~37 mol of *p*-nitrophenylacetate hydrolyzed $min^{-1}mol^{-1}$ of enzyme, the *C. perfringens* CA (Cpb) had no detectable esterase activity (<0.05 mol of *p*-nitrophenylacetate hydrolyzed $min^{-1}mol^{-1}$ of tetramer), also a property of Cab from *M. thermautotrophicus* (71, 72).

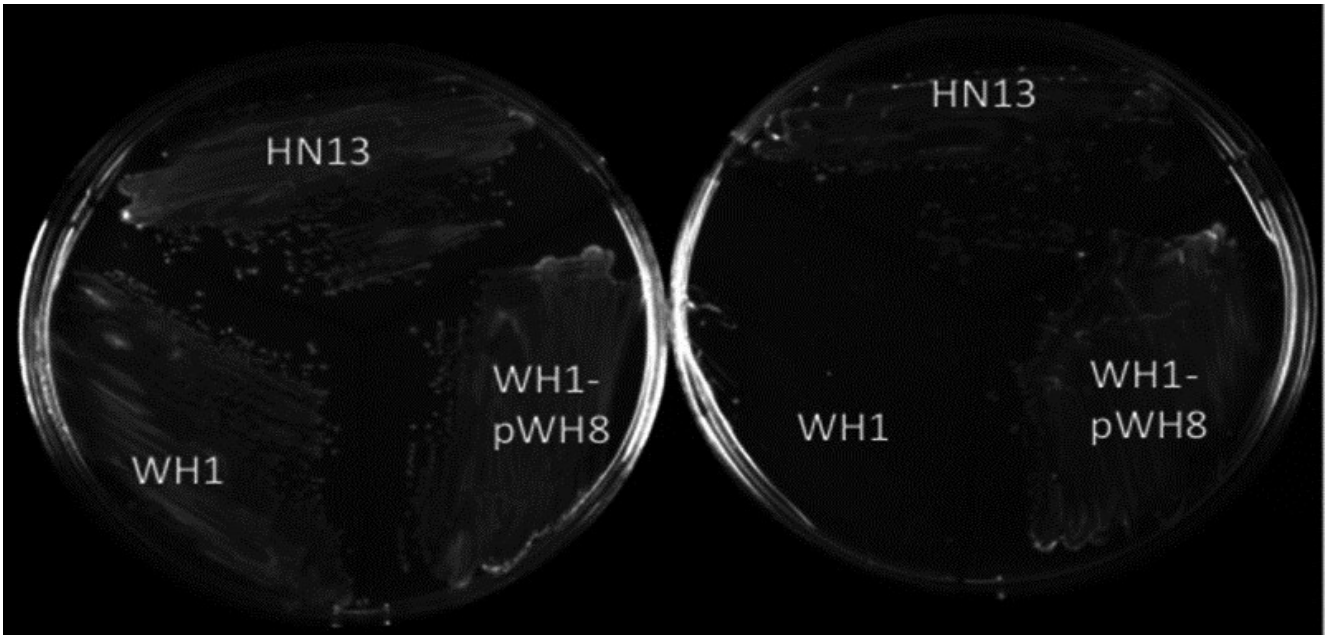

Figure 4.5 Growth of *C. perfringens* strains on solid semidefined medium.

Wild-type (HN13), *cpb* deletion mutant (WH1), and complemented mutant (WH1-pWH8) strains were cultivated on solid agar containing semidefined medium with 10% CO_2 (left) and without CO_2 (right) added to the atmosphere (see Materials and Methods).

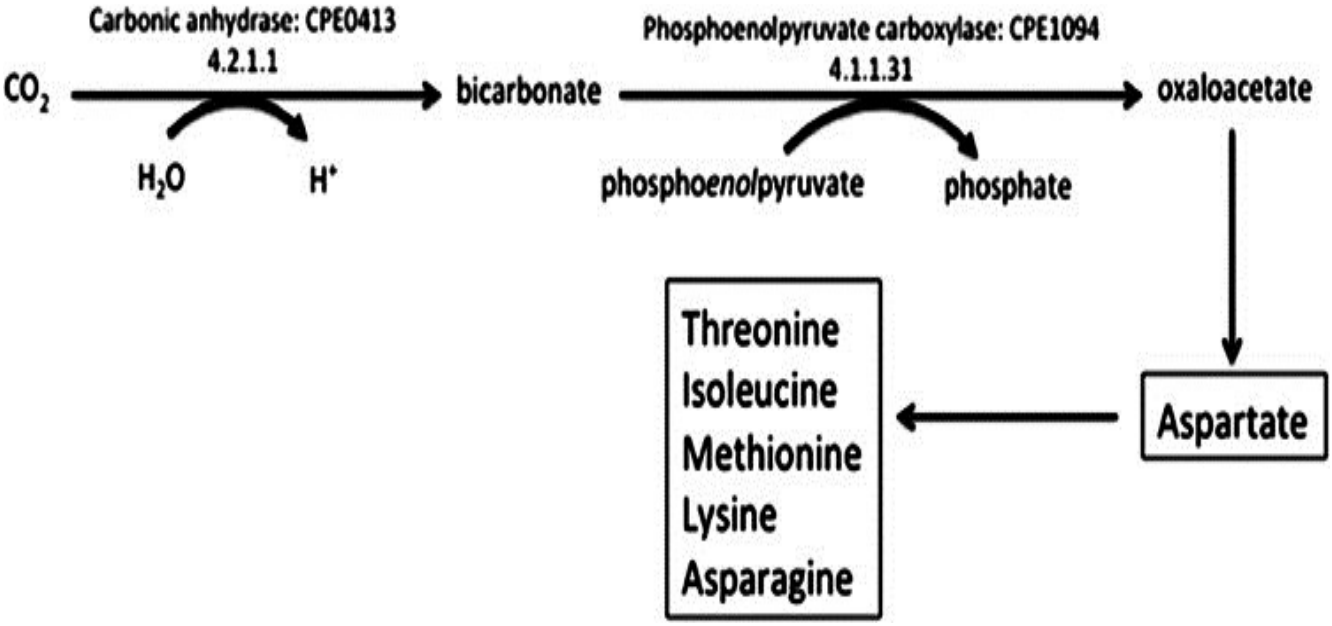

Figure 4.6 Proposed involvement of *C. perfringens* Cpb CA and PEP carboxylase leading to oxaloacetate and amino acid biosynthetic pathways.

Carbonic anhydrase is necessary for bicarbonate formation, which is the substrate for the anaplerotic enzyme, PEP carboxylase, leading to oxaloacetate formation and amino acid biosynthesis (boxes).

Supplementary Material

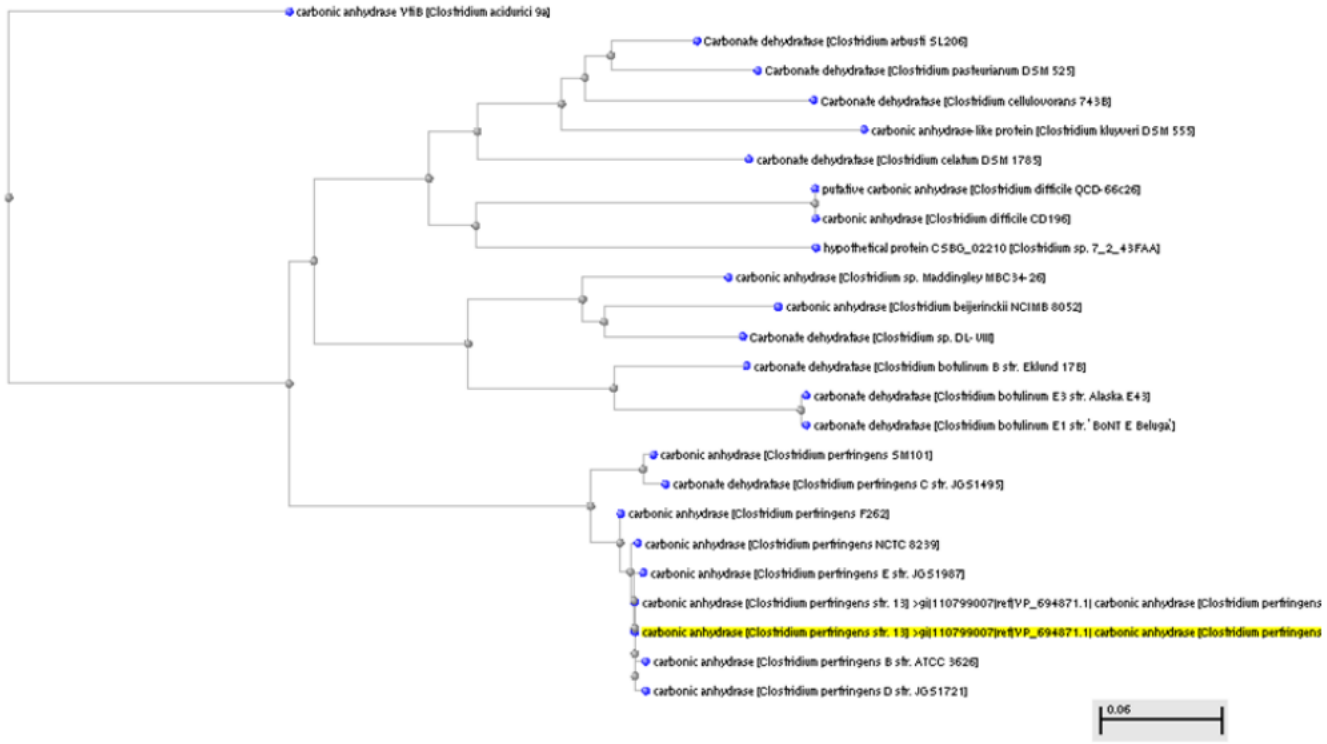

Figure 4.7 Phylogenetic tree showing the relationships among beta class carbonic anhydrase sequences from species of the genus Clostridia.

The tree was produced using the Fast Minimum Evolution algorithm (Desper R and Gascuel O, Mol Biol Evol 21:587-98, 2004) with BLAST pairwise alignments obtained from all non-redundant databases available from the National Center for Biotechnology Information (http://www.ncbi.nlm.nih.gov/). Bar indicates substitutions per site. Gene identification numbers follow. *Clostridium perfringens* str. 13 , GI:18309395; *Clostridium perfringens* E str. JGS1987, GI:168204407; *Clostridium perfringens* B str. ATCC 3626, GI:170763897; *Clostridium perfringens* NCTC 8239, GI:182420476; *Clostridium perfringens* D str. JGS1721, GI:182624627*; Clostridium perfringens* F262, GI:422872991; *Clostridium perfringens* SM101, GI:110802070; *Clostridium perfringens* C str. JGS1495, GI:169343003; *Clostridium arbusti* SL206, GI:399887674; *Clostridium* sp. DL-VIII, GI:359410832; *Clostridium beijerinckii* CIMB 8052, GI:150019236; *Clostridium cellulovorans* 743B, GI:302873277; *Clostridium* sp. Maddingley MBC34-26, GI:410729058; *Clostridium pasteurianum* DSM 525, GI:440781189; *Clostridium botulinum* B str. Eklund 17B, GI:187932534; *Clostridium celatum* DSM 1785, GI:429766678; *Clostridium difficile* QCD- 66c26, GI:254975813; *Clostridium difficile* CD196, GI:260683813; *Clostridium* sp. 7_2_43FAA, GI:404370481; *Clostridium kluyveri* DSM, GI:153953171; *Clostridium botulinum* E3 str. Alaska E43, GI:188589913; *Clostridium botulinum* E1 str. 'BoNT E Beluga', GI:251780513; *Clostridium acidurici* 9a, GI:407474874.

Acknowledgements

This work was supported by the Division of Chemical Sciences, Geosciences, and Biosciences, Office of Basic Energy Sciences of the U.S. Department of Energy through grant DE-FG02-95ER20198 MOD16 to J.G.F. and National Institutes of Health grants R21 AI088298 and NSF grant 1057871 to S.B.M.

Chapter 5 Conclusions

Type IV pili are incredible structures. They are the strongest known molecular motor, and can mediate a vast array of different functions. And yet, the basics of how they work are not well understood. It is known that pili are extended by adding pilin monomers to the base of a growing filament, but how? What is the mechanism of the transition from a stable, monomeric pilin in a membrane, to a stable position in a pilus?

In Chapter 2, the energy state of one of these, the pilin in membrane, was examined. Although the data gathered thus far do not support any definitive conclusions, the technique is promising and worthy of refining to get a proper answer. Once refined, the data generated can be fed back into the original molecular dynamics (MD) simulation and used to firm up the current theoretical limits. The solid state NMR technique shown here only addresses the angle of insertion, but by using selectively ^{15}N labeled amino acids, the depth of insertion also potentially becomes measurable. This would help refine the MD simulation even further. Electro-assembly of pili from pilin in an artificial membrane was an exciting, and as yet unconfirmed result. If this is found to be true, the possibility of using an electric field to directly probe the energy required to polymerize a pilus is an exciting prospect. Being able to combine the ssNMR data, MD simulations, and electro-assembly could potentially fill in a lot of current gaps in the knowledge base about how type IV pili are assembled. Knowing the energy barrier of removing a pilin from the membrane into solvent (MD and ssNMR data), and the actual amount of energy required to electro-assemble pilins from the same conditions into a membrane could help shed light on the mechanistic steps involved in assembly. The difference in energy required for these two situations could be used in an effort to highlight critical amino acid residues: for instance, if mutating the codon for a given residue results in no change in the barrier of removing a pilin from membrane to solvent, but increases the energy required for electro-assembly (or abolishes electro-assembly altogether), then it can be said that the residue plays a critical role in membrane-to-pilus transition, or is crucial to the structure of the pilin. Unfortunately, this scenario would likely prove difficult to analyze using ssNMR as any

residues critical for assembly would complicate the purification procedure used here. However, this can potentially be overcome by having an accurate MD model of the variant pilin.

In Chapter 3, one of the possible mechanisms of assembly was examined. After an exhaustive effort, it must be stated simply that PilB2 and PilC2 do not interact, and thus cannot form a 'core assembly apparatus'. In these investigations, however, some interesting divisions in type IV pili machinery began to slowly emerge. So far, distinctions have been drawn by examining the pilin proteins themselves, but not the actual mechanisms or machinery of assembly. It seems that there are several different ways of categorizing the machinery, which are not exclusive. There are the assembly ATPases that remain hexameric in the absence of ATP. This is likely an arbitrary distinction, as there will always be ATP present in the cell. There are the assembly ATPases that bind zinc: This likely has to do with hexamer stability, and can be related to the previous division. There are assembly ATPases that have an extended N-terminal domain versus those that do not, and a subset of those with the extra domain bind cyclic-di-GMP. And then there are the assembly ATPases that directly bind to their cognate integral membrane core protein versus those that do not. It becomes very difficult to organize and separate these different machinery types, and it also leads to the question: Does it matter? In other words, do these divisions show meaningful differences in assembly mechanism? It is my opinion that they do, simply because these divisions are maintained across a very large diversity of bacterial organisms, with multiple types found even in the same organism. This implies that each machinery architecture has its own advantages and disadvantages. All of this goes back to the idea of a 'core assembly apparatus' as put forward by Lisa Craig. It is still very possible that this is a viable model, just not the only viable model.

Bibliography

1. **Hassan KA, Elbourne LDH, Tetu SG, Melville SB, Rood JI, Paulsen IT.** 2015. Genomic analyses of *Clostridium perfringens* isolates from five toxinotypes. Res Microbiol **166:**255-263.
2. **Uzal FA, Freedman JC, Shrestha A, Theoret JR, Garcia J, Awad MM, Adams V, Moore RJ, Rood JI, McClane BA.** 2014. Towards an understanding of the role of *Clostridium perfringens* toxins in human and animal disease. Future Microbiol **9:**361-377.
3. **Smith LD, Gardner MV.** 1949. The occurrence of vegetative cells of *Clostridium perfringens* in soil. J Bacteriol **58:**407.
4. **Stevens DL.** 2000. The pathogenesis of clostridial myonecrosis. Int J Med Microbiol **290:**497-502.
5. **Ma M, Gurjar A, Theoret JR, Garcia JP, Beingesser J, Freedman JC, Fisher DJ, McClane BA, Uzal FA.** 2014. Synergistic effects of *Clostridium perfringens* enterotoxin and beta toxin in rabbit small intestinal loops. Infect Immun **82:**2958-2970.
6. **Varga JJ, Nguyen V, O'Brien DK, Rodgers K, Walker RA, Melville SB.** 2006. Type IV pili-dependent gliding motility in the Gram-positive pathogen *Clostridium perfringens* and other Clostridia. Mol Microbiol **62:**680-694.
7. **Rood JI.** 1998. Virulence genes of *Clostridium perfringens*. Annu Rev Microbiol **52:**333-360.
8. **McDonel JL.** 1980. *Clostridium perfringens* toxins (type A, B, C, D, E). Pharmacol Ther **10:**617-655.
9. **Huyet J, Naylor CE, Savva CG, Gibert M, Popoff MR, Basak AK.** 2013. Structural Insights into *Clostridium perfringens* Delta Toxin Pore Formation. PLoS ONE **8:**e66673.
10. **Jin F, Matsushita O, Katayama S, Jin S, Matsushita C, Minami J, Okabe A.** 1996. Purification, characterization, and primary structure of *Clostridium perfringens* lambda-toxin, a thermolysin-like metalloprotease. Infect Immun **64:**230-237.
11. **Rood JI, Cole ST.** 1991. Molecular genetics and pathogenesis of *Clostridium perfringens*. Microbiol Rev **55:**621-648.
12. **Flores-Díaz M, Alape-Girón A.** 2003. Role of *Clostridium perfringens* phospholipase C in the pathogenesis of gas gangrene. Toxicon **42:**979-986.
13. **Hatheway CL.** 1990. Toxigenic clostridia. Clin Microbiol Rev **3:**66-98.
14. **Sakurai J, Nagahama M, Oda M.** 2004. *Clostridium perfringens* Alpha-Toxin: Characterization and Mode of Action. Journal of Biochemistry **136:**569-574.
15. **Gurjar A, Li J, McClane BA.** 2010. Characterization of toxin plasmids in *Clostridium perfringens* type C isolates. Infect Immun **78:**4860-4869.
16. **Alves GG, de Ávila RAM, Chávez-Olórtegui CD, Lobato FCF.** 2014. *Clostridium perfringens* epsilon toxin: the third most potent bacterial toxin known. Anaerobe **30:**102-107.
17. **Harry KH, Zhou R, Kroos L, Melville SB.** 2009. Sporulation and enterotoxin (CPE) synthesis are controlled by the sporulation-specific sigma factors SigE and SigK in *Clostridium perfringens*. J Bacteriol **191:**2728-2742.
18. **Liu H, Bouillaut L, Sonenshein AL, Melville SB.** 2013. Use of a mariner-based transposon mutagenesis system to isolate *Clostridium perfringens* mutants deficient in gliding motility. J Bacteriol **195:**629-636.
19. **Craig L, Li J.** 2008. Type IV pili: paradoxes in form and function. Curr Opin Struct Biol **18:**267-277.
20. **El-Naggar MY, Wanger G, Leung KM, Yuzvinsky TD, Southam G, Yang J, Lau WM, Nealson KH, Gorby YA.** 2010. Electrical transport along bacterial nanowires from *Shewanella*

oneidensis MR-1. Proceedings of the National Academy of Sciences **107:**18127-18131.
21. **Maier B, Potter L, So M, Long CD, Seifert HS, Sheetz MP.** 2002. Single pilus motor forces exceed 100 pN. Proc Natl Acad Sci USA **99:**16012-16017.
22. **Lu S, Giuliani M, Harvey H, Burrows LL, Wickham RA, Dutcher JR.** 2015. Nanoscale Pulling of Type IV Pili Reveals Their Flexibility and Adhesion to Surfaces over Extended Lengths of the Pili. Biophys J **108:**2865-2875.
23. **Semmler AB, Whitchurch CB, Mattick JS.** 1999. A re-examination of twitching motility in *Pseudomonas aeruginosa*. Microbiology **145 (Pt 10):**2863-2873.
24. **Bischof LF, Friedrich C, Harms A, Søgaard-Andersen L, van der Does C.** 2016. The Type IV Pilus Assembly ATPase PilB of *Myxococcus xanthus* interacts with the Inner Membrane Platform Protein PilC and the Nucleotide Binding Protein PilM. J Biol Chem.
25. **Craig L, Volkmann N, Arvai AS, Pique ME, Yeager M, Egelman EH, Tainer JA.** 2006. Type IV pilus structure by cryo-electron microscopy and crystallography: implications for pilus assembly and functions. Mol Cell **23:**651-662.
26. **Tammam S, Sampaleanu LM, Koo J, Manoharan K, Daubaras M, Burrows LL, Howell PL.** 2013. PilMNOPQ from the *Pseudomonas aeruginosa* type IV pilus system form a transenvelope protein interaction network that interacts with PilA. J Bacteriol **195:**2126-2135.
27. **Touhami A, Jericho MH, Boyd JM, Beveridge TJ.** 2006. Nanoscale characterization and determination of adhesion forces of *Pseudomonas aeruginosa* pili by using atomic force microscopy. J Bacteriol **188:**370-377.
28. **van Schaik EJ, Giltner CL, Audette GF, Keizer DW, Bautista DL, Slupsky CM, Sykes BD, Irvin RT.** 2005. DNA binding: a novel function of *Pseudomonas aeruginosa* type IV pili. J Bacteriol **187:**1455-1464.
29. **Carter MQ, Chen J, Lory S.** 2010. The *Pseudomonas aeruginosa* pathogenicity island PAPI-1 is transferred via a novel type IV pilus. J Bacteriol **192:**3249-3258.
30. **Ajon M, Frols S, van Wolferen M, Stoecker K, Teichmann D, Driessen AJ, Grogan DW, Albers SV, Schleper C.** 2011. UV-inducible DNA exchange in hyperthermophilic archaea mediated by type IV pili. Mol Microbiol **82:**807-817.
31. **Allers T.** 2011. Swapping genes to survive - a new role for archaeal type IV pili. Mol Microbiol **82:**789-791.
32. **Strom MS, Lory S.** 1993. Structure-function and biogenesis of the type IV pili. Annu Rev Microbiol **47:**565-596.
33. **Folkhard W, Marvin DA, Watts TH, Paranchych W.** 1981. Structure of polar pili from *Pseudomonas aeruginosa* strains K and O. J Mol Biol **149:**79-93.
34. **Leighton TL, Buensuceso RNC, Howell PL, Burrows LL.** 2015. Biogenesis of *Pseudomonas aeruginosa* type IV pili and regulation of their function. Environ Microbiol **17:**4148-4163.
35. **Berry J-L, Pelicic V.** 2015. Exceptionally widespread nanomachines composed of type IV pilins: the prokaryotic Swiss Army knives. FEMS Microbiol Rev **39:**134-154.
36. **Pelicic V.** 2008. Type IV pili: e pluribus unum? Mol Microbiol **68:**827-837.
37. **Rodgers K, Arvidson CG, Melville S.** 2011. Expression of a *Clostridium perfringens* type IV pilin by *Neisseria gonorrhoeae* mediates adherence to muscle cells. Infect Immun **79:**3096-3105.
38. **Burrows LL.** 2012. *Pseudomonas aeruginosa* twitching motility: type IV pili in action. Annu Rev Microbiol **66:**493-520.
39. **Melville S, Craig L.** 2013. Type IV pili in Gram-positive bacteria. Microbiol Mol Biol Rev **77:**323-341.
40. **Lieberman JA, Petro CD, Thomas S, Yang A, Donnenberg MS.** 2015. Type IV pilus secretins have extracellular C termini. MBio **6**.
41. **Friedrich C, Bulyha I, Søgaard-Andersen L.** 2014. Outside-in assembly pathway of the type

IV pilus system in *Myxococcus xanthus*. J Bacteriol **196:**378-390.
42. **Gold VAM, Salzer R, Averhoff B, Kühlbrandt W.** 2015. Structure of a type IV pilus machinery in the open and closed state. Elife **4**.
43. **Li C, Wallace RA, Black WP, Li Y-z, Yang Z.** 2013. Type IV pilus proteins form an integrated structure extending from the cytoplasm to the outer membrane. PLoS ONE **8:**e70144.
44. **Roelofs KG, Jones CJ, Helman SR, Shang X, Orr MW, Goodson JR, Galperin MY, Yildiz FH, Lee VT.** 2015. Systematic Identification of Cyclic-di-GMP Binding Proteins in *Vibrio cholerae* Reveals a Novel Class of Cyclic-di-GMP-Binding ATPases Associated with Type II Secretion Systems. PLoS Pathog **11:**e1005232.
45. **Tripp BC, Smith K, Ferry JG.** 2001. Carbonic anhydrase: new insights for an ancient enzyme. J Biol Chem **276:**48615-48618.
46. **Tripp BC, Bell CB, 3rd, Cruz F, Krebs C, Ferry JG.** 2004. A role for iron in an ancient carbonic anhydrase. J Biol Chem **279:**6683-6687.
47. **Lemkul JA, Bevan DR.** 2011. Characterization of interactions between PilA from *Pseudomonas aeruginosa* strain K and a model membrane. J Phys Chem B **115:**8004-8008.
48. **Hartman AH, Liu H, Melville SB.** 2011. Construction and characterization of a lactose-inducible promoter system for controlled gene expression in *Clostridium perfringens*. Appl Environ Microbiol **77:**471-478.
49. **Salzer R, Herzberg M, Nies DH, Joos F, Rathmann B, Thielmann Y, Averhoff B.** 2014. Zinc and ATP binding of the hexameric AAA-ATPase PilF from *Thermus thermophilus*: role in complex stability, piliation, adhesion, twitching motility, and natural transformation. J Biol Chem **289:**30343-30354.
50. **Jones CJ, Utada A, Davis KR, Thongsomboon W, Sanchez DZ, Banakar V, Cegelski L, Wong GCL, Yildiz FH.** 2015. C-di-GMP Regulates Motile to Sessile Transition by Modulating MshA Pili Biogenesis and Near-Surface Motility Behavior in *Vibrio cholerae*. PLoS Pathog **11:**e1005068.
51. **Roelofs KG, Wang J, Sintim HO, Lee VT.** 2011. Differential radial capillary action of ligand assay for high-throughput detection of protein-metabolite interactions. Proc Natl Acad Sci USA **108:**15528-15533.
52. **Drozdetskiy A, Cole C, Procter J, Barton GJ.** 2015. JPred4: a protein secondary structure prediction server. Nucleic Acids Res **43:**W389-394.
53. **Chiang P, Habash M, Burrows LL.** 2005. Disparate subcellular localization patterns of *Pseudomonas aeruginosa* Type IV pilus ATPases involved in twitching motility. J Bacteriol **187:**829-839.
54. **Georgiadou M, Castagnini M, Karimova G, Ladant D, Pelicic V.** 2012. Large-scale study of the interactions between proteins involved in type IV pilus biology in *Neisseria meningitidis*: characterization of a subcomplex involved in pilus assembly. Mol Microbiol **84:**857-873.
55. **Nariya H, Miyata S, Suzuki M, Tamai E, Okabe A.** 2011. Development and Application of a Method for Counterselectable In-Frame Deletion in *Clostridium perfringens*. Applied and Environmental Microbiology **77:**1375-1382.
56. **Hartman AH, Liu H, Melville SB.** 2011. Construction and characterization of a lactose-inducible promoter system for controlled gene expression in *Clostridium perfringens*. Appl Environ Microbiol **77:**471-478.
57. **Rowlett RS.** 2010. Structure and catalytic mechanism of the beta-carbonic anhydrases. Biochim Biophys Acta **1804:**362-373.
58. **So AK, Espie GS.** 1998. Cloning, characterization and expression of carbonic anhydrase from the cyanobacterium *Synechocystis* PCC6803. Plant Mol Biol **37:**205-215.
59. **Sawaya MR, Cannon GC, Heinhorst S, Tanaka S, Williams EB, Yeates TO, Kerfeld CA.** 2006. The structure of beta-carbonic anhydrase from the carboxysomal shell reveals a distinct

subclass with one active site for the price of two. J Biol Chem **281:**7546-7555.

60. **Kupriyanova EV, Sinetova MA, Markelova AG, Allakhverdiev SI, Los DA, Pronina NA.** 2011. Extracellular beta-class carbonic anhydrase of the alkaliphilic cyanobacterium *Microcoleus chthonoplastes*. J Photochem Photobiol B, Biol **103:**78-86.
61. **Joseph P, Turtaut Fc, Ouahrani-Bettache S, Montero J-L, Nishimori I, Minakuchi T, Vullo D, Scozzafava A, Köhler S, Winum J-Y, Supuran CT.** 2010. Cloning, characterization, and inhibition studies of a beta-carbonic anhydrase from *Brucella suis*. J Med Chem **53:**2277-2285.
62. **Nishimori I, Minakuchi T, Kohsaki T, Onishi S, Takeuchi H, Vullo D, Scozzafava A, Supuran CT.** 2007. Carbonic anhydrase inhibitors: the beta-carbonic anhydrase from *Helicobacter pylori* is a new target for sulfonamide and sulfamate inhibitors. Bioorg Med Chem Lett **17:**3585-3594.
63. **Cronk JD, O'Neill JW, Cronk MR, Endrizzi JA, Zhang KY.** 2000. Cloning, crystallization and preliminary characterization of a beta-carbonic anhydrase from *Escherichia col*i. Acta Crystallogr D Biol Crystallogr **56:**1176-1179.
64. **Covarrubias AS, Larsson AM, Högbom M, Lindberg J, Bergfors T, Björkelid C, Mowbray SL, Unge T, Jones TA.** 2005. Structure and function of carbonic anhydrases from *Mycobacterium tuberculosis*. J Biol Chem **280:**18782-18789.
65. **Vullo D, Nishimori I, Minakuchi T, Scozzafava A, Supuran CT.** 2011. Inhibition studies with anions and small molecules of two novel beta-carbonic anhydrases from the bacterial pathogen *Salmonella enterica* serovar Typhimurium. Bioorg Med Chem Lett **21:**3591-3595.
66. **Merlin C, Masters M, McAteer S, Coulson A.** 2003. Why is carbonic anhydrase essential to *Escherichia coli*? J Bacteriol **185:**6415-6424.
67. **Amoroso G, Morell-Avrahov L, Müller D, Klug K, Sültemeyer D.** 2005. The gene NCE103 (YNL036w) from *Saccharomyces cerevisiae* encodes a functional carbonic anhydrase and its transcription is regulated by the concentration of inorganic carbon in the medium. Mol Microbiol **56:**549-558.
68. **Mitsuhashi S, Ohnishi J, Hayashi M, Ikeda M.** 2004. A gene homologous to beta-type carbonic anhydrase is essential for the growth of *Corynebacterium glutamicum* under atmospheric conditions. Appl Microbiol Biotechnol **63:**592-601.
69. **Guilloton MB, Lamblin AF, Kozliak EI, Gerami-Nejad M, Tu C, Silverman D, Anderson PM, Fuchs JA.** 1993. A physiological role for cyanate-induced carbonic anhydrase in *Escherichia coli*. J Bacteriol **175:**1443-1451.
70. **Strop P, Smith KS, Iverson TM, Ferry JG, Rees DC.** 2001. Crystal structure of the "cab"-type beta class carbonic anhydrase from the archaeon *Methanobacterium thermoautotrophicum*. J Biol Chem **276:**10299-10305.
71. **Smith KS, Ferry JG.** 1999. A plant-type (beta-class) carbonic anhydrase in the thermophilic methanoarchaeon *Methanobacterium thermoautotrophicum*. J Bacteriol **181:**6247-6253.
72. **Smith KS, Cosper NJ, Stalhandske C, Scott RA, Ferry JG.** 2000. Structural and kinetic characterization of an archaeal beta-class carbonic anhydrase. J Bacteriol **182:**6605-6613.
73. **Smith KS, Ingram-Smith C, Ferry JG.** 2002. Roles of the conserved aspartate and arginine in the catalytic mechanism of an archaeal beta-class carbonic anhydrase. J Bacteriol **184:**4240-4245.
74. **Supuran CT.** 2011. Bacterial carbonic anhydrases as drug targets: toward novel antibiotics? Front Pharmacol **2:**34.
75. **Joseph P, Ouahrani-Bettache S, Montero J-L, Nishimori I, Minakuchi T, Vullo D, Scozzafava A, Winum J-Y, Köhler S, Supuran CT.** 2011. A new beta-carbonic anhydrase from *Brucella suis*, its cloning, characterization, and inhibition with sulfonamides and sulfamates, leading to impaired pathogen growth. Bioorg Med Chem **19:**1172-1178.

76. **Burghout P, Cron LE, Gradstedt H, Quintero B, Simonetti E, Bijlsma JJE, Bootsma HJ, Hermans PWM.** 2010. Carbonic anhydrase is essential for *Streptococcus pneumoniae* growth in environmental ambient air. J Bacteriol **192:**4054-4062.
77. **Sassetti CM, Boyd DH, Rubin EJ.** 2003. Genes required for mycobacterial growth defined by high density mutagenesis. Mol Microbiol **48:**77-84.
78. **Melville SB, Labbe R, Sonenshein AL.** 1994. Expression from the *Clostridium perfringens cpe* promoter in *C. perfringens* and *Bacillus subtilis*. Infect Immun **62:**5550-5558.
79. **Zimmerman S, Ferry J.** 2008. The beta and gamma classes of carbonic anhydrase. Curr Pharm Des **145 (Pt 10):**716-721.
80. **Khalifah R.** 1971. The carbon dioxide hydration activity of carbonic anhydrase. I. Stop-flow kinetic studies on the native human isoenzymes B and C. J Biol Chem**:**2561-2573.
81. **Alber BE, Ferry JG.** 1996. Characterization of heterologously produced carbonic anhydrase from *Methanosarcina thermophila*. J Bacteriol **178:**3270-3274.
82. **GORNALL AG, BARDAWILL CJ, DAVID MM.** 1949. Determination of serum proteins by means of the biuret reaction. J Biol Chem **177:**751-766.
83. **Laemmli UK.** 1970. Cleavage of structural proteins during the assembly of the head of bacteriophage T4. Nature **227:**680-685.
84. **Peterson JD, Umayam LA, Dickinson T, Hickey EK, White O.** 2001. The Comprehensive Microbial Resource. Nucleic Acids Res **29:**123-125.
85. **WILBUR KM, ANDERSON NG.** 1948. Electrometric and colorimetric determination of carbonic anhydrase. J Biol Chem **176:**147-154.
86. **Rowlett RS, Tu C, Lee J, Herman AG, Chapnick DA, Shah SH, Gareiss PC.** 2009. Allosteric site variants of *Haemophilus influenzae* beta-carbonic anhydrase. Biochemistry **48:**6146-6156.
87. **Shimizu T, Ohtani K, Hirakawa H, Ohshima K, Yamashita A, Shiba T, Ogasawara N, Hattori M, Kuhara S, Hayashi H.** 2002. Complete genome sequence of *Clostridium perfringens*, an anaerobic flesh-eater. Proc Natl Acad Sci USA **99:**996-1001.
88. **Ueda K, Nishida H, Beppu T.** 2012. Dispensabilities of carbonic anhydrase in proteobacteria. Int J Evol Biol **2012:**324549.
89. **Cot SS-W, So AK-C, Espie GS.** 2008. A multiprotein bicarbonate dehydration complex essential to carboxysome function in cyanobacteria. J Bacteriol **190:**936-945.
90. **Marcus EA, Moshfegh AP, Sachs G, Scott DR.** 2005. The periplasmic alpha-carbonic anhydrase activity of *Helicobacter pylori* is essential for acid acclimation. J Bacteriol **187:**729-738.
91. **Sassetti CM, Rubin EJ.** 2003. Genetic requirements for mycobacterial survival during infection. Proc Natl Acad Sci USA **100:**12989-12994.
92. **Badger MR, Price GD.** 2003. CO2 concentrating mechanisms in cyanobacteria: molecular components, their diversity and evolution. J Exp Bot **54:**609-622.
93. **Kusian B, Sültemeyer D, Bowien B.** 2002. Carbonic anhydrase is essential for growth of Ralstonia eutropha at ambient CO(2) concentrations. J Bacteriol **184:**5018-5026.
94. **Smith KS, Ferry JG.** 2000. Prokaryotic carbonic anhydrases. FEMS Microbiol Rev **24:**335-366.
95. **Dharmarajan L, Kraszewski JL, Mukhopadhyay B, Dunten PW.** 2011. Structure of an archaeal-type phosphoenolpyruvate carboxylase sensitive to inhibition by aspartate. Proteins **79:**1820-1829.
96. **Patel HM, Kraszewski JL, Mukhopadhyay B.** 2004. The phosphoenolpyruvate carboxylase from *Methanothermobacter thermautotrophicus* has a novel structure. J Bacteriol **186:**5129-5137.
97. **Minakuchi T, Nishimori I, Vullo D, Scozzafava A, Supuran CT.** 2009. Molecular cloning,

characterization, and inhibition studies of the Rv1284 beta-carbonic anhydrase from *Mycobacterium tuberculosis* with sulfonamides and a sulfamate. J Med Chem **52:**2226-2232.

98. **Burghout P, Vullo D, Scozzafava A, Hermans PWM, Supuran CT.** 2011. Inhibition of the beta-carbonic anhydrase from *Streptococcus pneumoniae* by inorganic anions and small molecules: Toward innovative drug design of antiinfectives? Bioorg Med Chem **19:**243-248.
99. **Nishimori I, Minakuchi T, Vullo D, Scozzafava A, Supuran CT.** 2011. Inhibition studies of the beta-carbonic anhydrases from the bacterial pathogen *Salmonella enterica* serovar Typhimurium with sulfonamides and sulfamates. Bioorg Med Chem **19:**5023-5030.
100. **Heinhorst S, Williams EB, Cai F, Murin CD, Shively JM, Cannon GC.** 2006. Characterization of the carboxysomal carbonic anhydrase CsoSCA from *Halothiobacillus neapolitanus*. J Bacteriol **188:**8087-8094.